universität wien

DISSERTATION / DOCTORAL THESIS

Titel der Dissertation / Title of the Doctoral Thesis

„Viscoelastic properties of polymer nanocomposites“

verfasst von / submitted by

Mag. rer. nat. Marius Reinecker

angestrebter akademischer Grad / in partial fulfilment of the requirements for the degree of

Doktor der Naturwissenschaften (Dr. rer. nat.)

Wien, 2016 / Vienna 2016

Studienkennzahl lt. Studienblatt: degree programme code as it appears on the student record sheet:	A 796 605 411
Dissertationsgebiet lt. Studienblatt/ field of study as it appears on the student record sheet:	Physik
Betreut von / Supervisor:	ao. Univ.-Prof. Mag. Dr. Wilfried Schranz

Assertion

This work contains three articles. Major parts of these publications were contributed by Mag. Marius Reinecker.

Ao. Prof. Dr. Wilfried Schranz

Mag. Marius Reinecker

Contents

1 Abstract **5**

1.1 English 5

1.2 German 6

2 Introduction **7**

3 Samples **9**

3.1 Polyurea elastomers 9

3.1.1 Jeffamines 400, 2000 and 4000 11

3.2 Fillers: $Mo_6S_2I_8$, MoS_2 12

3.3 Composites 13

3.3.1 JD-2000 nanocomposites 14

3.3.2 JED-2003 nanocomposites 14

3.4 Preparation of samples 16

4 Measurements **21**

4.1 Method: DMA 21

4.2 Instrument: Perkin Elmer Diamond DMA 25

5 Results and discussion **28**

5.1 Polyurea nanocomposites with nanowires and nanotubes 28

5.2 Comparison of different polyurea nanocomposites 30

5.3 Hard and soft domains in polyurea elastomers 32

6 Summary and conclusions **39**

7 Glossary of abbreviations **41**

8 Publications **42**

8.1 Dynamic- and Thermo-mechanical Analysis of Inorganic Nanotubes/elastomer Composites 42

8.2 Influence of inorganic nanoparticles on the glass transitions of polyurea elastomers . . 52

8.3 Two glass transitions of polyurea networks: effect of the segmental molecular weight . 62

9 Acknowledgements **73**

List of Figures **74**

List of Illustrations **77**

Literature **78**

10 Curriculum vitae **84**

1 Abstract

1.1 English

Polymer-nanoparticle composites (PNCs) play an increasing role in technology. The properties of polymers can be significantly changed by incorporating nanoparticles, which yields a great potential for applications. We present dynamic mechanical analysis (DMA) measurements of a type of polyurea elastomer and nanocomposites based on polyurea elastomers containing inorganic MoS_2 nanotubes and $Mo_6S_2I_8$ nanowires. Polyurea is a spontaneously occurring PNC, exhibiting a phase segregated structure with hard nanodomains embedded in a soft (elastically compliant) matrix. Two distinct peaks can be observed in tan δ in both the pure elastomer and composites of elastomer and nanoparticles. The first peak at T_{g1} is attributed to a glass transition occurring in the soft matrix, the second peak at T_{g2} to regions near the hard domains which experience a slowing down of dynamics. This can be considered as being the inverse situation compared to glass forming liquids in rigid porous matrices, which also have been investigated by DMA-measurements in context with the glass-transition and comprehensively described[1]. It is demonstrated that the glass transition temperature T_{g1} of the nanocomposites is increased by adding small amounts of inorganic nanotubes, whereas the transition temperature T_{g2} remains unchanged. That influence of the filler leads to an upshift in T_{g1}, suggesting an attractive interaction between the nanoparticles and the polymer. Focusing on the already phase seperated structure of the pure polyurea elstomer, it has been discovered that the temperature T_{g1} of the glass transition related to the soft matrix can be tuned by chemically controlling the volume fraction of soft to hard domains ϕ_x during manufacture of the sample. The interaction between the soft matrix and the hard nanodomains is selfevidently attractive in the pure polymer. It is shown that increasing the fraction of the hard domains leads to an increase in T_{g1}. A further increase in the relative volume of the hard domains eventually causes the two transition temperatures to match at a certain volume-fraction $\phi_{xc} = 0.6$, i.e. $T_{g1} = T_{g2}$. It is found that ϕ_{xc} corresponds closely to the percolation threshold of randomly oriented overlapping ellipsoids of revolution with an aspect ratio of about 1:4 - 1:5. It is therefore concluded, that reaching a volume-fraction of ϕ_{xc} of hard domains, polyurea-elastomers are transformed from a system of hard domains inside a soft matrix to a hard matrix containing soft domains.

1.2 German

Polymer-Nanopartikel-Komposite (PNCs) spielen eine zunehmende Rolle im technologischen Bereich. Die Eigenschaften von Polymeren können durch die Zugabe von Nanopartikeln signifikant verändert werden und dies birgt ein großes Potential für verschiedene Anwendungen. Wie präsentieren DMA Messungen von Polyurea-Elastomeren und auf Polyurea-Elastomeren basierenden Nanokompositen, welche anorganische MoS_2 Nanoröhrchen und $Mo_6S_2I_8$ Nanodrähte beinhalten. Polyurea ist ein spontan auftretendes PNC und weist eine segregierte Struktur mit in einer im elastischen Sinne weichen Matrix eingebetteten harten Nanodomänen. Zwei verschiedene Peaks konnten in $tan\delta$ beobachtet werden – sowohl in reinen Elastomeren als auch bei Elastomer-Nanopartikel-Kompositen. Der erste Peak bei T_{g1} ist auf einen Glasübergang in der weichen Matrix zurückzuführen. Der zweite Peak bei T_{g2} ist einem Glasübergang in Regionen nahe an den harten Domänen zuzuordnen, welche eine Verlangsamung der Dynamik erfahren. Verglichen mit glasformenden Flüssigkeiten in rigiden porösen Matrizes, die auch durch DMA-Messungen in Zusammenhang mit Glasübergängen erforscht und ausführlich beschrieben worden sind[1], kann dies als umgekehrte Situation betrachtet werden. Die Glasübergangs-Temperatur T_{g1} der Nanokomposite wird durch die Zugabe kleiner Mengen anorganischer Nanoröhrchen erhöht, während die Temperatur T_{g2} des Glasübergangs der harten Domänen unverändert bleibt. Dieser Einfluss des Füllers führt zu einer Erhöhung in T_{g1} und verweist auf eine attraktive Interaktion zwischen den Nanopartikeln und dem Polymer. In Bezug auf die bereits phasenseparierte Struktur des reinen Polyurea-Elastomers wird gezeigt, dass die Temperatur T_{g1} des Glasübergangs der weichen Matrix beeinflußt werden kann, indem der Volumenanteil von weichen zu harten Domänen ϕ_x während der Probenherstellung chemisch eingestellt wird. Die Interaktion zwischen weicher Matrix und harten Nanodomänen ist im reinen Polymer selbstevident attraktiv. Es wurde gezeigt, dass die Erhöhung des Anteils der harten Domänen zu einer Steigerung in T_{g1} führt. Eine weitere Steigerung im relativen Volumen der harten Domänen verursacht schließlich eine Anpassung der beiden Übergangstemperaturen bei ϕ_{xc} , also $T_{g1} = T_{g2}$. Es zeigt sich, dass ϕ_{xc} eng mit der Perkulationsschwelle von zufällig angeordneten überlappenden Rotationsellipsoiden mit einem Längenverhältnis von ca. 1:4 bis 1:5 korrespondiert. Daraus wird geschlossen, dass Polyurea-Elastomere die einen Volumensanteil von ϕ_{xc} erreichen sich von einem System harter Domänen in einer weichen Matrix zu einer weiche Domänen beinhaltenden harten Matrix verkehren.

2 Introduction

The developement of new polymeric materials is a very broad and growing field, encompassing, for instance, protective coatings [2, 3], large area sensors [4], medical applications or novel photonic materials [5]. Polymers in general exhibit a wide range of physical and chemical properties, and can be well tailored to fit very specific requirements [6]. They can quite easily be optimized for strength or toughness in a given temperature range for the intended application. This can be done by first of all choosing the right type of polymer and for example changing chemical composition or cross-linking density. A possible approach of further expanding the range in which the properties of polymeric materials can be customized and enhanced is to use them as a host matrix for nanoscale filling components. This has been done with a variety of polymers and filling materials e.g. carbon particles and nanotubes to change electrical conductivity [7], functionalized carbon nanotubes to improve mechanical properties [8] or silver to influence optical properties [9] and many more. A very meaningful and well established way to characterize – not only, but in particular – polymers is dynamically measuring their mechanical properties in different geometries over their intended temperature range of operation. This approach of investigating materials by dynamic mechanical analysis, or in short DMA, is often found to be the most sensitive method available. It is also particularly well suited to gain information about the glass transition [10].

It has been shown previously [11] that polymers dispersed with nanoscale filling materials can exhibit two glass transitions at different respective temperatures $T_{g1}<T_{g2}$. This has been done for a variety of different polymer host matrices all filled with spherical silica nanoparticles to establish the generality of a second glass transition in polymer-nanoparticle systems. Achieved results have been interpreted by the authors using the morphological model presented by Eisenberg, Hird and Moore (EHM model) [12] which was originally intended to describe a similar effect in random ionomers. According to the mentioned model, regions of strongly restricted mobility of the polymer-chains changing to weakly restricted and unrestricted mobility with increasing distance to the filler particles are proposed. A distinct second glass transition temperature T_{g2} starts to become evident when the regions of weakly restricted mobility overlap, i.e. when the average distance between the nanodomains goes below the

limit of about 5 to 10 nm. Since this corresponds approximately to the range of sizes of dynamically correlated regions of glass forming polymers and liquids near T_g [13], the loosely bound regions are able to undergo their own glass transition. A very similar effect can also be observed in confined glass-forming molecular liquids [14, 15].
The emerging second glass-transition T_{g2} has been further studied and confirmed by Comer et al.[16] for another range of polymers with regard to surface properties of the filler material using pure SiO_2 and a number of different functionalized silica particles, again of spherical geometry. The reported $tan\,\delta$ curves of the complex mechanical susceptibility with a second peak pertaining to T_{g2} are shown to be dependent on the surface chemistry of the filler particles. This is in good agreement with MC- and MD-simulations [17, 18] on polymer/nanoparticle composites demonstrating a possible increase or decrease of T_g depending on the type of interaction between the nanoparticles and the polymer chains.

The materials to be investigated in the present thesis are different kinds of pure polyurea elastomers as well as polymer nanocomposites (PNCs) consisting of polyurea hosts containing several different inorganic filling materials, more specifically, uncoated MoS_2 nanotubes [19] and $Mo_6S_2I_8$ nanowires [20]. Polyurea is a very attractive material for several reasons. It is forming fast, removing the need for a catalyst to accelerate the reaction, making the process less sensitive to humidity or temperature changes which is a definite advantage over other polymers like e.g. polyurethanes. It exhibits high resistance against many chemicals, mechanical abraision and a remarkable capacity to disperse mechanical shock as occuring explosion blasts or ballistic impacts [3]. Furthermore it posesses good biocompatibility and is therefore also well suited for medical applications e.g. implants [21]. Polyurea has a block copolymer structure. It consists of hard areas embedded in a soft matrix, making it possible to adjust its mechanical properties by influencing the fraction of soft to hard segments through varying the stoichiometry of it's components and controlling reaction time [22]. This phase-separated nature of soft and hard domains makes polyurea especially interesting as it will be shown to exhibit a second glass transition T_{g2} even in the absence of any filler. This is due to the size scale of and distance between the hard segments, forming an intrinsic nanocomposite without the addition of any nanoparticles. These materials just described will be closely examined in relation to their respective glass forming behaviour and mechanical properties in the scope of this work.

3 Samples

The range of sample materials consists of various kinds of polyurea elastomers. They strongly differ in a number of characteristics, particularly average molecular weight, which is related to a specific average length of the polymer chains, and interaction with water, as some display hydrophilic and others hydrophobic characteristics. Also, a range of inorganic nanoscopic filling materials was used to create different polymer nanocomposites (PNCs) in addition to the pure elastomer samples.

All samples were manufactured using the same method and the different kinds of nanoparticles were also incorporated into the polymer in the same way as in the case of the composites. Furthermore, all were prepared in the same manner and to the same size in their charateristic dimension pertaining to the employed method of measurement, in this case length and width of the elastomer strip. There is some slight variation in thickness of the samples due to differences in preparation.

3.1 Polyurea elastomers

The actual manufacturing process of the materials was done by sol/gel chemistry at the ETH Zürich by A. Sánchez-Ferrer as discribed in detail in [22, 23, 24]. To summarize, the polymer and the crosslinker were each separately dissolved in acetone, then poured together and slowly stirred for several minutes before casting the mixture into a mold. All polyurea elastomers discussed here are comprised of a linear molecular backbone, but the possible structures are not limited to this simple shape, e.g. JT-series polyurea elastomers, which are not subject of this work, consist of a star-like polymer backbone.

At standard conditions polyurea forms a phase-seperated nanostructure of hard domains embedded in a matrix of soft polymer chains, with a chemically tunable ratio of the respective relative volumes of matrix and domains. The hard domains consist of clusters of hard segments linked together by hydrogen bonding between the urea-moieties (marked in green in figures 3.1 and 3.2), as shown in

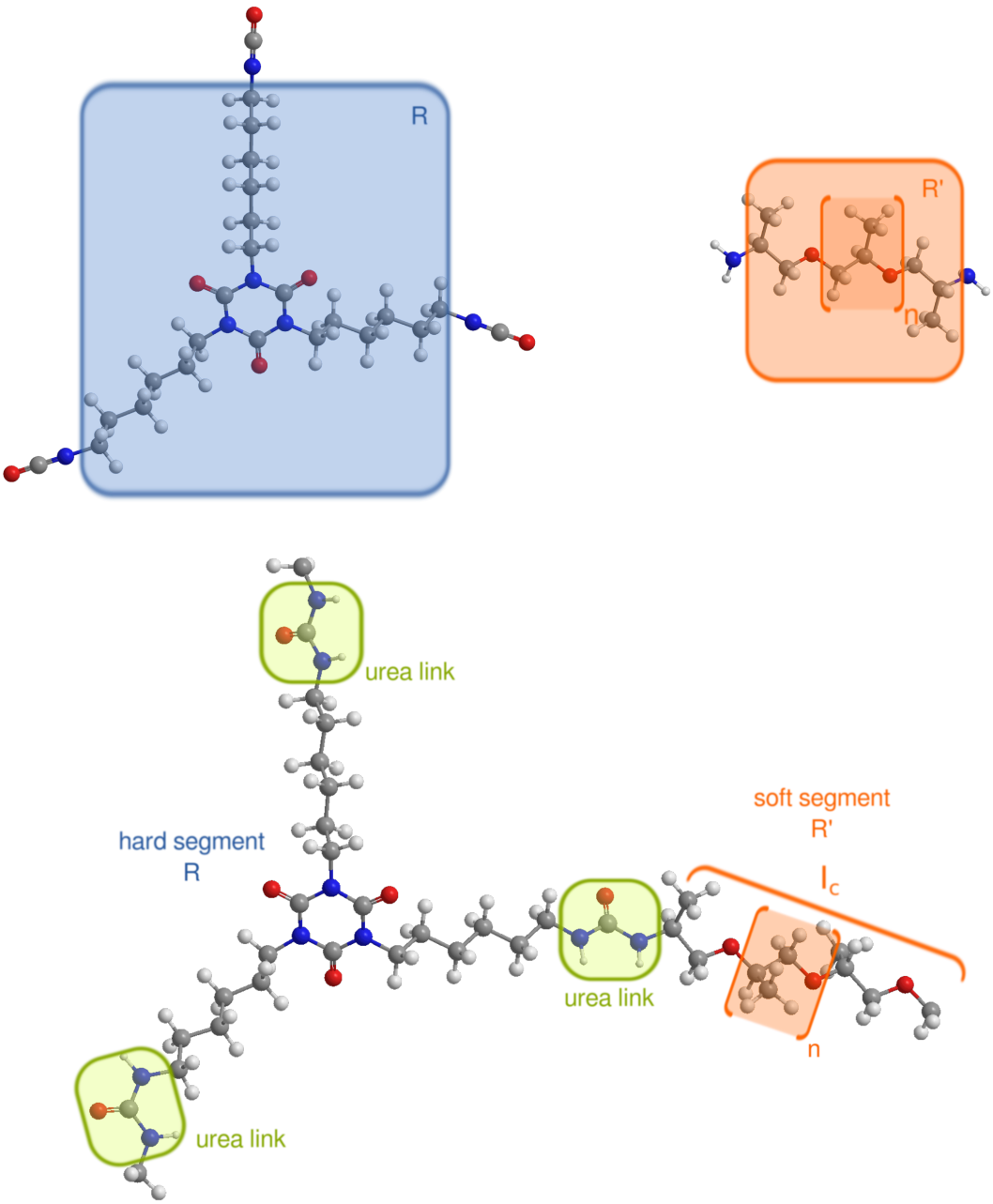

Illustration 3.1: Typical polyurea segment. Carbon atoms are shown in **black**, **hydrogen** in white, **nitrogen** in blue and **oxygen** in red.

figure 3.2. This considered, a rigid matrix dispersed with soft domains could form the far end of the spectrum at a certain ratio of volumes, as will be explored in more detail in 5.3 and 8.3, arriving at the conclusion that such is indeed the case.

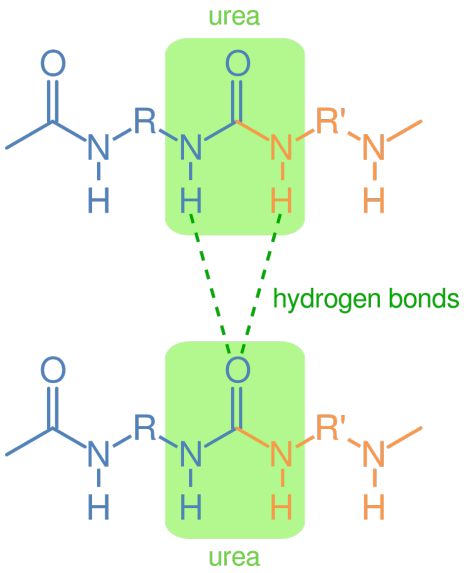

Illustration 3.2: Hydrogen bonds between urea-moieties

A comparison of selected qualitative properties of different kinds of polyurea is presented in the following table:

Name	molecular backbone	molecular mass	interaction with water
JD-400	linear	low	hydrophobic
JD-2000	linear	medium	hydrophobic
JD-4000	linear	high	hydrophobic
JED-2003	linear	medium	hygroscopic, hydrophilic

Table 3.1

3.1.1 Jeffamines 400, 2000 and 4000

The table below compares in detail the three linear hydrophobic diamino-terminated polyetheramines Jeffamine 400, 2000 and 4000 with respect to their molecular size and mass:

Name	Mn	DP	l_c	d	Φ	ρ
JD-400	528	13	5.2	4.4	0.39	972
JD-2000	1991	40	14.9	6.4	0.12	991
JD-4000	4024	75	27.4	7.3	0.07	994

Table 3.2

Mn	$[g \cdot mol^{-1}]$	molecular mass of soft domains
DP		number of repeating units (monomers)
l_c	$[nm]$	contour length (maximum length)
d	$[nm]$	distance between hard and soft segments
Φ		volume fraction of hard domains
ρ	$[kg \cdot mol^{-3}]$	density

The average size of the hard domains in JD-2000 was determined to be a few nanometers and the distance between them was found to be 6.4 nm by performing SAX and WAXS measurements [23]. Figure 3.7 shows atomic force microscopy (AFM) images of the three different polyurea elastomers described in table 3.2.

3.2 Fillers: $Mo_6S_2I_8$, MoS_2

No specific information was available about the nanoparticles used in the first set of composites based on JD-2000 other than their chemical composition. This, at least, ascertains the same type of interaction between elastomer and filler, which is attractive for the materials discussed here. Regardless, wires and tubes have distinctly different surface to volume ratio even without any further detailed knowledge of the actual dimensions, or even distribution of lengths, the particular particles might have. The surface area of the nanoparticles is of course a determining factor for the size of the interfacial regions between the filler and the polymer matrix. These arguments led to expect noticeably dissimilar results for each kind of sample.

For the JED series of PNCs two different kinds of multiwalled MoS_2 nanotubes [19, 25] were used. The samples denoted $C1$ contain the thinner and shorter species of the two, samples denoted $C2$ the thicker and longer tubes. For these fillers more data pertaining to their size and shape was available, which ist given in the table below. $C1$-tubes were the result of desulfurization of MoS_7, whereas the

variant labeled $C2$ is obtained from the decomposition of multiwall $Mo_6S_2I_8$ nanowires. It was not possible to obtain any information as to the exact width of the length-distribution of the tubes.

Designation	label	length $[\mu m]$	diameter$[nm]$	wall type
MoS_2170	$C1$	10	$80-100$	multi
MoS_2628	$C2$	100	~ 250	multi

Table 3.3

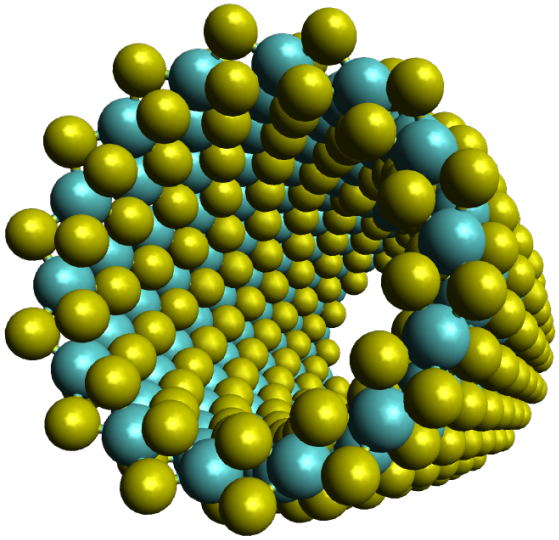

Illustration 3.3: Typical single wall MoS_2-nanotube sulfur shown in yellow, molybdenum colored turquoise

3.3 Composites

Concerning the manufacturing process in the case of polyurea-nanoparticle composites, the filler material was added in the shape of a dry powder to the solution containing the crosslinker and then ultrasonicated before it was stirred together with the solution containing the polymer. In the next step the mix was cast into a mold in the same way as with the pure elastomers, see 3.1 and [23, 24].

3.3.1 JD-2000 nanocomposites

These consist of the hydrophobic elastomer JD-2000 with a linear molecular backbone of medium molecular weight as described in 3.1, which were filled with approximately 0.1 wt-% nanowires $Mo_6S_2I_8$ to create one kind of PNC and ≈0.1 wt-% nanotubes MoS_2 to form another. Scant information was available about the precise characteristics of the filling materials and their distribution inside the polymer matrix. A third variant of JD-2000 PNC was made at a later time, containing ≈1 wt-% MoS_2 nanotubes. The samples were received as small pieces of translucent film. The pieces containing nanoparticles showed a light grey tint of different shades to the naked eye, depending if they contained nanowires or tubes, the samples containing the nanotubes appearing darker.

3.3.2 JED-2003 nanocomposites

This is a hydrophilic elastomer composed of linear polymer-chains with medium molecular weight. 2 sets of PNCs were received, one containing 0.1, 0.5 and 1 weight-% of $C1$-nanotubes, the other filled with the same percentages of $C2$-nanotubes, which are both described in detail in 3.2 and 8.2. As with the JD-2000 PNCs, the JED-2003 samples were also received as small pieces of grey-tinted film. The filler content was also easily discernible with the naked eye, but the difference between the samples containing the same percentage of $C1$- or $C2$-tubes was not readily apparent.

To get a clearer picture of the actual distribution of the filler particles inside the PNCs Small angle X-ray scattering (SAXS) measurements were performed on the samples to gain some information about agglomerates of nanowires/tubes in the samples and more specifically, their shape, size and orientation. The images were recorded using a Bruker AXS Nanostar.
Because of the rather wide size-distribution and irregular spatial distribution of the clusters results were not very conclusive and viable fits concerning the shape of the agglomerates could not be achieved. The best results were obtained by using strongly elongated rotational ellipsoids or rods capped with half-spheres to model the shape of the aggregates. This still gives a very good hint for a rough estimate of the general shape of the clusters. Figure 3.8 shows some slight preference of direction in the orientation of the clusters, note the elliptical distortion of the diffraction image. This could not be observed at higher concentrations of filler, as can be seen in Figure 3.9, where the diffraction rings appear perfectly concentric. In both images the rings appear very wide and not sharply defined, which suggests a rather large range of many different lengths and widths of the clusters. This is in reasonable agreement with atomic force microscope (AFM) pictures [3], showing rod-like hard domains of different length and width in a comparable material.

Scanning electron microscopy (SEM) images were also obtained, using a Zeiss Supra 55 VP microscope. The images selected for figures 3.10 and 3.11 are typical for all variants of the JED-composites. They clearly show that despite the quick formation of the polyurea elastomer and all efforts to disperse the nanoparticles, the filler has already in part accumulated at the bottom of the elastomer and almost disappeared from the top surface, resulting in a distinct gradient of concentration over the thickness of the PNC-film. The terms "top" and "bottom" refer to the horizontal orientation of the PNC-film as it is cast into the Petri-dish during manufacture. During the DMA-measurements the samples were oriented vertically, changing this references to "front" and "back" respectively, with stress applied parallel to the surfaces shown in 3.10 and 3.11. This means there is no gradient in the concentration of the tubes in the direction the sample is deformed during the measurements, which otherwise would have rendered the gathered data invalid. The absolute values obtained still exhibit an uncertainty which is difficult to quantify, but affects all samples consistently in the same fashion. Therefore, although the inhomogenous distribution along the thickness of the samples is disadvantageous, it was nevertheless possible to compare the samples to each other in a meaningful way.

3.4 Preparation of samples

The samples were received as thin circular films $\approx 100\ mm$ in diameter. From these 3 mm-wide strips were marked with a sliding caliper and cut by hand with a razorblade. These strips were then cut down to a length of $\approx 10\ mm$. This particular step does not need to be done very precisely, as the quantity actually entering into the calculation of the complex modulus is the free length of the mounted sample. This length is very accurately defined by the fixture clamps of the DMA. The position of the clamps can be controlled with an accuracy of 1 μm. The strip of the material to be tested can be easily attached to the clamps with an extra length of $\approx 1\ mm$ at each end. The thickness of the film was measured by micrometer gauge. As the material is quite soft at room temperature, at which the measuring and cutting was done, sample dimensions are affected by the largest uncertainty of all quantities, $\pm 10\ \mu m$, amounting to $\approx 3\%$ of the sample width.

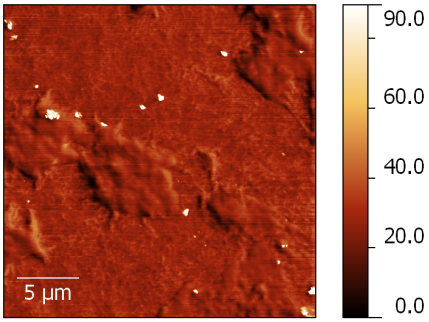

Figure 3.1: The phase image of polyurea JD-400 shows small hard islands which appear elevated from the soft matrix

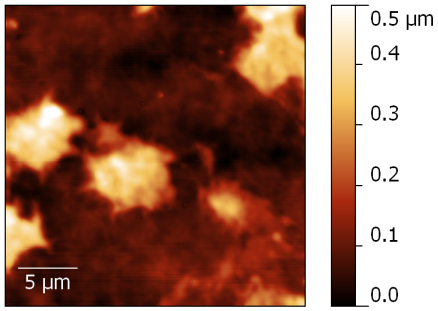

Figure 3.2: In the topographic view of polyurea JD-400 the small hard islands can be clearly seen as light spots

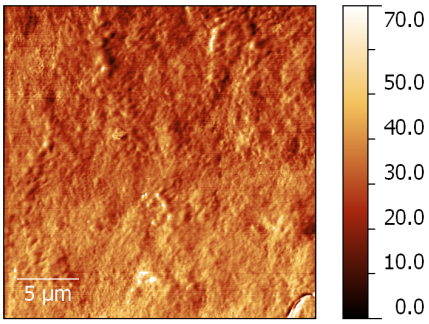

Figure 3.3: The phase image of JD-2000 is less conclusive than the one of JD-400, but the hard domains are still discernible.

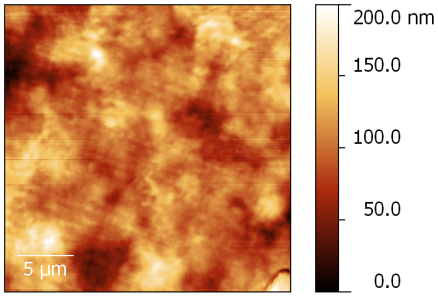

Figure 3.4: In the topographic view of polyurea JD-2000 more hard islands can be discerned, and the dark areas representing the soft matrix occupy less space compared to JD-400. Extensive areas of restricted molecular mobility are also visible, indicated by mid-tone colors.

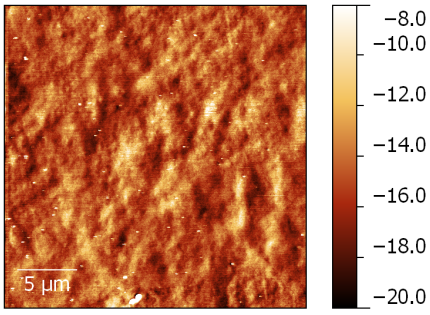

Figure 3.5: On the phase image of JD-4000 it is very difficult to recognize the difference between the soft from the hard areas.

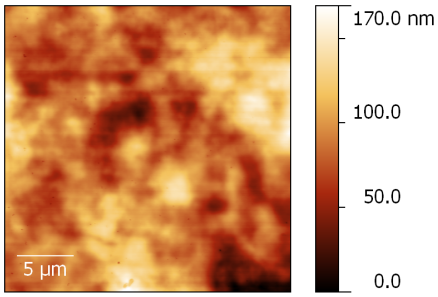

Figure 3.6: Only a few small dark spots representing the soft matrix remain in the topographic image of JD-4000.

Figure 3.7: AFM phase (left column) and topographic (right column) images of JD-400 (top row), JD-2000 (second row) and JD-4000 (bottom row)

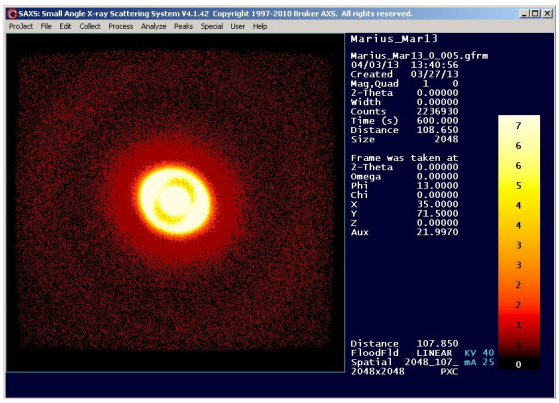

Figure 3.8: SAX-image of JED with C1 MoS_2 nanotubes, $1 \cdot 10^{-}1$ weight-% . The slightly elliptic shape suggests a direction of preference in the distribution of the nanotubes. As the rings are not sharply defined, but rather diffuse, the clusters of nanotubes have a rather wide size distribution.

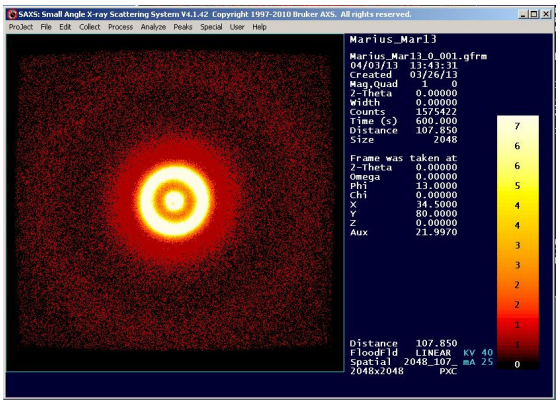

Figure 3.9: SAX-image of JED with C1 MoS_2 nanotubes, 1 weight-% . The diffraction rings appear to be perfectly concentric, leading to the conclusion that the nanotube-clusters are randomly oriented.

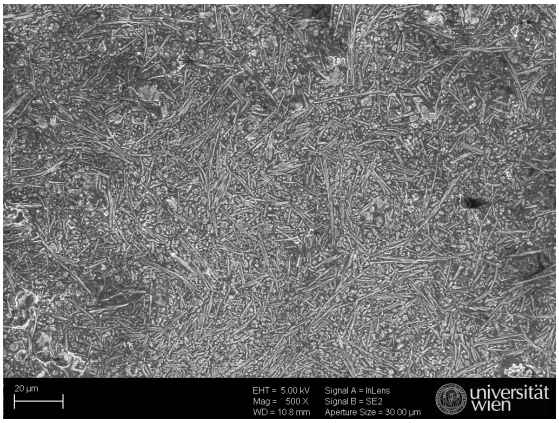

Figure 3.10: SEM-image of JED with C2 MoS_2 nanotubes, „bottom“ side with respect to the orientation during manufacture of the sample in horizontal orientation in a petri dish, showing that the nanotubes have sunk to the bottom during the polimerization process in spite of having been stirred as long as possible.

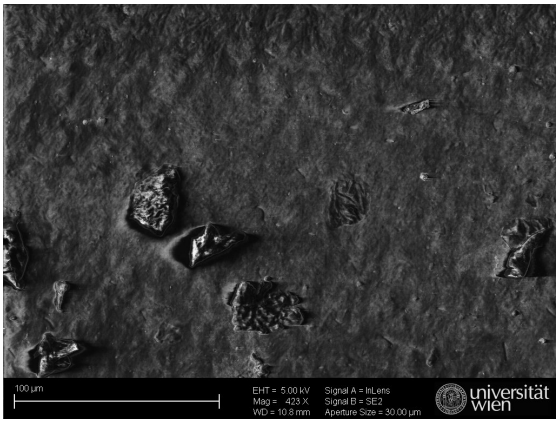

Figure 3.11: SEM-image of JED with C2 MoS_2 nanotubes, „top“ side with only very few individual nanotubes visible as most have sunk down into the sample in relation to the orientation during manufacture.

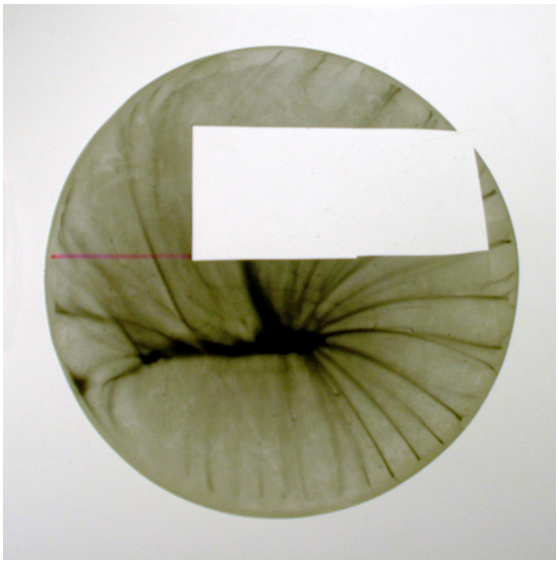

Figure 3.12: JED with C1 MoS_2 nanotubes

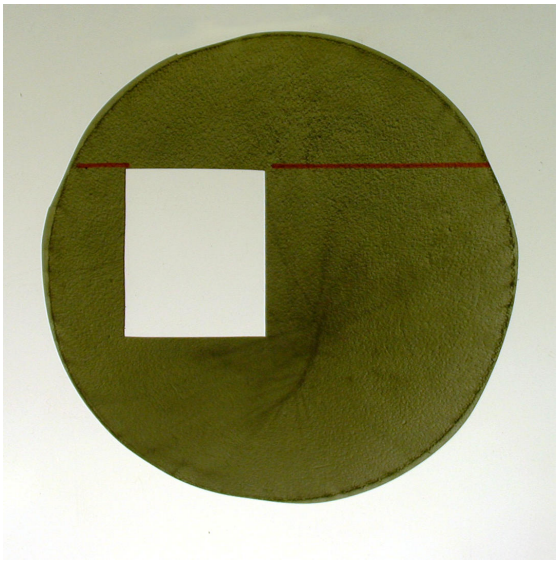

Figure 3.13: JED with C1 MoS_2 nanotubes

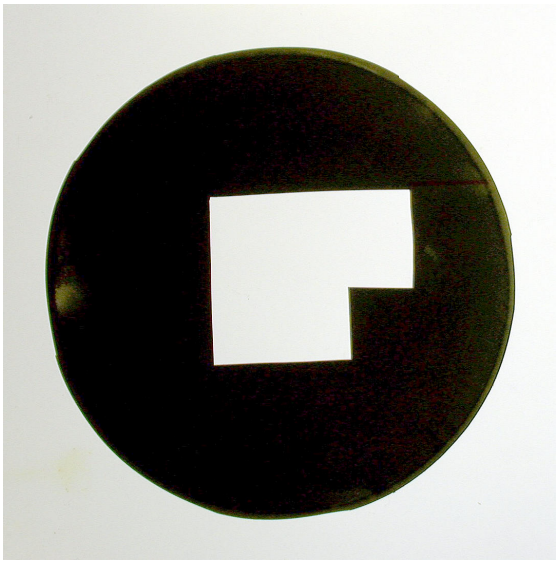

Figure 3.14: JED with C1 MoS_2 nanotubes

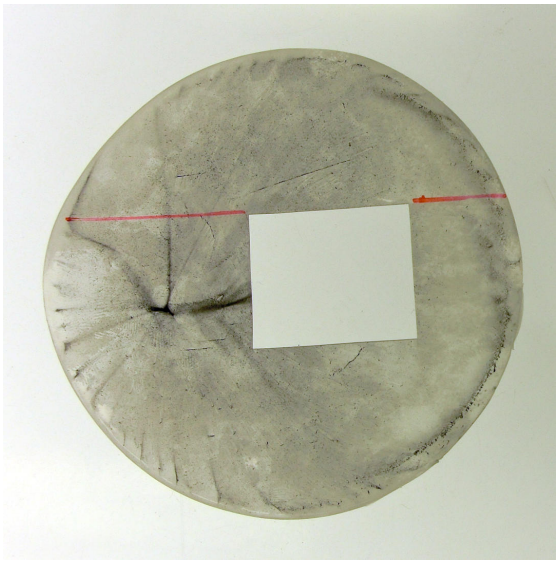

Figure 3.15: JED with C2 MoS_2 nanotubes

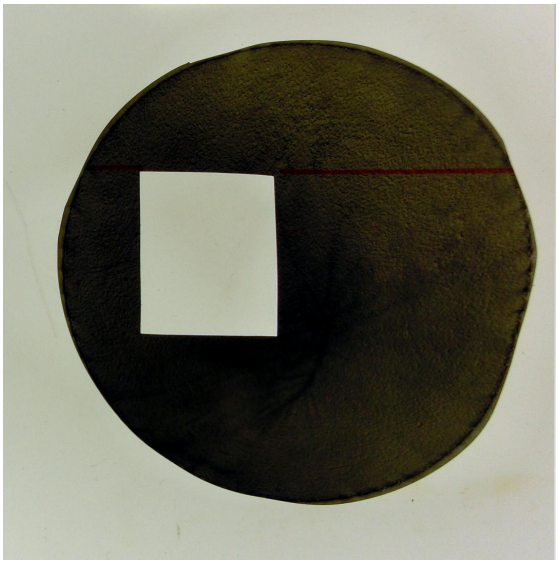

Figure 3.16: JED with C2 MoS_2 nanotubes

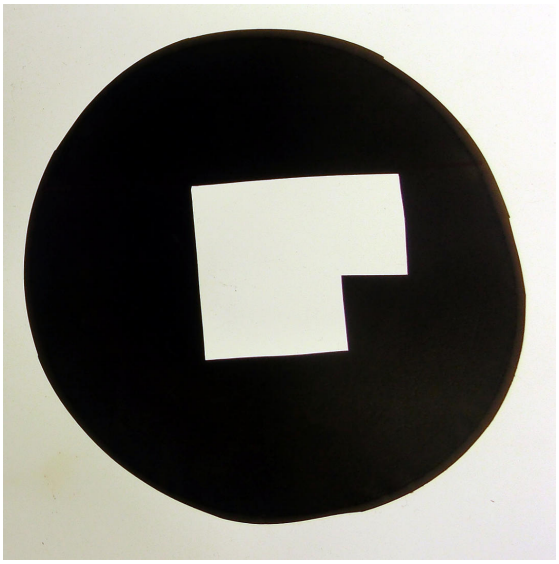

Figure 3.17: JED with C2 MoS_2 nanotubes

4 Measurements

4.1 Method: DMA

Dynamic mechanical analysis (DMA), also sometimes called dynamic thermomechanical analysis or DTMA, is a very well suited method for detecting and analysing phase transitions, and has been used for investigating the viscoelastic properties especially of polymers for some time now.
In comparison with differential scanning calorimetry (DSC), which is also widely used to measure phase transition temperatures, DMA is said to be an order of magnitude more sensitive and has the ability to detect even sidechain and bend-and-stretch movement (or β- and γ-relaxations, respectively) [10], which cannot be discerned in DSC. Also, the lack of need for a very pure reference sample with a perfectly well defined heat capacity makes it a very convenient method. DMA can only measure changes in the bulk of the sample material and cannot detect small localized effects or distinguish surficial influences.

A sinusoidal force is applied at a given frequency in addition to a static force to a piece of material and the displacement is measured. This change in position is recorded in relation to time and temperature. All other DMA data is calculated from these basic quantities.

At any given oscillation period and temperature, Hooke's Law is used to calculate the elastic modulus:

$$\sigma = E\epsilon \tag{4.1}$$

As the quantities actually measured by the DMA are not stress and strain, but force and displacement, it may be more conveniently written as:

$$F = \frac{E}{s}\Delta l \tag{4.2}$$

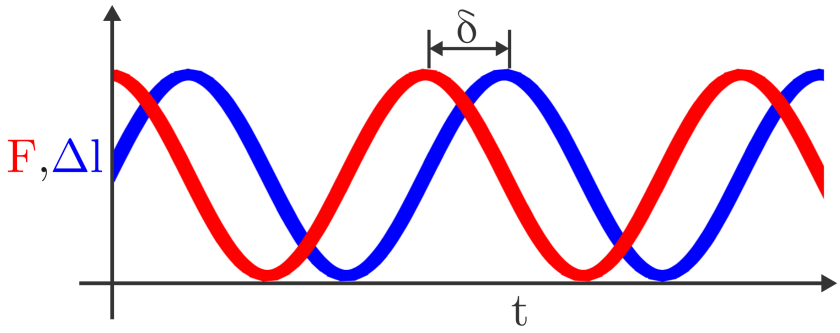

Illustration 4.1: Principle of DMA measurements. The periodically modulated force ***F*** is shown in red, the corresponding length change of the sample $\boldsymbol{\Delta l}$ in blue. δ denotes the phase shift between them. The time-axis is labeled t.

σ	stress
E	elastic modulus
ϵ	strain
F	force
s	shape factor
Δl	displacement

The shape factor s depends on the particular geometry, which is used to perform the measurements. Calculating the phase shift between force and displacement from their respective time dependencies allows to determine the complex elastic modulus E^*.

$$|E^*| = \frac{max_t(\sigma(t))}{max_t(\epsilon(t))} \tag{4.3}$$

$$E^* = E' + iE'' \tag{4.4}$$

$$E' = E^* cos(\delta)$$

$$E'' = E^* sin(\delta) \tag{4.5}$$

$$\frac{E''}{E'} = tan(\delta)$$

t	time
E^*	complex elastic modulus
δ	phase shift of force and displacement
E'	$Re[E^*] \propto$ elastic energy storage
E''	$Im[E^*] \propto$ proportional to viscous energy dissipation

In DMA, the oscillating force can be applied to the tested material in two fundamental ways: torsionally or linearly. Instruments constantly shearing the sample in one direction are commonly called rheometers and are accordingly used for testing liquids and pastes. Most modern examples though are also able to measure solid samples by applying torsional force in an oscillating manner and using appropriate fixtures, thus measuring shear modulus G^*. Instruments going by the name of dynamic mechanical analyzer typically use linear force and determine Young's modulus or E^*, but usually can also be configured to measure shear modulus G^*. This creates considerable overlap in the area of application for these types of instrument. Both are best suited for soft (meaning low modulus) solid materials, although also very hard and brittle materials can be tested if the measurement geometry is chosen accordingly and samples can be obtained or prepared in an advantageous shape, e.g. a long rod or bar for extension mode, a thin film for shear mode or a long, thin bar for cantilever or 3-point-bending mode.
There are several options concerning measurement geometry and sample shape with using DMA.

The particular geometry best suited for measuring thin films is extension of a strip of material. The associated shape factor thus becomes very simple, reading $\frac{xy}{z}$, x, y, z being the width, depth and length of the sample, stress, strain as well as l_0 and Δl parallel to the z-axis. The longer the sample is in z-direction, the better the resolution regarding strain. The usual method for calculating strain, as employed by software of the used instruments, is Cauchy- or engineering strain:

$$\epsilon = \frac{\Delta l}{l_0} \tag{4.6}$$

l_0	length of the sample at rest without any mechanical stress applied
Δl	maximum length change

In theory, E^* should be identical to Young's modulus, but in reality there often is a considerable mismatch. This stems from the fact that Young's modulus is obtained from the slope of the linear region of a stress-strain curve at a given temperature, the sample bearing static load. The data used to calculate the complex modulus E^* as evaluated by DMA would represent a single point on such a σ vs ϵ curve.

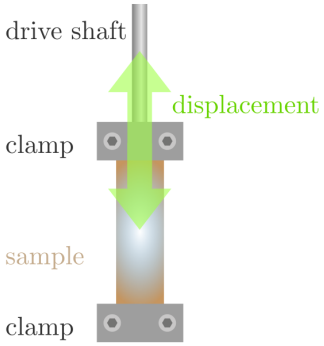

Illustration 4.2: Tension mode

The drawback of extension geometry is, if the sample starts to melt and flow at a certain temperature, signal noise increases and quickly renders the recorded data unusable in this temperature region. This is the case for the polyurea-elastomers examined in this work. The situation can be remedied by switching to a shear setup, measuring the complex shear modulus G^*. The corresponding shape factor for this geometry is $\frac{2zy}{x}$, force and therefor also stress being applied along the y-axis. To employ this method with DMA, two identical samples are needed, as shown in illustration 4.3.

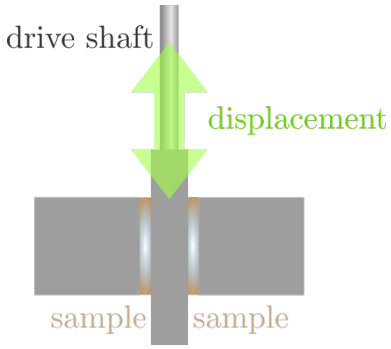

Illustration 4.3: Shear mode. Two identical samples are needed for this setup.

In the case of an isotropic material, the shear modulus G^* can be reconverted to modulus E^* and vice versa using the following relation: $E^* = \frac{2G^*}{1-\nu}$ For the data presented here, this means the shear modulus is equal to half of the value of E^*, assuming Poisson's ratio ν to be as close to zero to be of no consequence. As the DMA operates in the linear viscoelastic region of the material and the strain amplitudes are kept at least 3 orders of magnitude below sample dimensions, no necking of the sample is expected and any influence on the width and depth of the sample described by Poisson's ratio $\nu = -\frac{d\epsilon_x}{d\epsilon_z}$ is negligible. This has to be kept in mind because DMA is not able to detect any lateral contraction of the sample and the data would just reflect a virtually lowered value of the modulus, as the applied force would affect a smaller cross-sectional area. Taking care that the whole measurement

is as a matter of fact performed within the linear viscoelstic region of the material and checking sample dimensions afterwards usually ascertains this simplification concerning ν to be valid.

A typical representation of a DMA measurement on a polymer sample over the temperature range where the glass transition occurs is shown in figure 4.1. The real part of E' starts out at a relatively high value below the glass transition temperature T_g, with the sample in the so called glassy state. Close to the transition temperature E' starts to drop and the sample exhibits a leatherlike behaviour. After the glass transition E' settles at a value up to several orders of magnitude lower than in the glassy state. This region is called the rubbery plateau. In the glassy state at temperatures below T_g the $tan\ \delta$, also called damping, is small, rising to a distinctive peak at the transition temperature, and dropping down again afterwards. On the rubbery plateau the $tan\ \delta$ stays at a more or less constant value. Typically the damping in the rubbery state is higher than in the glassy state. There exist several different ways to determine the glass transition temperature T_g from data collected by DMA. The particular method employed here is using the temperature value at the apex of the peak in $tan\ \delta$, which is well established in literature [10].

4.2 Instrument: Perkin Elmer Diamond DMA

The two most common methods in measuring displacement used by DMA are optical and electrical. In the Diamond DMA, position is detected via linear voltage differential transformer (LVDT), marking it to be of the latter kind. The acronym is also sometimes rendered in full as linear vertical displacement transducer, but it nevertheless refers to the same kind of device.
Specifications of the instrument state a temperature range of -150 to $600°C$ with the available accessories. The lowest temperature consistently achieved by the particular DMA used was $-138°C$.

The instrument had to be modified for cooling by liquid nitrogen to achieve suitable temperature stability and operational duration for temperature scans with low ($< 5K/min$) heating rates in the range from the onset of the glass transition to around $100C°$. Specifically, the insulated hose

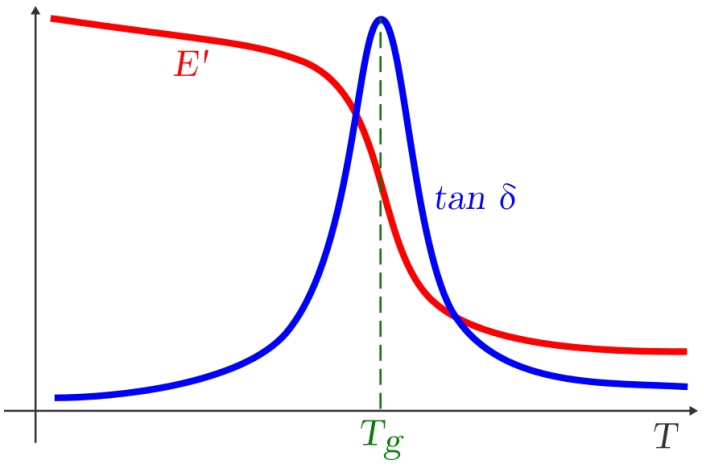

Figure 4.1: Typical representation of a glass transition measured with DMA. The elastic contribution E' to the complex modus, shown in **red**, changes very little until the glass transition temperature is approached, when it drops drastically, possibly severeal orders of magnitude. The damping $tan(\delta)$, shown in **blue**, which is defined as the ratio of the viscous contribution E" to E', exhibits a pronounced peak in the same temperature region as the drop in E' occurs. The dashed line marks the definition of the glass transition temperature $\boldsymbol{T}_g$ used in this work.

connecting the furnace to the dewar was removed and the temperature controller connected to the valve on the dewar was switched off. The connecting piece of the furnace was directly attached to an open-topped vessel made from expanded polystyrene, effectively making the former and the latter communicating vessels. The level at which the surface of a liquid filled into this assembly would touch the lowest metal parts of the sample fixtures inside the closed up furnace during a measurement was marked on the polystyrene. A styrofoam lid was cut to cover the opening. In this way the furnace could be partially flooded with liquid nitrogen without any danger of immersing the sample or the moving upper part of the fixture connecting to the LVDT (see 4.2). the directly connected liquid nitrogen reservoir has the advantage of effecting a much more static and closed enviroment compared to the turbulent gas stream used as the default method of cooling. Moreover, in this way the sample is not only cooled by the nitrogen gas evaporating from the liquid directly below it, but by thermal contact to metal parts all around it, which in turn directly touch the liquid nitrogen reservoir inside the furnace. To keep the system at a constant temperature, it is only necessary to monitor the liquid level in the polystyrene vessel and refill it to the level corresponding to the

Figure 4.2: Unmodified Perkin Elmer Diamond DMA. An insulated hose connects the liquid nitrogen dewar to the instrument's furnace.

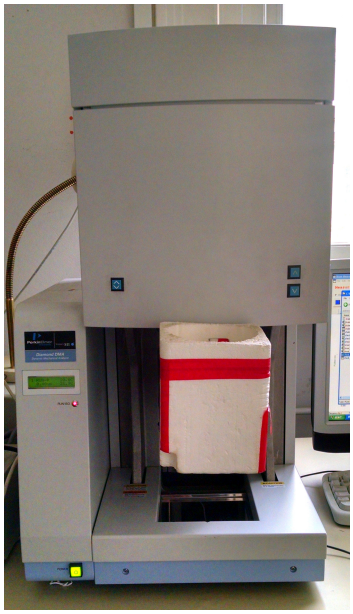

Figure 4.3: Modified Perkin Elmer Diamond DMA. The insulated liquid nitrogen reservoir is mounted directly on the furnace. The top covering of the reservoir was removed and is not shown in the picture.

desired temperature, which can easily be done without opening the furnace chamber or causing any noticeable disturbance in the measurement. A possible drawback of this configuration consisted in the loss of direct temperature control and a steady heating rate. A previous measurement in the original setup with full temperature control and heating rates of $2K/min$, which turned out to be extremely wasteful concerning nitrogen usage, showed no noticeable difference in the recorded viscoelastic data to a test-run after the modifications were made. This suggests that, even at the highest heating rate, the samples were thin enough with an adequately large surface as to be sufficiently near to thermal equilibrium with the surroundings during the whole run.

The temperature scan with the adapted instrument was effected in such a way that the furnace chamber was rapidly cooled down with liquid nitrogen, kept at nitrogen boiling point for at least 30 min and then allowed to heat up by thermal conduction from the surroundings through the furnace insulation. At $0°C$ the resistance heater kicked in and supplied a more steady rate up to the upper temperature limit of the measurement. Heating rates with the fluid bath setup ranged from $\approx 0,2$ to $3,2K/min$. Liquid nitrogen consumption was cut down from $50l$ to $2l$ per measurement because of the change in configuration.

5 Results and discussion

5.1 Polyurea nanocomposites with nanowires and nanotubes

The experiments' performed on the first set of samples (see 8.1) main goal was to compare the pure sample to PNCs consisting of the same polymer but filled with particles of different geometries [26], although the used filler materials are somewhat similar chemically. The particular polyurea elastomer used was Jeffamine JD-2000. Two different composites containing MoS_2 nanotubes and $Mo_6S_2I_8$ nanowires, as well as a batch of pure elastomer to be used as a reference were made. The DMA measurements show a noticeable upshift in the glass transition temperature, which is larger for the nanotubes than for the nanowires. The filler materials also cause a reinforcement of the real part E' of the elastc modulus of up to 15%.

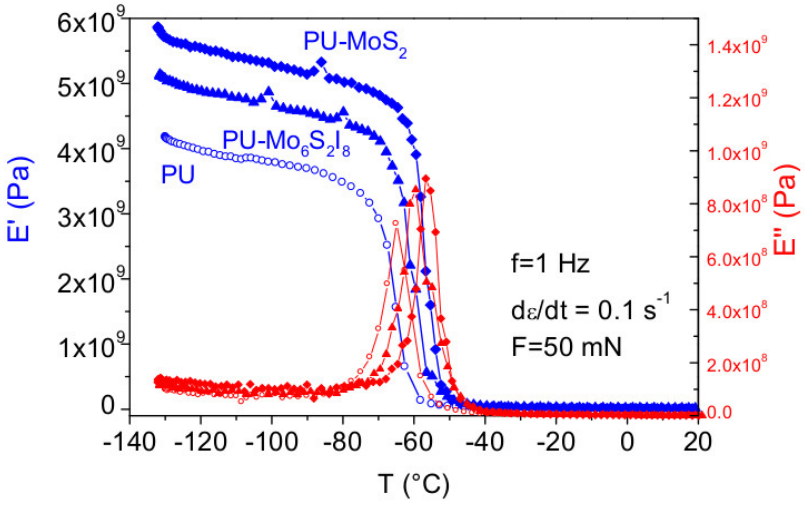

Figure 5.1: Real (E') and imaginary (E'') part of the complex Young's modulus for the pure polyurea elastomer (PU) and the two nanocomposites (PU-MoS_2 and PU-$Mo_6S_2I_8$).

Material	T_g [°C]	ΔT_g [°C]
PU	-65	–
$PU - Mo_6S_2I_8$	-60	$+5$
$PU - MoS_2$	-56.5	$+9$

Table 5.1: T_g shift in polyurea PNCs

Depending on the type of interaction between matrix and filler, the glass transition temperature T_g can either increase or decrease compared to the pure material [27]. For the repulsive case, T_g shifts to a lower temperature, if the matrix interacts attractively with the particles, the glass transition occurs at a higher temperature T_g. Therefore, the materials in table 5.1 are clearly characterized to be of the latter kind.

Furthermore, a second peak in the *tan* δ curve has been observed (figure 5.2). This occurs not only in the PNCs, but also in the pure reference material without the presence of nanoparticles. The additional peak can be attributed to regions of restricted mobility [11] near the hard nanodomains in polyurea already described in section 3.1. The peak in *tan* δ representing the bulk transition at T_{g1} is denoted α, and the one related to the glass transition near the hard domains at T_{g2} as α'.

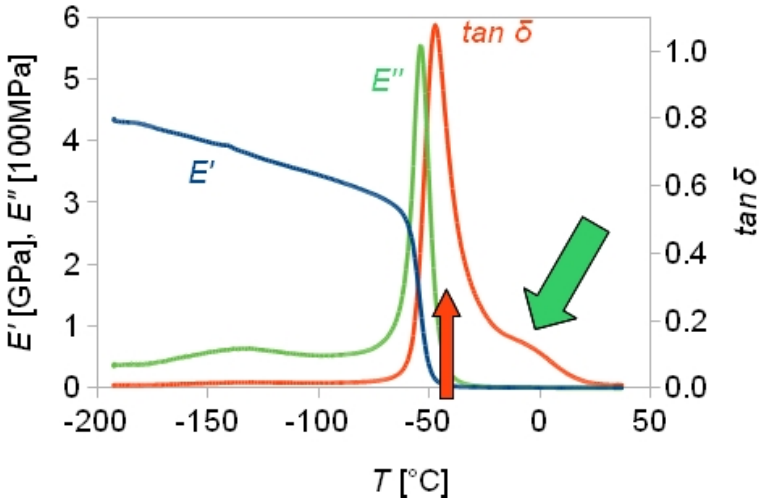

Figure 5.2: Second *tan* δ-peak in polyurea JD-2000

The so called EHM-model [12] states that a second glass transition α' starts to appear when the distance between the hard nanodomains is smaller than around $5 - 10\,nm$, which corresponds to the approximate size of the dynamically correlated regions in glass forming polymers near T_g [13]. If this is the case, these regions can undergo their own glass transition, at a higher temperature than the soft matrix. This is in good agreement with data available from literature, where the distance was

measured to be $d = 5.2\ nm$ [24, 23, 22]. The relationship between the size of the correlated regions and the glass transition temperature is explored in more detail in section 5.3.

5.2 Comparison of different polyurea nanocomposites

The focus of the second series of measurements was to investigate the influence of the loading percentage and the size of particles with the same basic shape and chemistry. To achive this, further experiments were conducted on JD-2000 PNCs containing ≈ 1 weight-% MoS_2 nanotubes as well as new samples. These PNCs were chosen based on the knowledge gained through previous results with JD-2000/MoS_2. Two kinds of well-characterized nanotubes labeled $C1$ and $C2$ were chosen as a filler materials, described in a more detailed fashion in table 3.3. This decision was based on the fact that tubes showed a stronger influence on the complex elastic modulus E^* than wires. Though both kinds of nanotubes share a lot of characteristics, e.g. basic shape and chemical composition, they are very different in their average length and diameter. $C1$ tubes are much thinner and shorter than the $C2$ kind. The reason for this choice of filler material was to maximize the effect the size of the particles has on the properties of the PNC. Polyurea elastomer JED-2003 served as a host matrix for both types of nanotubes. JED-2003 possesses an almost identical segmental length l_c and average molecular weight $\overline{M}_c$ compared to JD-2000, which results in a more or less identical volume fraction $\Phi_x = 0.12$ of hard domains. Using these materials, two sets of PNCs with three different loading percentages were manufactured as described in sections 3.3 and 3.3.2.

The DMA measurements were performed on the samples as received without any prior treatment. The insets in figures 5.3 and 5.5 show a distinctive stepped decrease in the real part E' of the complex elastic modulus caused by the desintegration of the network formed by hydrogen bonds. A distinctive influence of the MoS_2 nanotubes on the temperature at which the hydrogen bonds are removed is visible in both kinds of composites. For JED-2003 (figure 5.5) this is already noticeable at a typical scale of the graph showing the whole measurement. For JD-2000 (figure 5.3) it only becomes apparent by a closer look at the interval of E' in question. A more detailed view of this is shown in the insets of both figures. Repeating the experiments with the same samples and also fresh samples annealed at $80°C$ for two hours beforehand showed no significant effect on T_g. Moreover, the stepped decrease in E' vanishes with the values smoothly levelling out towards the minimum before the melting point of the sample is reached.

The temperature scans were also performed at multiple frequencies, but the influence on the complex elastic modulus E^* in the range accessible by DMA turns out to be only slight, for more details see

section 8.2.

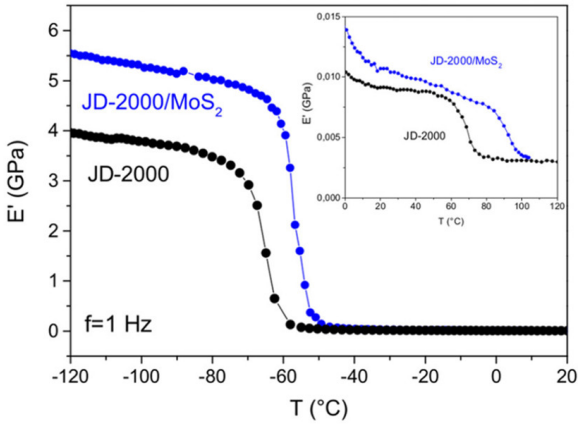

Figure 5.3: E' of PNC JD-2000/MoS_2

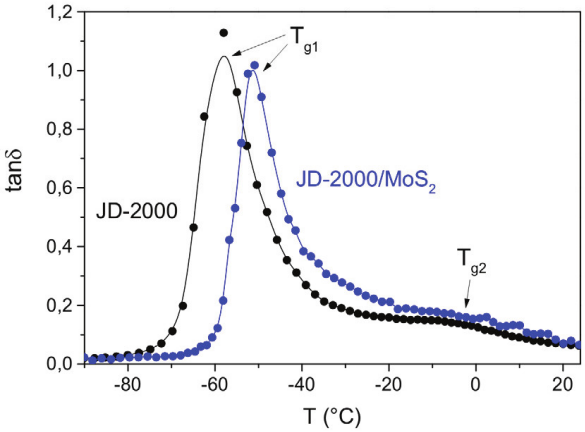

Figure 5.4: $tan\ \delta$ of PNC JD-2000/MoS_2

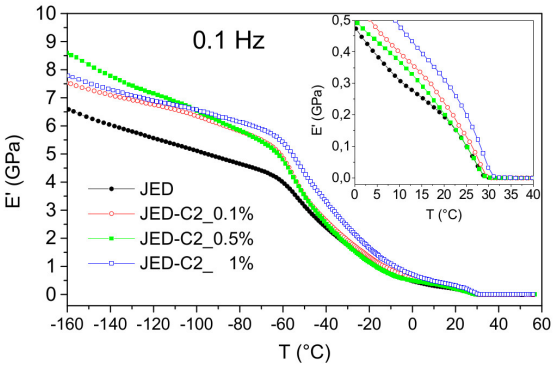

Figure 5.5: E' of PNC JED-2003/MoS_2 The inset shows the drop in the elastic modulus E' due to the removal of the hydrogen bonds.

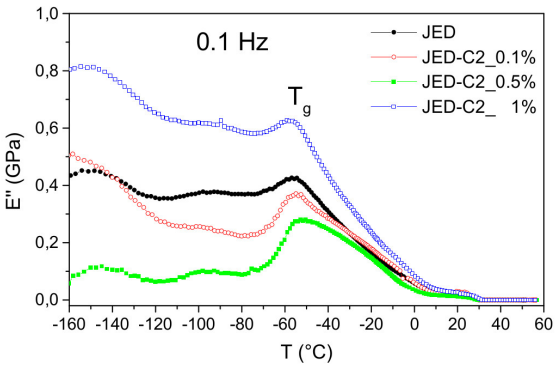

Figure 5.6: E'' of PNC JED-2003/MoS_2

5.3 Hard and soft domains in polyurea elastomers

The third set of experiments main concern was to explore the influence of the average chain length of the polymer on the size and distance of the hard domains in polyurea, which in turn has an effect on the glass-transition in those materials [28]. To accomplish this, the Jeffamines JD-400, 2000 and 4000 were prepared, the properties of which are summarized in table 3.2. Because of the long backbone chains in JD-4000 the hard domains are more widely dispersed and the regions of restricted mobility around them farther apart than in the other two polyurea elastomers. The α'-peak in $tan\ \delta$ related to the area around the hard domains at T_{g2} is relatively small in comparison to the α-peak at T_{g1}, and is seperated from T_{g1} by a relatively large temperature interval. This means the material mostly consists of a soft matrix and is only moderately influnced by the presence of the hard clusters, which only occupy a small fraction of the total volume. The results for JD-4000 and JD-2000 show very similar behaviour, but the in comparison to JD-4000 and JD-2000 much shorter polymer chains in JD-400 result in drastically larger and more interconnected hard domains, considerably slowing down the dynamics throughout the material. This causes the first glass transition at temperature $T_{g1} < T_{g2}$ to merge into T_{g2}, making it impossible to discern the two transitions directly. Only a single peak is recognizable at any scale of the graph.

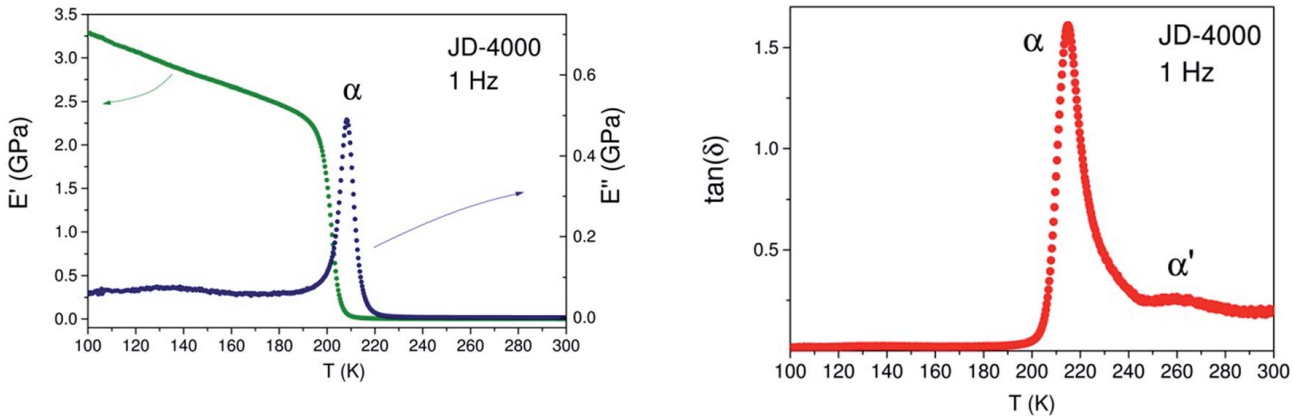

Figure 5.7: E', E'' and $tan\ \delta$ of JD-4000

In order to describe the broad distribution of relaxation times for the glass transitions in polyurea, the Havriliak-Negami model presents a suitable choice to fit the data. The reason for that is the models ability to account for the breadth and asymmetry of the relaxation curve. One instance of the model is applied to each of the transitions and they are then combined in relation to a common high frequency limit, as shown in equation 5.1.

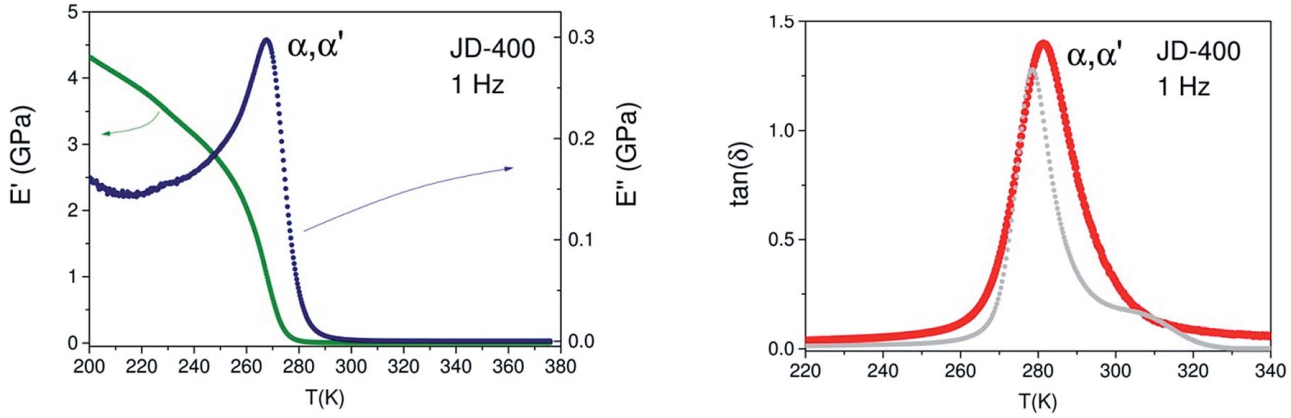

Figure 5.8: ***E′***, ***E″*** and ***tan(δ)*** of JD-400. The grey discs show the ***tan(δ)*** of **JD-2000**, shifted with respect to temperature, to illustrate the relative breadth of the ***tan(δ)*** of **JD-400**.

$$E^*(\omega) = E^\infty - \sum_{j=1}^{2} \frac{\Delta E_j}{1 + (i\omega\tau_j)^{\alpha_j})^{\beta_j}} \tag{5.1}$$

$j = 1, 2$	indices representing the α and α' transition
τ_j	relaxation times
ω	mechanical excitation frequency
α_j, β_j	exponents related to the broadness and asymmetry of the peak
E_{sj}	static elastic modulus for the corresponding $j = 1, 2$ process
E_∞	elastic Modulus at the high frequency limit
$\Delta E_1 = E_\infty - E_{s1}$	
$\Delta E_2 = E_{s1} - E_{s2}$	

The relaxation times τ_j are dependent on temperature, which can be expressed by using a Vogel-Fulcher relationship:

$$\tau_j = \tau_{0j}\, \mathrm{e}^{\frac{B_j}{T - T_{0j}}} \tag{5.2}$$

τ_j	relaxation time
τ_{0j}	attempt rate
B_j	activation energies
T_{0j}	Vogel-Fulcher-temperatures of the α and α' relaxation

This procedure allowed to accurately describe the measured data. Although JD-400 seems to display just a single peak in $tan\ \delta$, it proved impossible to achieve a viable fit result by using just a single

Havriliak-Negami term, i.e. fitting a single transition. Moreover, there remained the problem of separating the respective contributions of the two relaxation processes. Varying the static moduli E_{sj} resulted in fits with χ^2 values ranging from 0.28 to 0.39. Albeit T_{g1} could be determined very accurately, the resulting uncertainty for T_{g1} is comparatively large, amounting to $\pm 10.6\ K$. A table listing the fit parameters can be found in table 5.3 and in section 8.3.

The temperature dependence of the volume of the correlated regions was calculated using the approach described in [29], resulting in the following relationship:

$$N_{corr,4}(T) = \frac{k_B N_A}{\Delta C_p \overline{M}_c} T^2 \{max_\omega(\frac{1}{E_\infty}\frac{dE'(\omega,T)}{dT})\}^2 \tag{5.3}$$

$N_{corr,4}$	number of correlated units
k_b	Boltzmann constant
N_a	Avogadro constant
$\overline{M}_c$	segmental molecular weight
$\Delta C_p\ [Jg^{-1}K^{-1}]$	specific heat anomaly at T_g
T	temperature
ω	excitation frequency
E'	real part of the complex elastic modulus E^*

	JD-4000	JD-2000	JD-400
$T_{01}[K]$	156.6	153.8	221.5
α_1	0.78	0.7	0.66
β_1	0.48	0.39	0.001
$\tau_{01}[s]$	10^{-15}	10^{-15}	10^{-15}
$B_1[K]$	1755	1755	1755.2
$\Delta E_1/E_\infty$	0.99	0.97	0.7
$T_{02}[K]$	206.3	92	171.8
α_2	0.16	0.57	0.61
β_2	0.36	0.098	0.17
$\tau_{02}[s]$	10^{-13}	10^{-13}	10^{-13}
$B_2[K]$	565.7	4010	1388
$\Delta E_2/E_\infty$	0.009	0.026	0.299

Table 5.2: Havriliak-Negami fit parameters

A more exhaustive breakdown of the intermediary steps is given in section 8.3. In order to estimate the actual spatial correlations of hard and soft domains in polyurea two different approaches were used, both assuming that the dynamic correlations are string-like. First, the number of correlated soft segments $N_{corr,4}(T)$ was calculated with formula 5.3 to determine the correlated volume $V_{corr}(T) = N_{corr,4}(T)/\rho$. The partial derivative of the real part of the elastic modulus $dE'(\omega, T)/dT$ was calculated from fits to experimental data.

One approach estimates the correlation length ξ using cylindrical strings with the approximate thickness of a polyurea-molecule, $d = 2r \approx 0.56\ nm$, consequently arriving at:

$$\xi(T) = \frac{V_{corr}(T)}{r^2\pi} \tag{5.4}$$

Alternatively, $\xi(t)$ was calculated by multiplying the number of correlated segments $N_{corr,4}(T)$, equation 5.3, with the segmental length of polymer, listed in section 3.1.1.

$$\xi(T) = N_{corr,4}(T) \cdot l_c \tag{5.5}$$

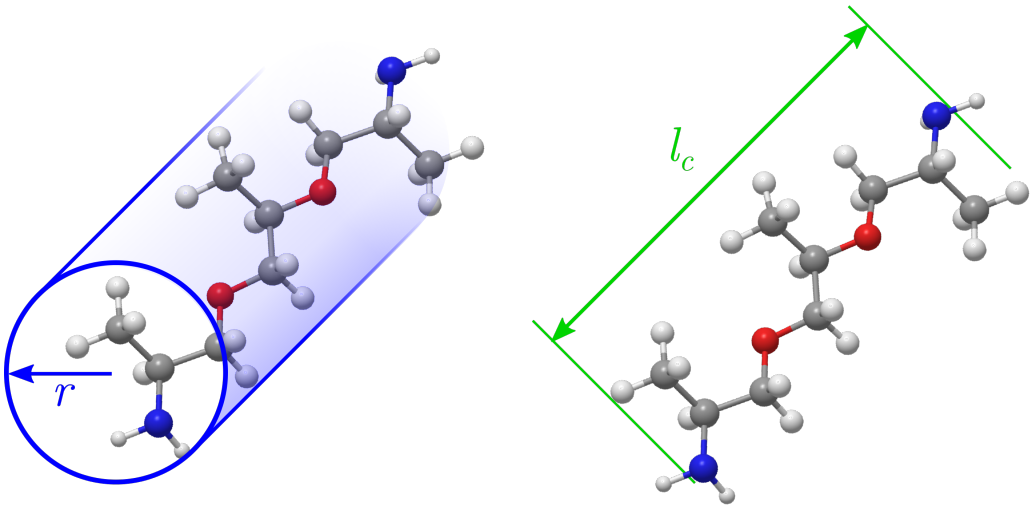

Illustration 5.1: 2 methods for calculating the correlation length in polyurea based on DMA-data

Both methods yield almost identical results, arriving at a correlation length of $\xi(T_{g1}) \approx 43\ nm$. Figure 5.9 shows the temperature dependencies of the dynamically correlated regions near the α-glass transition in JD-2000. Full circles are calculated with equation 5.3, with values for $E'(\omega, T)$ calculated from experimental data. The red disks denote $\boldsymbol{V_{corr} = N_{corr,4}/\rho}$, blue disks represent $\boldsymbol{\xi = V_{corr}/r^2\pi}$ and green disks show $\boldsymbol{\xi = N_{corr,4} \cdot l_c}$. Full lines are fits using parameters listed in section 8.3 and

equation 5.6.

$$V_{corr}(T) = \frac{N_{corr,4}(T)}{\rho} \propto \frac{k_B}{\rho \Delta C_p} T^2 \frac{B^2}{(T - T_0)^4} \tag{5.6}$$

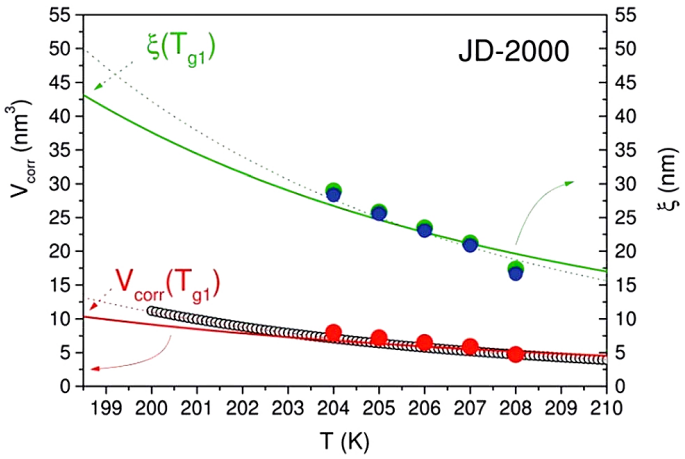

Figure 5.9: Temperature dependencies of dynamically correlated regions

This leads to the conclusion that the dynamical correlations between the polymer chains increase with decreasing temperature for the α-process related to T_{g1}. It can be argued that the α'-process connected with T_{g2}, which has only marginal influence on the real part E' of the complex elastic modulus compared to the α-transition, is related to a freezing of motion in only a small volume of restricted mobility directly around the hard nanodomains. The restriction is the result of the direct chemical attachment of the polymer chains to the hard domains, as shown in section 3.1.1. The estimation of this volume is explained in more detail in section 8.3 and arrive at a value of $\approx 30\ nm^3$. This is significantly larger than the correlation volume V_{corr} in figure 5.9, thus implying that the volume influenced by the hard domains is sufficiently large to show its own glass transition. This holds true for all three elastomers JD-400, JD-2000 and JD-4000. Plotting the volume fractions of the hard domains, see table 3.2, against the respective glass transition temperatures T_{g1} and T_{g2} and fitting the data with equation 5.7 [30], as shown in figure 5.10, a critical volume fraction of $\Phi_x^c = 0.19$ is observed, where the two glass transitions reverse order. As this value matches the percolation threshold of randomly oriented overlapping ellipsoids [31], this suggests that around a critical volume-fraction $\Phi_x^c = 0.19$ the topology of the system changes completely. The system consists of a soft matrix containing hard domains, but below this threshold the percolating hard domains form a rigid matrix with soft inclusions.

$$T_{g1} = T_{g1}^{0} + k\frac{\Phi_x}{1-\Phi_x} \tag{5.7}$$

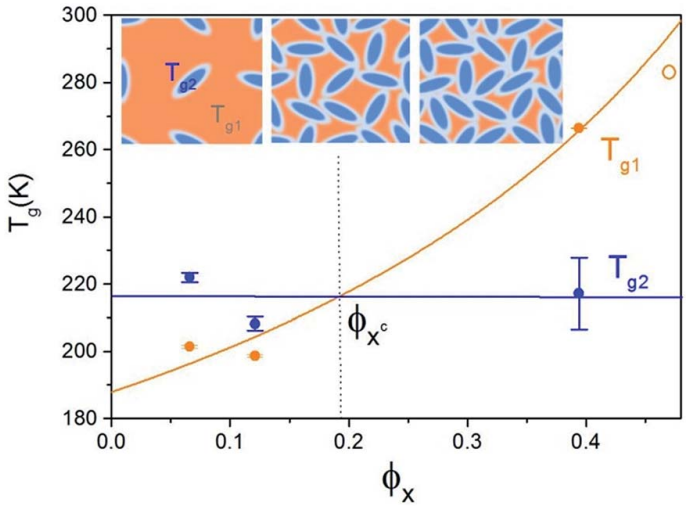

Figure 5.10: Glass transition temperatures dependent on the volume fraction of hard domains. Insets show 2-dimensional comics of the configurations of the hard domains and their shells of restricted mobility inside the soft matrix. The first inset on the left shows widely dispersed hard domains without any contact of the slowed down regions around it, corresponding to the situation in JD-2000 and JD-4000. The inset in the middle gives an impression of how the hard domains start to continuously interconnect over long distances, and the third inset on the right shows densely interlocked hard domains, as they can be found in JD-400. The actual situation is more complex because the domains are not perfectly eliptically shaped. They are also not of precisely the same size. Moreover, the real arrangement of the domains is naturally 3-dimensional.

The strong increase in T_g with increasing Φ_x can be explained by arguments pertaining to their physical origin. As the size of the correlated regions increases for the temperature T approaching the glass transition at T_{g1}, the surface induced slowing down of dynamics will start to affect polymer chains farther away from the surface of the hard domains. Since the approximate correlation length at the glass transition temperature $\xi(T_{g1})$ is bigger than the average distance between the hard domains, the soft domains are drastically impeded in their mobility, accounting for the increased glass transition temperature T_{g1}.

6 Summary and conclusions

The addition of $Mo_6S_2I_8$ nanowires and MoS_2 nanotubes to polyurea to form a PNC causes a noticeable increase in the real part E' of the complex elastic modulus. $Mo_6S_2I_8$ and MoS_2 interact attractively with the polyurea matrix, as the glass transition temperature T_g of the PNCs is also shown to increase, compared to a reference sample without nanoparticles. The influence of the tubes is more pronounced than that of the wires, probably due to the larger interfacial area. Focusing on the influence of different MoS_2-nanotubes at various loading percentages, it turns out they are most probably attached to the polyurea-matrix by hydrogen bonding. DMA data show that the effects attributed to the presence of the nanotubes vanishes after removing the hydrogen bonds by annealing the samples. This is in good agreement with theoretical studies by computer simulations [32]. As polyurea-elastomers can exhibit two glass transition temperatures T_{g1} and T_{g1} even without the addition of nanoparticles, it can be described as an intrinsic nanocomposite. Polyurea is phase-separated into soft and hard domains, the size of which can be controlled during manufacture. Depending on the volume fraction Φ_x of hard domains, polyurea behaves as a soft matrix interdispersed by hard domains. If a critical value Φ_x^c for the hard domains is exceeded, the properties change to those of a rigid matrix of percolated hard domains with soft inclusions, comparable to glass forming liquids in nanoporous materials [14, 33, 15, 1]. This picture is complemented by a strong reinforcement of E' measured in $JD-400$ samples when compared to the other two species of polyurea-elastomers. The former contains a larger, the latter a smaller fraction of hard domains than denoted by this calculated critical threshold.

The findings in this work are mostly based on a more or less macroscopic and phenomenological approach and further steps should be taken to complement them by computer simulations and micro- to nanoscale measurements. Modelling the hard nanodomains with rotational ellipsoids of a single size works well to describe the principle of the processes investigated in justifiable agreement with the experimental results. Nevertheless inital AFM, SAXS and SEM measurements already show that the precise situation is more heterogenous and complicated on a microscale than any simplified geometrical model. The relaxation times $\tau(r,T)$ are found to be larger near the hard domains than

in the pure polymer for $r \to \infty$, but their exact spatial dependence – i.e. r dependency of τ_0, B and T_0 in the Vogel-Fulcher-equation – is completely unknown. Knowledge of these interrelations would considerably reduce the number of fitting parameters. This necessitates further study employing the above-mentioned methods.

Apart from the expanded fundamental understanding of the materials investigated, there has been also gained valuable information regarding possible applications. Based on the data presented here, it can be expected to be possible to further increase the glass transition temperature T_g and considerably extend the thermal operational range of similar polymers by increasing the packing density of the hard domains. This also would result in a drastic mechanical reinforcement with a much higher elastic modulus E'.

7 Glossary of abbreviations

AFM	atomic force microscope
DMA	dynamic mechanical analysis or analyzer
DSC	differential scanning calorimetry
DTMA	dynamic thermo-mechanical analysis or analyzer
LVDT	linear voltage differential transformer
PNC	polymer-nanocomposite
SAXS	small angle X-ray scattering
SEM	scanning electron microscopy
TMA	thermo-mechanical analysis or analyzer

8 Publications

8.1 Dynamic- and Thermo-mechanical Analysis of Inorganic Nanotubes/elastomer Composites

Sensors & Transducers Journal, Vol. 12, Special Issue, October 2011, pp. 71-79

www.sensorsportal.com

Sensors & Transducers

ISSN 1726-5479

http://www.sensorsportal.com

Dynamic- and Thermo-mechanical Analysis of Inorganic Nanotubes/elastomer Composites

[1] Armin FUITH, [1] Marius REINECKER, [2] Antoni SÁNCHEZ-FERRER, [2] Raffaele MEZZENGA, [3] Aleš MRZEL, [4] Maris KNITE, [5] Ilze AULIKA, [6] Marija DUNCE and [1] Wilfried SCHRANZ

[1] University of Vienna, Functional Materials, Boltzmanngasse 5, A-1090 Vienna, Austria
[2] ETH Zurich, Institute of Food, Nutrition & Health, Food & Soft Materials Science Group, Schmelzbergstrasse 9, LFO, E23-E29, CH-8092 Zurich, Switzerland
[3] J. Stefan Institute, Jamova 39, SI 1000 Ljubljana, Slovenia
[4] Institute of Technical Physics, Riga Technical University, Azenes Str. 14/24, LV-1048, Riga, Latvia
[5] Center for Space Human Robotics – IIT@Polito, Corso Trento 21, 10129, Turin, Italy
[6] Institute of Solid State Physics, University of Latvia, Kengaranga Str. 8, LV-1063, Riga, Latvia
E-mail: armin.fuith@univie.ac.at, marius.reinecker@univie.ac.at, wilfried.schranz@univie.ac.at, antoni.sanchez@agrl.ethz.ch, raffaele.mezzenga@agrl.ethz.ch, ales.mrzel@ijs.si, knite@latnet.lv, ilze.aulika@iit.it, mdunce@gmail.com

Received: 15 June 2011 /Accepted: 18 July 2011 /Published: 31 October 2011

Abstract: We present dynamic mechanical analysis (DMA) and thermomechanical analysis (TMA) measurements of a new type of polyurea elastomer nanocomposites based on inorganic MoS_2 nanotubes and $Mo_6S_2I_8$ nanowires. The addition of a small amount of nanoparticles (<1 wt-%) leads to an increase of the glass transition temperature T_g as compared to the pure elastomeric matrix. A second peak observed in tanδ in the pure and mixed elastomer is attributed to a second glass transition occurring in regions near the hard nanodomains of the microphase separated polyurea system. It is also found that the small amount of nanoparticles leads to an increase in the Young´s modulus of up to 15 % in the whole measured temperature range (from -130 °C to 20 °C). The thermal expansion of doped samples is considerably larger above T_g. Below T_g, this difference vanishes completely. A very similar behaviour was also found in measurements of polyisoprene/multiwall carbon nanotube (MWCNT) composites. *Copyright © 2011 IFSA.*

Keywords: Inorganic nanotubes, Polymer nanocomposites, Dynamic mechanical analysis, Thermomechanical analysis, Glass transition, Elastomer, Polyurea.

1. Introduction

Polymer nanostructured composites have gained much interest due to their potential use as flexible large size sensors with superior mechanical and/or electrical properties [1]. TMA (thermomechanical analysis) and DMA (dynamic mechanical analysis) were performed to study thermal expansion, as well as temperature and frequency dependence on the nanostructured composite materials. In this work we present recent results based on TMA and DMA measurements on the nanotubes/elastomer (MoS_2) and nanowires/elastomer ($Mo_6S_2I_8$) nanocomposites. The polyurea matrix was chosen as the reference elastomeric system in order to compare the effect due to the presence of nanoparticles in the matrix. Polyurea synthesis is similar to the one used for polyurethane, which was introduced in 1937 by Otto Bayer for replacement of natural rubber. Polyurea is an attractive material with many applications such as coatings, implants or medical devices. It forms by the rapid reaction of isocyanates (rigid molecules) with polyetheramines (flexible chains). Polyurea exhibits a phase separated structure with rigid urea domains (hard domains) embedded in a matrix of flexible polymer chains (soft domains) [2-4]. The mechanical properties of polyurea can be tuned over a broad range by varying the molecular weight of the components, the relative amount of hard and soft domains, and the loading of nanoparticles [3, 4]. In the present work, we study the influence of inorganic nanotubes (MoS_2) [5] and nanowires ($Mo_6S_2I_8$) [6] to the mechanical properties and to the glass transition temperature in the polyurea matrix. The results are compared to recent measurements on polyisoprene/multiwall carbon nanotube (MWCNT) composites [7].

2. Experimental Part

2.1. Samples Preparation

Three elastomers were synthesized: a reference elastomer (PU) without any nanoparticle, and two elastomer nanocomposites containing nanotubes (PU-MoS_2) and nanowires (PU-$Mo_6S_2I_8$). For the synthesis of the three elastomers, two solutions in acetone were prepared as described in literature [2-4]: one containing the diamino-terminated polymer, and the other the trifunctionalized crosslinker with or without nanoparticles. In order to obtain a final solid content of 15% w/v, 3.85 g of Jeffamine D-2000 (Hunstman) was dissolved in 11.1 mL of acetone, and 0.65 g of Basonat HI-100 (BASF) was dissolved in 14.5 mL of acetone. In the case of elastomers containing nanoparticles, the Basonat HI-100 was dissolved in an ultrasonicated acetone dispersion of the corresponding nanoparticles to be incorporated. The two solutions were mixed and gently stirred for 5 min, and the final solution was cast onto the glass surface of a Petri dish. One day after the samples were cast, the obtained film was allowed to dry in the atmosphere and peeled from the surface. Samples were cut from their corresponding free-standing films ($14.6 \times 5.0 \times 0.75$ mm^3). The final concentration of nanoparticles was less than 1 wt-%.

2.2. Experimental Methods

Dynamic mechanical analysis (DMA) is one of the most commonly applied methods for the determination of the mechanical properties of materials, together with thermomechanical analysis (TMA) for the determination of the thermal expansion. Materials such as polymers and polymer networks can be characterized as a function of temperature and frequency. The complex elastic compliance can be measured in a frequency range from 0.01 Hz to 100 Hz, and for temperatures between 80 K and 850 K.

The principle of the DMA technique is based on the sinusoidally modulated dynamic force $F_{dyn}e^{i\omega t}$ at a chosen amplitude and frequency when applying a static force F_{stat}. The resulting amplitude u and phase shift δ of the resulting elastic response of the sample are registered via inductive coupling with a resolution of $\Delta u \approx 10$ nm and $\Delta\delta \approx 0.1°$. The knowledge of u and δ allows determining the real and imaginary parts of a certain component of the complex elastic compliance tensor S_{ii}

$$S_{ii}' = S_{ii}\cos\delta \text{ and } S_{ii}'' = S_{ii}\sin\delta \quad (1)$$

The inverse compliances are the so-called storage ($E'=1/S_{ii}'$) and loss ($E''=1/S_{ii}''$) modulus. We employ two different kinds of DMA instruments: the Perkin Elmer DMA 7 and the Perkin Elmer Diamond DMA. Table 1 compares the specifications of both instruments as commercially available.

Table 1. Specifications of the Perkin Elmer DMA 7 and the Perkin Elmer Diamond DMA.

	DMA 7	**Diamond DMA**
F_{stat} (maximal force)	2.5 N	10 N
ΔF (resolution)	10^{-5} N	10^{-5} N
ω (frequency range)	0.01 Hz – 50 Hz	0.01 Hz – 100 Hz
T (temperature range)	90 K – 850 K	120 K – 850 K

The minimal force that can be applied in both instruments is 10^{-3} N. The force is transmitted by a rod, which is also the probe for the position of the upper end of the sample. The Perkin Elmer DMA-7 can work with quartz or steel rods and sample holders, whereas the Perkin Elmer Diamond DMA works only with steel holders, which has restricted low temperature performance. The presently used geometries are the parallel plate stress (PPS) and the tensile stress (TS) arrangements as shown in Fig. 1.

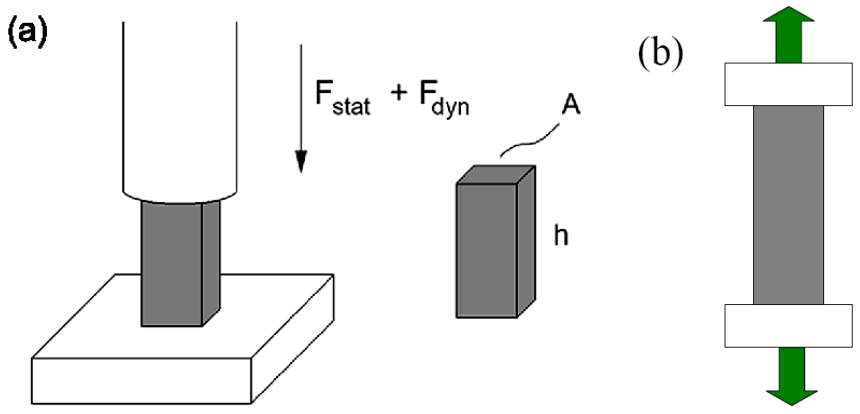

Fig. 1. Typical sample geometries for the PPS (a), and the TS (b) methods.

In PPS geometry, a force F_3 is applied in the z-direction, and the corresponding change in length Δh in the same direction is measured. This yields the Young's or elastic modulus of the sample in the elastic regime $E \equiv 1/S_{33}$. The strain ε_3 is defined as the ration between the change in length with respect to the initial length of the sample $\varepsilon_3 = \Delta h/h$, and the measured stress σ_3 as the applied force divided by the cross section of the element $\sigma_3 = F_3/A$. In the elastic region (for small deformations), both magnitudes are connected by the Young's modulus:

$$\sigma_3 = E\ \varepsilon_3 = 1/S_{33}\ \varepsilon_3 \tag{2}$$

In this way, the effective spring constant of a material $k = F_3/\Delta h = 1/S_{33}\ A/h$ is measured [8, 9].

The Perkin Elmer TMA uses a similar measuring principle as the Perkin Elmer DMA, i.e. the sample position is measured via inductive coupling at nominally zero applied force. The sample geometry is usually the same as for the PPS method (Fig. 1a). A small static force of 10^{-3} N was applied to keep good mechanical contact between the quartz or steel rod and the sample for all our TMA measurements.

3. Results

3.1. TMA Experiments

TMA experiments were carried out in order to analyze the differences in the thermal expansion of both nanocomposites with respect to the pure elastomer matrix. Fig. 2 shows the temperature dependence of the thermal expansion of the pure polyurea system (PU) and the two polyurea nanocomposites PU-MoS_2 and PU-$Mo_6S_2I_8$.

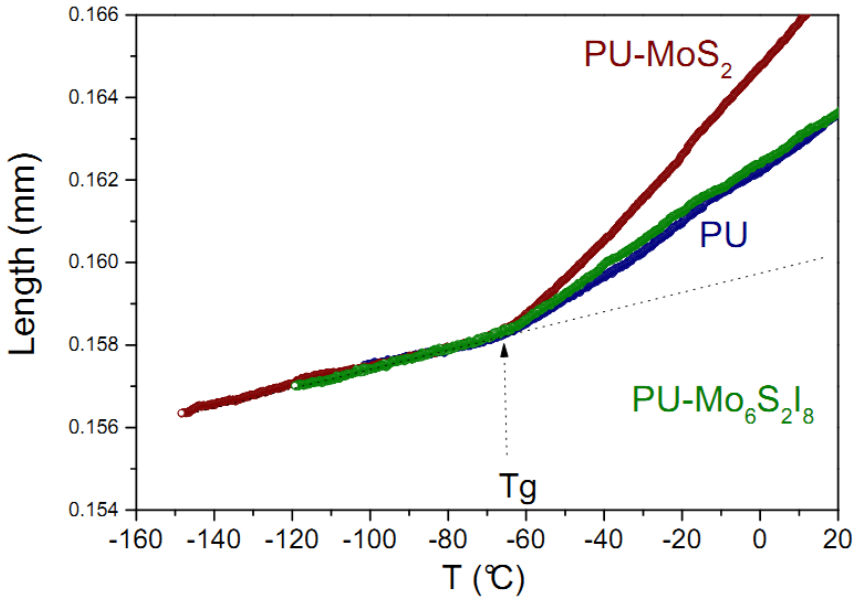

Fig. 2. Thermal expansion as function of temperature for the pure polyurea elastomer (PU), and the polyurea nanocomposites (PU-MoS_2 and PU-$Mo_6S_2I_8$). The curves are normalized to the length of the PU at -120 °C.

Above T_g, the thermal expansion of the nanocomposite PU–MoS_2 is considerably increased, whereas the thermal expansion below T_g is not affected by the presence of the nanotubes (Table 2). This behaviour is very similar to the one found in polyisoprene/multiwall carbon nanotube (MWCNT) and polyisoprene/carbon black (CB) composites as shown in Fig. 3. The nanowires containing nanocomposite (PU-$Mo_6S_2I_8$) has a similar behaviour than the pure polyurea matrix. It seems that nanowires do not affect that much the thermal properties of the polymer matrix.

Table 2. Linear thermal expansion coefficients $\alpha_L = (1/L_0)(\Delta L/\Delta T)$ of PU, PU-MoS_2 and PU-$Mo_6S_2I_8$ calculated from Fig. 2 with $L_0 = L(T = -120\ °C)$. The volume thermal expansion coefficient is $\alpha = 3\alpha_L$.

	$\alpha_L (T < T_g)$	$\alpha_L (T > T_g)$
PU, PU $Mo_6S_2I_8$	1.3 10^{-4} K^{-1}	3.9 10^{-4} K^{-1}
PU-MoS_2	1.3 10^{-4} K^{-1}	6.5 10^{-4} K^{-1}

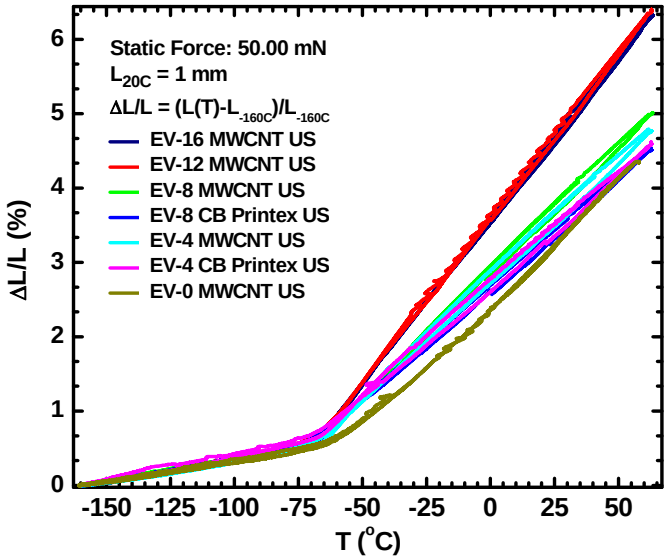

Fig. 3. Relative length $\Delta L/L$ ($\Delta L/L = L(T) - L(T = -160\ °C)/L(T = -160\ °C)$) as function of temperature for the polyisoprene/multiwall carbon nanotube (MWCNT) and polyisoprene/carbon black (CB) nanocomposites.

The thermal expansion coefficient α of polymer nanocomposites depends on many factors: the type of interaction between the nanoparticles and the polymer backbones, the shape of the nanoparticles, the volume fraction of the nanoparticles, and the thermal expansion coefficient of the nanoparticles [19]. Since some of these ingredients like the thermal expansion coefficient of MoS_2 and $Mo_6S_2I_8$ are not yet known, a quantitative analysis of the present thermal expansion data has to wait for a future work.

3.2. DMA Experiments

DMA experiments were performed for the determination of the Young's modulus and tanδ as function of temperature, as well as the glass transition temperatures upon heating the sample. Fig. 4 shows the temperature dependences of the real (E') and the imaginary (E") part of the complex Young's modulus of pure polyurea (PU) and the two polyurea nanocomposites (PU-MoS_2 and PU-$Mo_6S_2I_8$). The measurements were performed in TS mode at 1 Hz frequency, with a strain rate of $d\varepsilon/dt = 0.1\ s^{-1}$. Recently performed DMA measurements on polyurea/polyurethane systems at 1 Hz [10] show a very similar behaviour, where in addition to the $T_{g\alpha}$ around –47 °C some elastic anomalies at $T_{g\beta} = -80$ °C and $T_{g\gamma} = -141$°C were found, whose origins are not yet clear.

With the addition of nanotubes (MoS_2) and nanowires ($Mo_6S_2I_8$), a clear upwards shift in the glass transition temperature can be observed from the decays in the storage modulus (E') and the maxima in the loss modulus (E") of both nanocomposite samples. The same tendency has been also obtained by analyzing the thermal expansion data in Fig. 2. The results are summarized in Table 3. A possible origin for this increase of T_g with filler content will be discussed below.

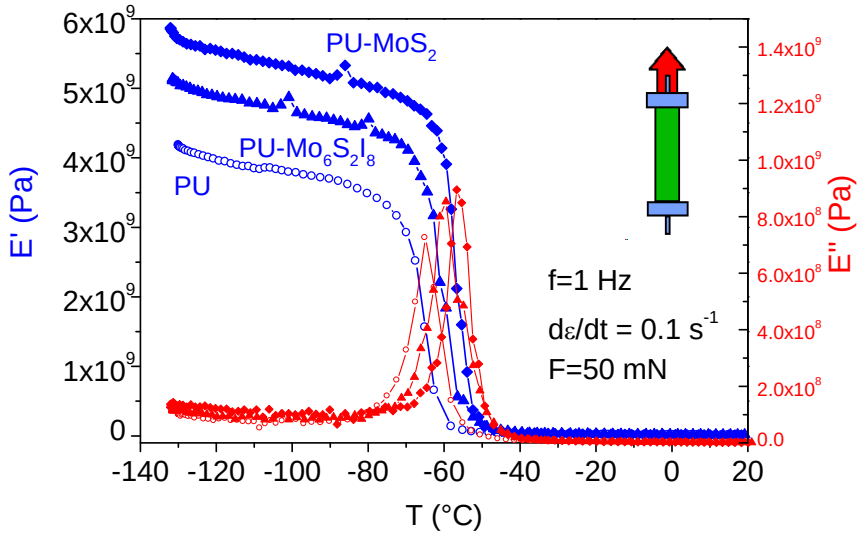

Fig. 4. Real (*E*') and imaginary (*E*") part of the complex Young's modulus for the pure polyurea elastomer (PU) and the two nanocomposites (PU-MoS_2 and PU-$Mo_6S_2I_8$).

Table 3. Glass transition temperature (T_g) and shift of the glass transition temperature (ΔT_g) for the polyurea elastomer (PU) and the two nanocomposites (PU-MoS_2 and PU-$Mo_6S_2I_8$).

	T_g (°C) (DMA)	ΔT_g (°C) (DMA)	T_g (°C) (TMA)	ΔT_g (°C) (TMA)
PU	-65		-68	
PU-$Mo_6S_2I_8$	-60	+5	-62	+6
PU-MoS_2	-56.5	+9	-60	+8

For the nanocomposite with nanotubes (PU-MoS_2), an increase in the Young's modulus up to 15 % was observed in the whole measured temperature range, while for the nanocomposite with nanowires (PU-$Mo_6S_2I_8$) was up to 12 %.

The reinforcement of a polymer nanocomposite crucially depends on the polymer-nanoparticle interfacial interaction, the modulus of the filler component, the shape of the filler as well as the relative orientation of the filler particles with respect to the applied stress [19].

Assuming a simple law of mixture we can estimate the Young´s modulus E_c of the composite as

$$E_c = E_p(1-\phi_f) + E_f\phi_f, \tag{3}$$

where E_p and E_f are the Young´s moduli of the polymer matrix and filler, respectively and ϕ_f is the volume fraction of the filler.

With $\phi_f \approx 0.01$, $E_p(-120°C) = 4$ GPa and $E_f(MoS_2) \approx 120$ GPa [20], we obtain $E_c \approx 1.3E_p$, thus a reinforcement of ≈ 30 % is obtained for the PU-MoS_2 nanocomposite. Using the more elaborated Halpin-Tsai model [21] and an aspect ratio (length/thickness) of the inorganic nanotubes or nanowires of ≈ 100, we obtain even better agreement with our data from Fig. 4: $E_c \approx 1.16E_p$.

However, similar as for the thermal expansion coefficient α, a more quantitative analysis of the reinforcement effect of PU-MoS_2 and PU-$Mo_6S_2I_8$ needs additional knowledge about the polymer-nanotube interaction and the value of the Young´s modulus of the PU-nanoparticle system.

Having a close look to the DMA experiments, a second relatively broad peak (T_{g2}) at slightly higher temperatures in the tanδ profile (or equivalently in the loss modulus, E") was found in addition to the T_{g1} (Fig. 5). The origin of this second peak or shoulder will be discussed in the next section. It seems that this broad peak is related only to the polyurea matrix, since it appears already in the reference system (PU).

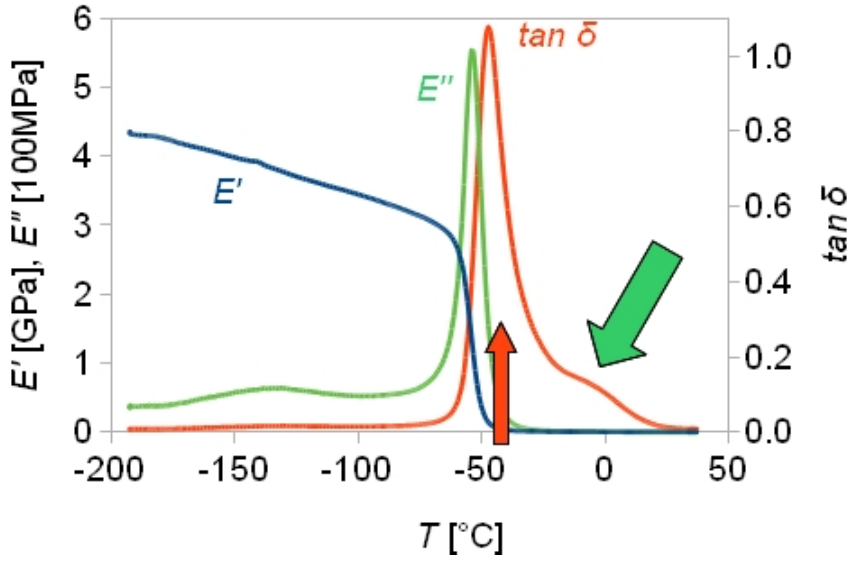

Fig. 5. Young's modulus E' (blue line), tanδ (red line) and E'' (green line) for the pure polyurea matrix (PU) measured in TS mode. The read and green arrows show the two glass transitions at T_{g1} and T_{g2}, respectively.

4. Discussion

The most significant findings of the present work on inorganic nanotubes-elastomer nanocomposites are the upshift of the glass transition temperature T_g with addition of nanoparticles, as well as the occurrence of a second peak or shoulder in tanδ and E" above the T_{g1} peak already observed in pure elastomeric matrix and both nanocomposites. Molecular dynamics simulations have shown [11] that the presence of nanoscale structures in the polymer network affects the glass transition temperature due to a change of the polymer dynamics. In the case of attractive interactions between the polymer and the nanoparticles, the chain relaxation time is increased and leads to a higher T_g relative to the pure system. For non-attractive interactions, a slight downshift in T_g is expected. Such influence of nanoparticles to polymer chain dynamics and glass transitions was indeed experimentally verified [12]. In our case, an attractive interaction between the polymer chains and the MoS_2 nanotubes and $Mo_6S_2I_8$ nanowires should then be proposed to explain the observed increase in T_g relative to the pure polyurea elastomer.

The second peak observed above T_{g1} in tanδ and in E" (Fig. 5) was also observed in the reference sample (PU). Therefore, it cannot be attributed to the presence of inorganic nanoparticles. However, as mentioned above even pure polyurea is a heterogeneous material consisting of hard nanodomains embedded in a soft matrix. It was shown [13] that such systems can exhibit *two glass transitions* at two different temperatures $T_{g1} < T_{g2}$. If the nanodomain-chain interactions are strong enough, the polymer chains near to a nanodomain exhibit reduced mobility compared to the regions far from the nanodomain. According to the so called EHM model [14], the second glass transition temperature at T_{g2} starts to be detectable when the regions of restricted mobility overlap, i.e. when the distance between nanodomains goes below the limit of about 5 to 10 nm. Then, the regions of reduced mobility

can undergo their own glass transition, since the value of 5 to 10 nm is approximately the size of dynamically correlated regions of glass forming polymers or liquids near T_g [15]. In previous works [2-4], the microphase separated domains were measured by means of SAXS, and the authors found distances of d =5.2nm. Thus, this second glass transition at T_{g2} might well be explained in terms of the nanoconfined hard domains in the polyurea elastomer.

The finding of a second peak in tanδ and E" is reminiscent of our recent results in a physically and chemically different but topologically similar system, i.e. the study of molecular liquids (salol, toluene, ortho-terphenyl, etc) confined in mesoporous Vycor and Gelsil with pore sizes between 2.5 nm and 10 nm [16, 17]. Here the restricted mobility of the molecules occurs due to an attractive interaction of the molecules near the pore walls, since the molecules form hydrogen bonds with the hydroxyl groups of the silica surface. Due to the dynamically decoupled motions of molecules far from the pore walls (faster motion → T_{g1}) and near the pore walls (slower motion → T_{g2}), two tanδ peaks could be clearly resolved for pore diameters bigger than 5 nm [16]. By silylating the surface of the pores, we could suppress the pore wall-molecule interaction and also the second glass transition temperature vanished [18].

5. Conclusions

We have presented thermomechanical and dynamic mechanical measurements on a polyurea elastomer and polyurea nanocomposites doped with inorganic nanotubes (MoS_2) and nanowires ($Mo_6S_2I_8$). The addition of nanoparticles causes a rather strong (up to 15 %) increase in the Young's modulus in the whole measured temperature range (from -130 °C to 20 °C), as well as an increase in the thermal expansion above the glass transition temperature T_g. The thermal expansion below T_g is unaffected by the presence of nanoparticles. The same behavior was also found in polyisoprene nanocomposites doped with carbon black (CB) and multiwall carbon nanotubes (MWCNT).

Adding inorganic nanoparticles to a polyurea matrix leads to an increase in the T_g, implying an attractive interaction between the nanoparticles and the polymer. An attractive interaction is also consistent with the observed remarkable reinforcement of PU-MoS_2 and PU-$Mo_6S_2I_8$.

A significant feature was the observation of a second broad peak in tanδ and E" above the glass transition temperature peak in pure and in doped samples. Since this second damping peak is also observed in pure polyurea, we argue that this second glass transition is occurring in regions near to the hard nanodomains. According to the arguments presented above, a separated second glass transition temperature can only be observed if the average distance between the hard nanodomains is not larger than 5 to 10 nm, as has been actually measured (d = 5.2 nm) for this system [2-4].

Although many interesting results have been found here for pure polyurea and polyurea/nanotube or polyurea/nanowire composites, clearly more measurements on well characterized samples with a larger range of doping concentrations are needed to reach final conclusions.

Acknowledgements

The present work was performed in the frame of the COST Action MP0902 (COINAPO – Composites of Inorganic Nanotubes and Polymers).

References

[1]. T. Hanemann and D. V. Szabó, Polymer-Nanoparticle Composites: From Synthesis to Modern Applications, *Materials*, Vol. 3, 2010, pp. 3468-3517.

[2]. A. Sánchez-Ferrer, R. Mezzenga, H. Dietsch, Orientational Behavior of Ellipsoidal Silica-Coated Hematite Nanoparticles Integrated within an Elastomeric Matrix and its Mechanical Reinforcement, *Macromol. Chem. Phys.,* Vol. 212, 2011, pp. 627-634.

[3]. A. Sánchez-Ferrer, M. Reufer, R. Mezzenga, P. Schurtenberger, H. Dietsch, Inorganic-Organic Elastomer Nanocomposites from Integrated Ellipsoidal Silica-Coated Hematite Nanoparticles as Crosslinking Agents, *Nanotechnology*, Vol. 21, 2010, pp. 185603/1-7.

[4]. A. Sánchez-Ferrer, D. Rogez and P. Martinoty, Synthesis and Characterization of New Polyurea Elastomers by Sol/Gel Chemistry, *Macromolecular Chemistry and Physics,* Vol. 211, 2010, pp. 1712-1721.

[5]. M. Remskar, A. Mrzel, Z. Skraba, A. Jesih, M. Ceh, J. Demsar, P. Stadelmann, F. Lévy and D. Mihailovic, Self-Assembly of Subnanometer-Diameter Single-Wall MoS_2 Nanotubes, *Science,* Vol. 292, 2001, pp. 479-481.

[6]. A. Kis, G. Csanyi, D. Vrbanic, A. Mrzel, D. Mihailovic, A. J. Kulik and L. Forró, Nanomechanical Investigation of $Mo_6S_{9-x}I_x$ Nanowire Bundles, *Small,* Vol. 3, No. 9, 2007, pp. 1544-1548.

[7]. M. Knite, V. Tupereina, A. Fuith, J. Zavickis and V. Teteris, Polyisoprene – multi-wall carbon nanotube composites for sensing strain. *Mat. Sci. Eng*., C, Vol. 27, 2007, pp. 1125-1128.

[8]. K. P. Menard, Dynamic Mechanical Analysis, *CRC Press, Taylor & Francis Group,* 2008.

[9]. E. K. H. Salje and W. Schranz, Low amplitude, low frequency elastic measurements using Dynamic Mechanical Analyzer (DMA) spectroscopy, *Z. Kristallographie*, Vol. 226, 2011, pp. 1-17.

[10].J. Yi, M. C. Boyce, G. F. Lee and E. Balizer, Large deformation rate-dependent stress-strain behavior of polyurea and polyurethanes, *Polymer*, Vol. 47, 2006. pp. 319-329.

[11].F. W. Starr, T. B. Schroder and S. C. Glotzer, Molecular Dynamics Simulation of a Polymer Melt with a Nanoscopic Particle, *Macromolecules*, Vol. 35, 2002, pp. 4481-4492.

[12].H. Oh and P. F. Green, Polymer chain dynamics and glass transition in athermal polymer/nanoparticle mixtures, *Nature Materials*, Vol. 8, 2008, pp. 139-143.

[13].G. Tsagaropoulos and A. Eisenberg, Dynamic Mechanical Study of the Factors Affecting the Two Glass Transition Behavior of Filled Polymers, Similarities and Differences with Random Ionomers. *Macromolecules*, Vol. 28, 1995, pp. 6067-6077.

[14].A. Eisenberg, B. Hird and R. B. Moore, A New Multiplet-Cluster Model for the Morphology of Random Ionomers, *Macromolecules*, Vol. 23, 1990, pp. 4098-4107.

[15].E. Hempel, G. Hempel, A. Hensel, C. Schick and E. Donth, Characteristic Length of Dynamic Glass Transition near *T*g for a Wide Assortment of Glass-Forming Substances, *J. Phys. Chem. B,* Vol. 104, 2000, pp. 2460-2466.

[16].J. Koppensteiner, W. Schranz and M. R. Puica, Confinement effects on glass forming liquids probed by dynamic mechanical analysis, *Phys. Rev. B*, Vol. 78, 2008, pp. 054203-1 – 054203-9.

[17].J. Koppensteiner and W. Schranz, Dynamic Mechanical Analysis of Confined Glass Forming Liquids, *Phase Transitions*, Vol. 83, 2010, pp. 744-757.

[18].J. Koppensteiner, W. Schranz and M. A. Carpenter, Revealing the pure confinement effect in glass-forming liquids by dynamic mechanical analysis, *Phys. Rev. B*, Vol. 81, 2010, pp. 024202-1 – 024202-8.

[19].G. D. Sims and W. R. Broughton, In: Polymer Matrix Composites, *Elsevier,* Oxford, 2001.

[20].A. Kis, D. Mihailovic, M. Remskar, A. Mrzel, A. Jesih, I. Piwonski, A. J. Kulik, W. Benoit and L. Forró, Shear and Young´s Moduli of MoS_2 Nanotube Ropes, *Adv. Mater.,* Vol. 15, 2003, pp. 733-736.

[21].J. C. Halpin and J. L. Kardos, The Halpin-Tsai Equations: A Review, *Polym. Eng. Sci*., Vol. 16, 1976, pp. 344-352.

8.2 Influence of inorganic nanoparticles on the glass transitions of polyurea elastomers

ISSN 1862-6300
Phys. Status Solidi A
210 · No. 11 November
2241–2528 (2013)

physica status solidi pss a

www.pss-a.com

applications and materials science

11
2013

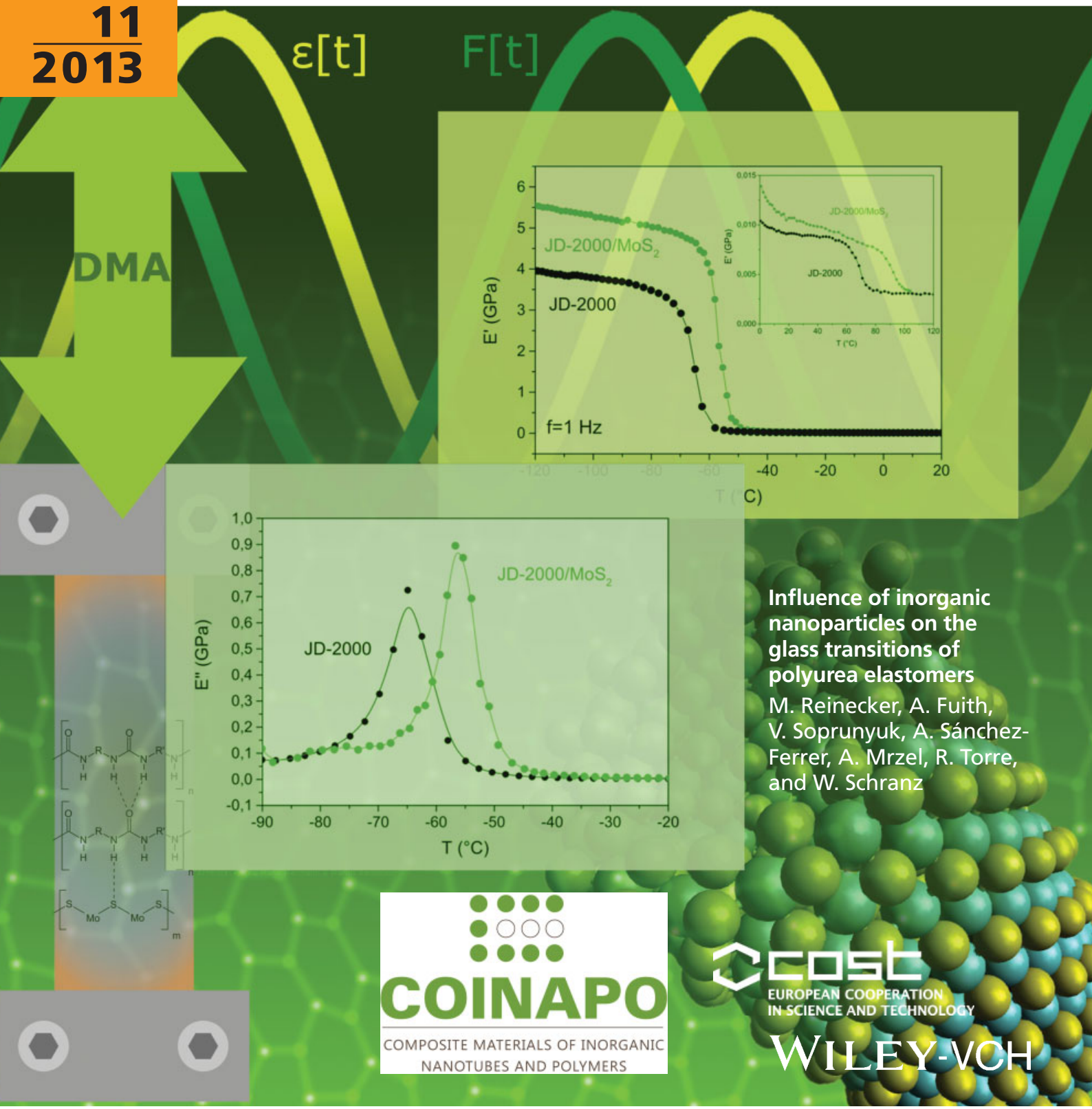

Influence of inorganic nanoparticles on the glass transitions of polyurea elastomers

M. Reinecker, A. Fuith, V. Soprunyuk, A. Sánchez-Ferrer, A. Mrzel, R. Torre, and W. Schranz

COINAPO
COMPOSITE MATERIALS OF INORGANIC NANOTUBES AND POLYMERS

cost
EUROPEAN COOPERATION IN SCIENCE AND TECHNOLOGY

WILEY-VCH

Influence of inorganic nanoparticles on the glass transitions of polyurea elastomers

Marius Reinecker [*,1], Armin Fuith[1], Viktor Soprunyuk[1], Antoni Sánchez-Ferrer[2], Aleš Mrzel[3], Renato Torre[4] and Wilfried Schranz [,1]**

[1] Faculty of Physics, University of Vienna, Boltzmanngasse 5, A-1090 Vienna, Austria
[2] ETH Zurich, Department of Health Sciences and Technology, Institute of Food, Nutrition & Health, Food & Soft Materials Science Group, Schmelzbergstrasse 9, LFO, E29, CH-8092 Zurich, Switzerland
[3] J. Stefan Institute, Jamova 39, SI 1000 Ljubljana, Slovenia
[4] European Laboratory for Non-Linear Spectroscopy, Universitá di Firenze, via Carrara 1, I-50019 Sesto Fiorentino, Italy

Received ZZZ, revised ZZZ, accepted ZZZ
Published online ZZZ (Dates will be provided by the publisher.)

Keywords . inorganic nanoparticles, composites, dynamic elasticity, glass transitions.

* Corresponding author: e-mail marius.reinecker@univie.ac.at, Phone: +43 1 4277 51171, Fax: +43 1 4277 51181
** e-mail wilfried.schranz@univie.ac.at, Phone: +43 1 4277 51171, Fax: ++43 1 4277 51181

The properties of polymers can be significantly changed by incorporating nanoparticles, which yields a great potential for applications. In the present study we use nanocomposites of new polyurea elastomers filled with 0.1, 0.5 and 1 wt-% MoS_2 nanotubes. Using dynamic mechanical analysis (DMA) measurements we show, that the glass transition temperatures T_g of the nanocomposites are increased by small amounts of inorganic nanotubes. In line with results from computer simulations of polymer melts with nanoscopic particles, we explain the observed shift of T_g to be due to a gradual slowing down of polymer chain dynamics in the proximity of nanotubes.

1 Introduction Composites of nanoparticles (NPs) and polymers are attractive materials with a high potential for applications [1], due to their flexibility and superior electrical, magnetic, mechanical, thermoelectric and optical properties, etc. [2]. The properties of polymers can be tuned by adding nanoparticles of different shapes, i.e. spheres, tubes or sheets. Since nanoparticles have large surface areas their performance depends strongly on the properties of the interfacial regions between the polymer and the nanoparticles, i.e. on the type of interaction (attractive or repulsive) between the nanoparticles and the polymer matrix, the degree of dispersion of the nanoparticles, etc.

Polyurea networks synthesized by sol/gel chemistry [3] are relatively new elastomers with extreme resistance to chemical abrasion and service temperatures between -60°C and +200 °C.

In the present work we have to deal with a problem of many scales of length (and time) for the following reason. Polyurea elastomers exhibit a phase separated structure [3] with rigid urea domains (hard domains) embedded in a matrix of flexible polymer chains (soft domains). The average size of the hard domains is of the order of several nanometers and the same holds for the average distance between them [3]. As we shall show below, the average distance between MoS_2 nanotubes is of the order of several micrometers, i.e. thousand times larger.

The mechanical properties of polyurea elastomers can be tuned by the relative amount of hard and soft domains – average molecular weight between crosslinking points – and also by the loading with NPs [4]. Pure polyurea elastomers exhibit two glass transition temperatures at $T_{g1} \approx -65$ °C and $T_{g2} \approx T_{g1}+25$ °C [9] attributed to cooperative motions of molecular segments in the soft domains of pure polyurea (T_{g1}) and to regions near the hard nanodomains (T_{g2}).

Although there are several techniques available to evaluate T_g, one of the most sensitive techniques is dynamic mechanical analysis (DMA). Here we present new DMA experiments where the presence of inorganic MoS_2 nanotubes [5] in different PU elastomer nanocomposites influences the polymer chain dynamics and the glass transition temperatures of the polymer network.

2 Experimental Part

2.1 Samples For the present study, the linear hydrophobic diamino-terminated polyetheramine Jeffamine D-2000 (M_n = 2060 g·mol^{-1}, ρ = 991 kg·m^{-3}) and the hydrophilic Jeffamine ED-2003 (M_n = 2300 g·mol^{-1}, ρ = 1068 kg·m^{-3}), from Huntsman International LLC, and the triisocyanate crosslinker Basonat HI-100 (mw = 504 g·mol^{-1}, ρ = 1174 kg·m^{-3}), from BASF SE, were used as received. Details of the synthesis of these PU elastomers are well described in the literature [4].

PU polymers are formed by the chemical reaction between a diisocyanate and a diamine to build urea moieties, as shown in Scheme 1. When one of these components – the isocyanate- or amino-containing chemicals - has more than two reacting groups, then networks are obtained.

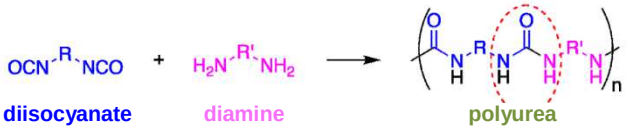

Scheme 1 Chemical reaction between a diisocyanate and a diamine yielding the corresponding polyurea compound (in the red oval, the urea moiety is shown).

In these PU networks, intermolecular hydrogen bonds are formed between the active hydrogen atoms from one urea group (-NH-) and the oxygen coming from the carbonyl group (>C=O) from another urea moiety (Scheme 2), bringing additional properties to the system.

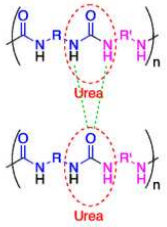

Scheme 2 Intermolecular hydrogen bonds between two urea motifs.

At room temperature polyurea shows microphase segregation, with hard segments dispersed in a soft matrix (Figure 1). From SAXS and WAXS experiments [4], the average size of the hard domains and the distance between them were determined for the Jeffamine D-2000-based PU network, with values in the order of few nanometers and 6.4 nm, respectively.

Two reference elastomeric samples JD-2000 and JED were synthesized when crosslinking the two linear diamino-terminated polyetheramine Jeffamine D-2000 and Jeffamine ED-2003, respectively, with the triisiocyante crosslinker Basonat HI-100. The volume fraction of hard domains for both PU systems was ϕ_x = 0.12.

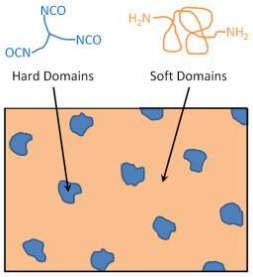

Figure 1 Phase separated structure of polyurea elastomers.

A first PU nanocomposite containing around 1 wt-% of MoS_2 nanotubes (JD-2000/MoS_2) was synthesized after crosslinking the corresponding Jeffamine D-2000 [8, 9]. Moreover, two sets of nanocomposites filled with 0.1, 0.5 and 1 wt-% of MoS_2 multiwall-nanotubes (MoS_2/170: 80-100 nm diameter, 10 µm length) obtained from the desulfurization of MoS_7 nanotubes (JED-C1-X) and of MoS_2 multiwall-nanotubes (MoS_2/628: 250 nm diameter, 100 µm length) obtained from the decomposition of multiwall $Mo_6S_2I_8$ nanowires (JED-C2-X) were prepared after crosslinking the Jeffamine ED-2003.

2.2 Experimental methods Dynamic mechanical analysis (DMA) is a technique to measure the low frequency elastic moduli and damping of materials [7]. A static force F_{stat} is sinusoidally modulated by a dynamic force $F_{dyn}\exp(i\omega t)$ at a chosen amplitude and frequency. The elastic and anelastic response of the sample leads to a change in length u and phase shift δ between force and amplitude, which is registered via inductive coupling. Normal resolutions for the length and phase shift are $\Delta u \approx 10$ nm and $\Delta\delta \approx 0.1°$, respectively. The knowledge of the sample length u and the phase shift δ allows determining the real and imaginary parts of a certain component of the complex elastic compliance tensor S_{ii}^*

$$S_{ii}' = S_{ii}\cos\delta \quad \text{and} \quad S_{ii}'' = S_{ii}\sin\delta \qquad (1)$$

The corresponding storage (E´) and loss modulus (E´´) are defined as E´:=1/S_{ii}´ and E´´:=1/S_{ii}´´, respectively.

DMA experiments were performed on a Perkin Elmer DMA 7 or on the Perkin Elmer Diamond DMA. In both setups the complex elastic compliance can be measured in a frequency range between 0.01 Hz and 100 Hz, and for temperatures between 80 K and 850 K. The minimal force that can be applied is 10^{-3} N with a resolution of 10^{-5} N. The maximal forces are 2.5 N for DMA 7 and 10 N for the Diamond DMA. In both instruments the force is transmitted via a quartz- (DMA 7) or steel- (DMA 7 and Diamond DMA) rod, which also probes the sample size. The present experiments were performed in tensile stress (TS) geometry (Figure 2). For more details concerning the DMA method see e.g. [7]. Typical sample size was l=9 mm b=2 mm t=0.2 mm. The samples were cooled down to about -183 °C and heated again with a heating rate between 0.5 and 2 °C/min. Up to 5 heating/cooling cycles were per-

formed. In the present work we always compare data for pure and filled samples that were taken from the same heating sequence.

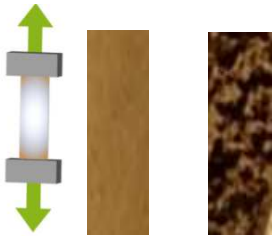

Figure 2 Tensile stress measurement geometry (left). The two right hand pictures show two JED samples with 0.1 and 0.5 wt-% MoS_2, respectively. Sample size is about 2 mm x 9 mm and 0.2 mm thick.

3 Results and discussion In Figures 3-5 optical and scanning electron microscopy images of polyurea JD-2000 filled with ≈1 wt-% MoS_2 (Fig. 3) and JED-C1 filled with 0.1 wt-% MoS_2/170 (Fig. 4) and 0.5 wt-% MoS_2/170 (Fig. 5) are shown for comparison.

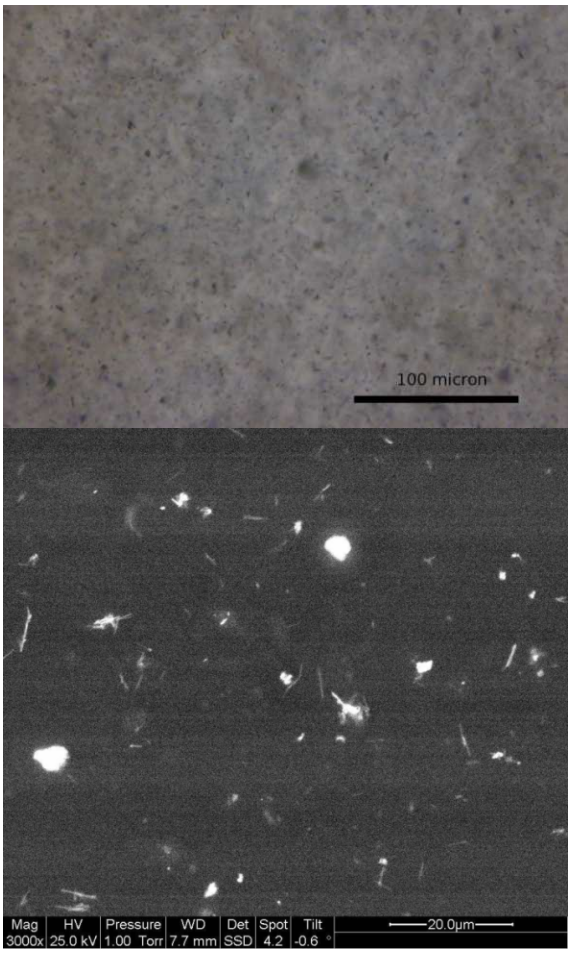

Figure 3 Optical (top) and scanning electron microscopy (bottom) [6] images of JD-2000 filled with ≈1 wt-% MoS_2.

The nanotubes are well dispersed, with an average distance between the NPs of several micrometers (Fig. 3 and Fig. 4), i.e. several tens of the diameter (≈100 nm) of a multiwall-nanotube. The JED-C1 samples filled with 0.5 wt-% show "clouds" of agglomerated nanotubes with regions between, where the NPs are relatively well dispersed (Fig. 5). A similar inhomogeneous distribution of NPs was also observed for the 1 wt-% JED-C1 samples. For comparison, pristine MoS_2 nanotubes usually form bundles or ropes of up to 10^6 individual tubes [5] which can be up to many tens of micrometers long.

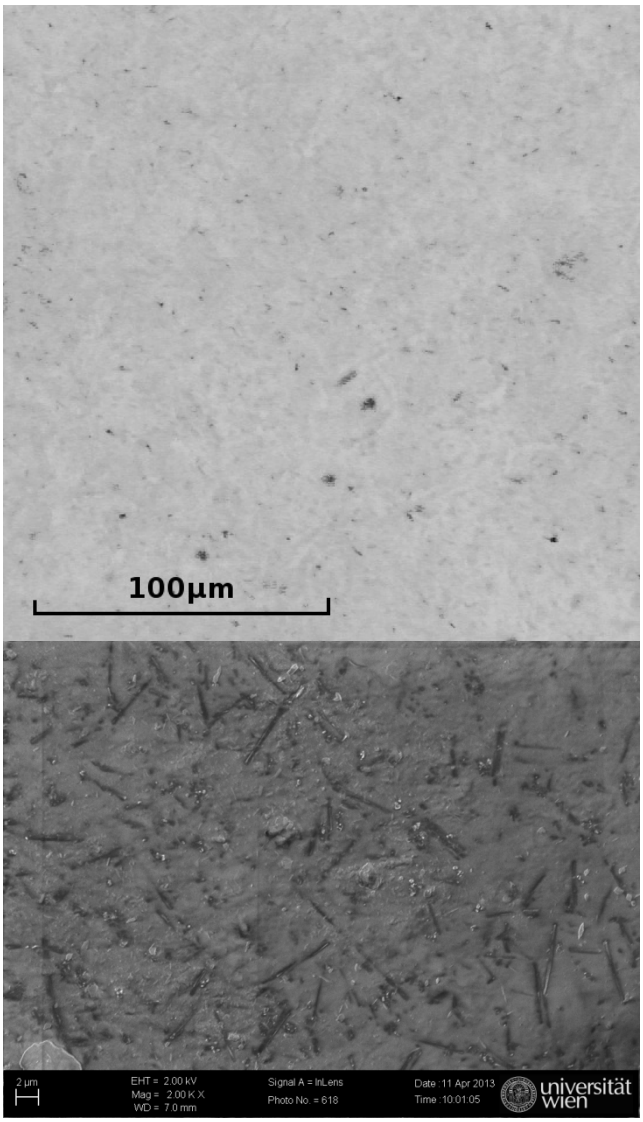

Figure 4 Optical (top) and scanning electron microscopy (bottom) of JED-C1 filled with 0.1 wt-% MoS_2/170. On the SEM picture separated multiwall-nanotubes are visible as "sticks" of about10 µm length.

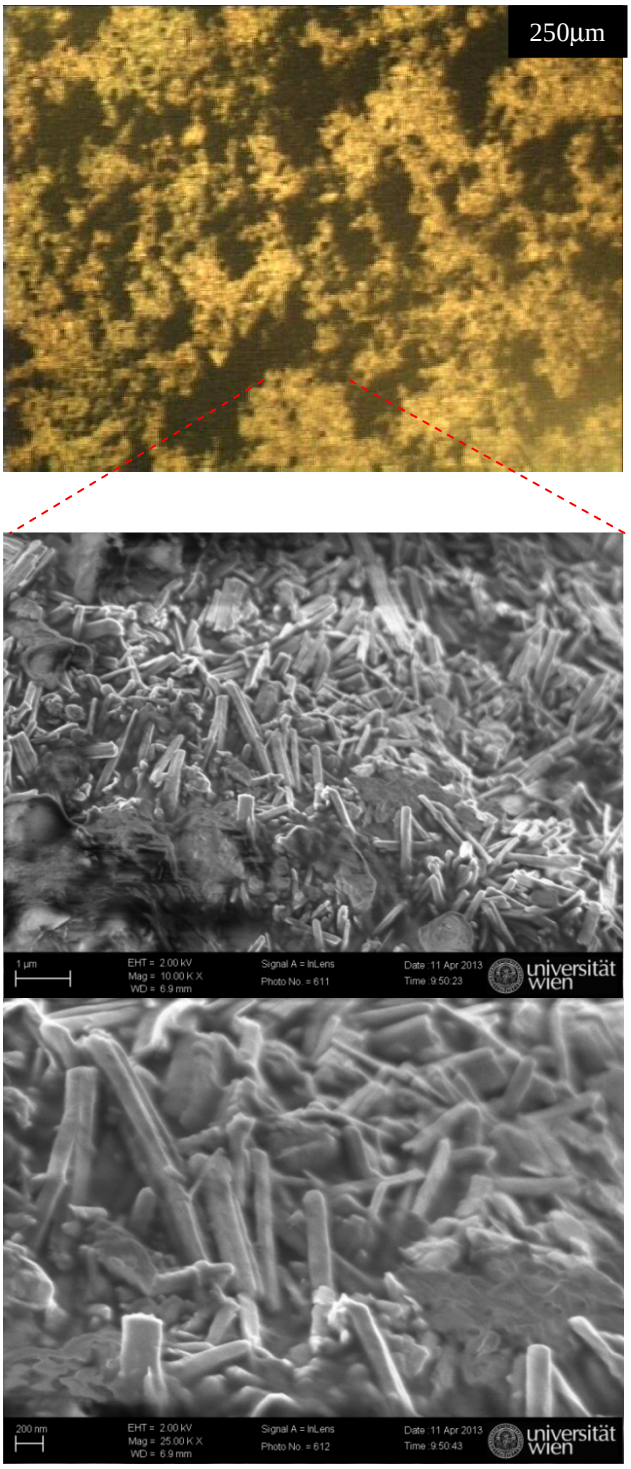

Figure 5 Optical microscopy (top) and SEM (bottom) images of JED-C1 filled with 0.5 wt-% MoS_2, showing "clouds" of MoS_2 aggregates (top) with relatively well dispersed regions in between (bottom). Individual multiwall-nanotubes of about 100 nm thickness and 10 µm length are perfectly discernible.

In order to study the effect of NPs in the polymer matrices, DMA experiments as a function of temperature and frequency were performed.

Figure 6 displays the temperature and frequency dependencies of tanδ=E´´/E´ of pure polyurea JD-2000, showing two glass transitions at $T_{g1} \approx -65$ °C and $T_{g2} \approx T_{g1}+25$ °C.

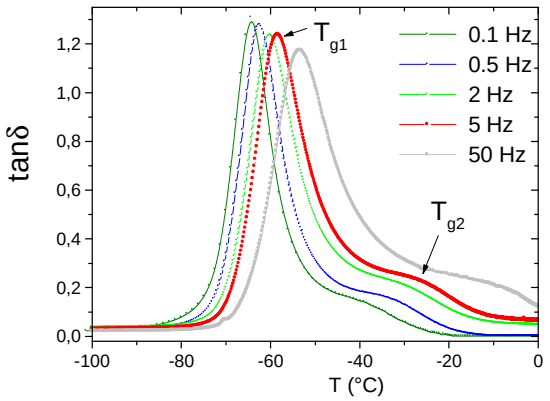

Figure 6 Temperature and frequency dependence of tanδ of the pure polyurea elastomer JD-2000. The measurements were performed at a heating rate of $dT/dt = 1$ °C·min^{-1}.

The glass transition at T_{g1} is attributed to the regions in the soft domains whereas the higher T_{g2} originates from regions near the hard domains [9]. Such a two glass transition behaviour can be observed when sufficiently strong particle enthalpic interactions lead to a permanent attachment of chain segments to the nanoparticles [24], which obviously is the case in the vicinity of the hard domains in polyurea. A discussion of this two-glass transition behaviour as well as detailed measurements for polyureas with different molecular weight of the polyetheramines (soft domains) will be the subject of a forthcoming paper.

The storage E' and loss E" moduli and tanδ as function of temperature are compared for the pure polyurea elastomer JD-2000 and the elastomeric nanocomposite JD-2000/MoS_2 (≈1wt-% of MoS_2) in Figure 7. Several methods are commonly used to determine the glass transition temperature T_g from DMA measurements [10]. They either relate T_g to the onset-temperature of E´ or to the temperature of the E´´-peak or the tanδ-peak respectively. Irrespectively which method we use to locate T_g, we obtain a shift of T_{g1} to higher temperatures by the addition of the inorganic nanoparticles. For 1 wt-% MoS_2 we obtain a shift of T_{g1} of about +8 °C (Figure 7). Averaging 10 successive temperature scans for pure and filled JD-2000, respectively we obtain $\Delta T_{g1}=8\pm3$ °C. For JD-2000 filled with 0.1 wt-% MoS_2 the change in T_{g1} was smaller than 0.8 °C. In contrast, T_{g2} is not affected by the presence of inorganic nanoparticles.

It is important to note, that all these measurements shown here were performed on samples that were not annealed at high temperatures, i.e. the intermolecular hydrogen bonds

between polyurea chains were not removed. Starting from room temperature they were cooled down to low temperatures and then heated until the hydrogen network broke down.

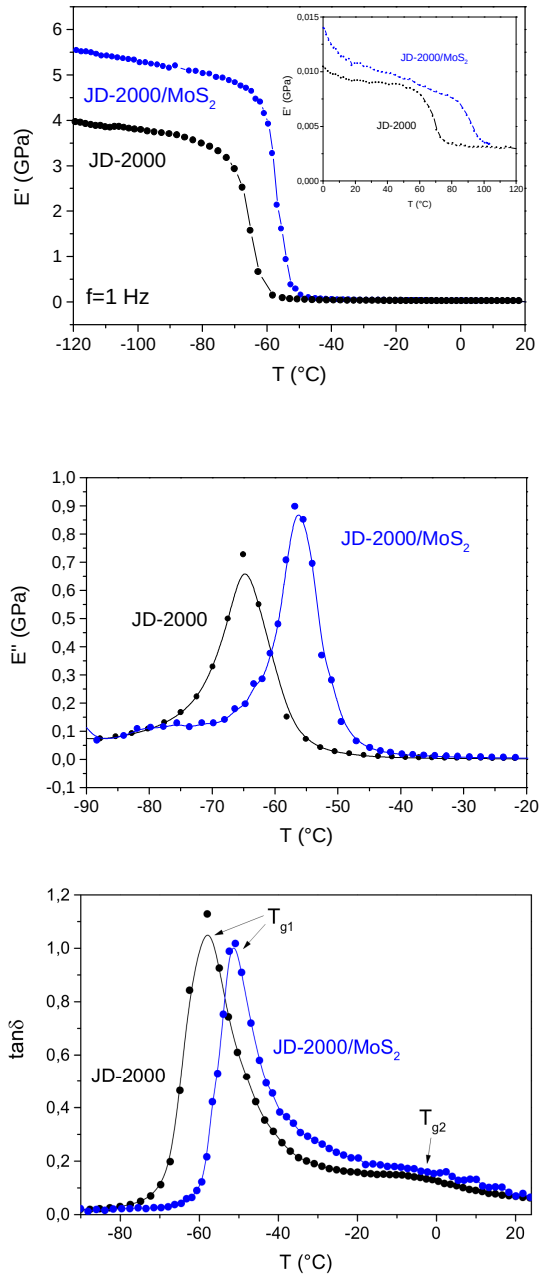

Figure 7 Storage $E´$, loss $E´´$ moduli and tanδ of pure polyurea JD-2000 compared with the nanocomposite JD-2000/MoS_2 (1 wt-% of MoS_2). The measurements were performed at the heating rate dT/dt = 1.5 °C·min^{-1} and frequency of 1 Hz.

The inset of Fig. 7 displays the high temperature part of E´(T) drawn on a larger scale to show the changes in Young´s moduli due to the breakdown of the hydrogen bonded network. One clearly observes an increase of the annealing temperature due to the presence of MoS_2 NPs. On the other hand, samples that were annealed at about 80°C for at least two hours prior to measurements, did not show any significant effects of nanoparticles on T_g.

To study the influence of inorganic nanofillers for another polymer we have performed DMA measurements of the elastomer JED (empty as reference system) and JED filled with 0.1, 0.5 and 1 wt-% MoS_2/170 (called JED-C1) and MoS_2/628 (called JED-C2). Pure JED exhibits a glass transition around T_g≈-51°C. Similar as for JD-2000 we found an increase of the glass transition for increasing concentration of MoS_2/170 NPs. (Fig. 8) for not annealed samples. Also here the effect of nanoparticles on T_g vanishes with annealing.

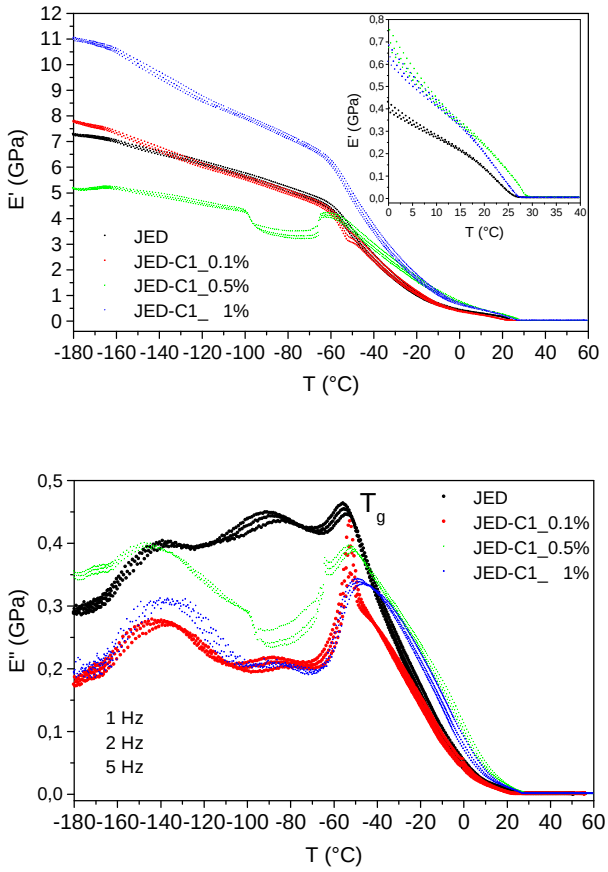

Figure 8 Storage E´ and loss modulus E´´ of pure elastomer JED compared with JED filled with 0.1, 0.5 and 1 wt-% MoS_2/170. The measurements were performed at the heating rate dT/dt = 1 °C·min^{-1} with frequencies of 1, 2 and 5 Hz.

The maximum shift of T_g=+7 °C was observed in not annealed samples for 1 wt-% of MoS_2. $\Delta T_g \approx$ +3 °C for 0.1 wt-% and +4 °C for 0.5 wt-% of MoS_2. For the samples filled with larger nanotubes (JED-C2) no significant shift in T_g was observed (Fig. 9). In both types of composites (JED-C1 and JED-C2) an increase in E´ (reinforcement)

was observed at least at temperatures above T_g (inset of Figures 8 and 9). It is also notable that in both composites the annealing temperature for removing the hydrogen bonds is influenced by the presence of nanotubes. With increasing concentration it shifts to higher temperatures by an amount up to 5 °C for 1 wt-% nanotubes (inset of Figures 8 and 9). For JD-2000 the shift was more than 20 °C (inset of Fig. 7)

Such changes of T_g in nanocomposites are not unusual. It is well established, that many properties of polymer nanocomposites depend crucially on the polymer-nanoparticle interface [11]. E.g. Bansal, *et al.* [12] have shown, that the thermomechanical properties of polymer nanocomposites are critically affected by the polymer-nanoparticle wetting behaviour. They used SiO_2 nanoparticles with a diameter of 14 ± 4 nm dispersed in a polysterene matrix. For untreated silica surfaces which are non-wetting to polysterene, they found a rather moderate decrease in T_g. For 1 wt-% SiO_2 they obtain $|\Delta T_g(1\ \%)| \approx 1.5$ K, for 5 wt-% the shift is about 4 K. For silica nanoparticles grafted with dense polystyrene brushes ("hairy" nanoparticles), silica surfaces provide intimate surface-polymer contact and T_g is shifted to higher temperatures, i.e. up to 4 K for 5 wt-% of grafted (wetting) nanoparticles.

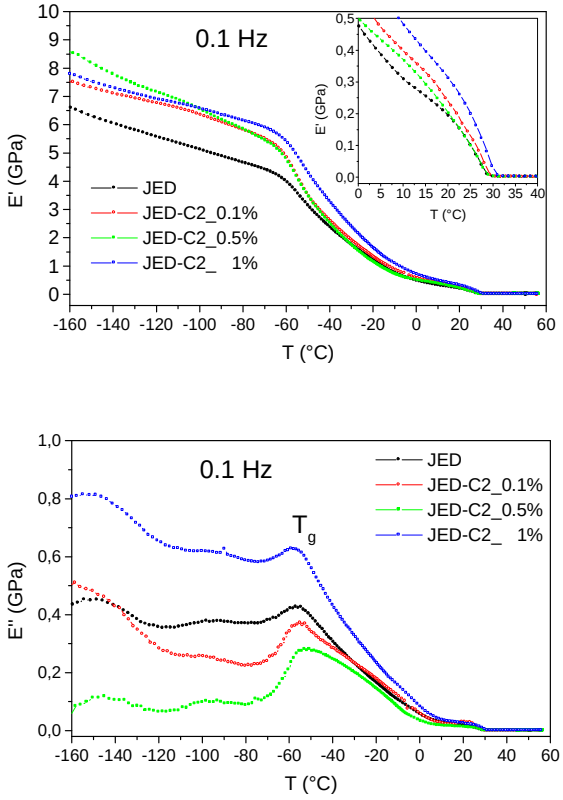

Figure 9 Storage E´ and loss modulus E´´ of pure elastomer JED compared with JED filled with 0.1, 0.5 and 1 wt-% MoS_2/628. The measurements were performed at a heating rate of $dT/dt = 1.5$ °C·min^{-1}.

The details of the mechanisms giving rise to the changes of T_g measured in polyurea-nanoparticle composites are difficult to resolve, since the glass transition mechanism itself is not yet fully understood. A possibility to explain the observed increase of T_g is based on the results of extensive molecular dynamics simulations of polymers with nanoscopic particles [15]. According to these results the polymer dynamics is affected in the proximity of the nanoparticles. Depending on the type of interaction between the nanoparticles and the polymers, the chain relaxation dynamics can accelerate (for non-wetting conditions, i.e. repulsive interactions) or slow down considerably (for attractive interactions, i.e. wetting or for neutral interfaces). In the present case the prevalent polymer-nanotube interaction is most probably attractive [28] occurring due to bonding of the hydrogens with the S-atoms of MoS_2 (Fig. 10).

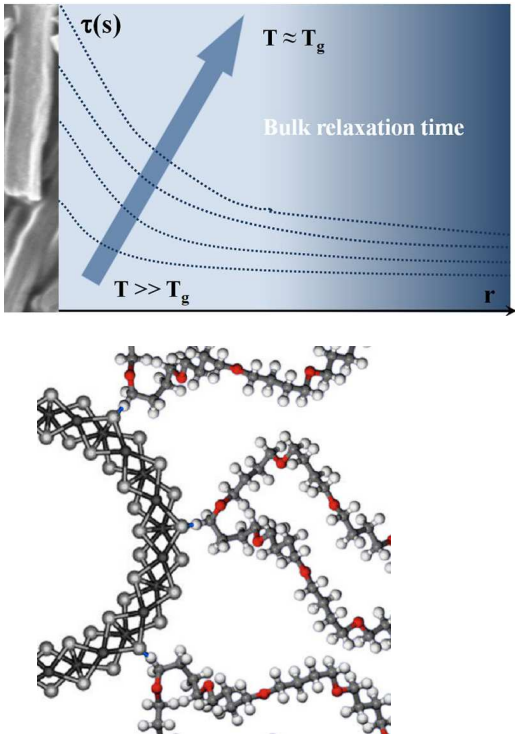

Figure 10 Top: Polymer chain relaxation time τ(r) as a function of distance *r* from the nanoparticle surface, at various temperatures approaching T_g. The arrow indicates the spatial increase of the slowed down regions due to the increase of correlation length with T→T_g. Bottom: Schematic illustration of the bonding between the hydrogen atoms of polyurea chains and the sulphur atoms of MoS_2 nanotubes as proposed in [28].

Because the size of CRRs increases for T→T_g, the dynamics of polymer chains at certain distances away from the nanoparticle surface will slow down, which then will reduce the dynamics of the whole sample, rationalizing the observed increase of the glass transition temperature. This picture is in good agreement with our observations (Fig.7),

showing that only the glass transition in the soft domains at T_{g1} is influenced by the addition of inorganic nanoparticles, whereas the regions near the hard domains yield a glass transition at T_{g2} that is independent of the presence of nanoparticles: the molecules near the hard domains are already strongly (chemically) attached, so that their dynamics is substantially slowed down and thus T_{g2} is not expected to be much influenced by the interaction with inorganic nanoparticles.

A similar decrease of mobility was recently observed in natural rubber-silica nanocomposites [21]. Even in the absence of specific polymer-filler interactions, polymer segments within a few nanometers of the filler particles exhibit relaxation times up to 2-3 orders of magnitude slower leading to an increase of the glass transition temperature of few Kelvin compared to bulk natural rubber.

In PMMA-C60 nanocomposites with NPs up to 6 wt-% a maximal increase of T_g of about 4 K was detected [22], and was also explained in terms of slowed down interfacial polymer/NP regions.

This picture of slowed down interfacial regions near MoS_2 NPs may be complemented by the observation, that the annealing temperatures for removing the hydrogen bonds are increased with increasing NP concentration (Figures 7 – 9). It suggests that the nanoparticles support the formation of intermolecular hydrogen bonding between the polymer chains (Scheme 2). Such an increase in cross-links between polyurea chains could explain the observed increase in tensile strength and would also explain the observed reduced chain mobility in the vicinity of NP induced cross-linking points and the resulting increase in T_g. Similar observations have been made very recently by Dodiuk, *et al.* [27]. The authors have studied the influence of WS_2 nanoparticles on the thermo-mechanical and adhesive peel properties of polyurethane. They also came to the conclusion, that the WS_2 nanoparticles may induce formation of intermolecular hydrogen bonding within the polyurethane.

An interesting observation has been made recently by Taschin *et al.* [6] with transient grating experiments of polyurea JD-2000 filled with ≈1 wt-% MoS_2 nanotubes. An intermediate dynamics was clearly detected at room temperature at the time scale of $\tau \approx 5 \cdot 10^{-5}$ s. Since this signal was absent in the pure samples, the authors argued that the effect is coming from the interfacial polymer chains in the vicinity of the nanotube surfaces. Taking into account that the relaxation time τ_α of the alpha-relaxation in pure polyurea [21] is of the order of $\tau_\alpha \approx 10^{-7}$ s at room temperature, one could speculate that the observed intermediate dynamics becomes visible in the filled samples due to an increase of local relaxation times from 10^{-7} s in the bulk to 10^{-5} s close to the nanoparticles. This explanation is in good agreement with our findings. However, to draw more specific conclusions detailed investigations, like e.g. temperature dependent transient grating experiments or local dielectric spectroscopy measurements [26] have to be performed on polyurea/MoS_2 nanocomposites.

4 Conclusions We have presented extensive DMA measurements of pure polyurea elastomers and nanocomposites of polyurea filled with various concentrations of inorganic nanotubes MoS_2. An upshift of T_g of several °C was observed together with a slight increase of the Young´s moduli of the composites. The increase of T_g is explained in terms of slowing down of local polymer chain dynamics, i.e. for polymer chains in the vicinity of the nanotubes. A clear cut analytic theory concerning such a suppression of dynamics is still missing. However, molecular dynamics simulations [15, 25] have shown a gradual slowing down of the polymer dynamics approaching the surface of nanoparticles, that do interact with the polymer matrix. In the present case, such an interaction between polyurea chains and MoS_2 NPs could be mediated via hydrogen bonding. Indeed, recent computer simulations [23] have shown that hydrogen may form stable chemical bonds with some low Miller-indexed edges of MoS_2. First principles calculations on a MoS_2 monolayer [28] yielded that hydrogen atoms prefer to bond to S atoms with a length of 1.41 Å and a formation energy of 1.91 eV. Although the detailed local geometry of the polymer-nanotube interface cannot be resolved at the moment, it seems clear, that the observed slowing down comes from such an interaction between the hydrogen atoms and sulphur atoms of MoS_2 nanotubes. Also our observation, that for annealed samples (hydrogen bonds are removed) the effect of nanotubes on T_g vanishes, is in accordance with such a picture.

As we have shown here, in the absence of permanent attachments of the polymer chains to the MoS_2 NPs the system yields a single, but larger average T_g, due to the increase of the longest relaxation time. On the other hand, polyurea opens a unique possibility to study also the effect of very strong NP/chain enthalpic interactions. Due to its phase separated nanostructure into so called hard and soft domains (Figure 1), two glass transitions appear which are related to cooperative motions of molecular segments in the soft domains (T_{g1}) and to regions near the hard nanodomains (T_{g2}), respectively. Due to the strong attractive nanoparticle – polymer chain interactions the polymer chain motions near the hard nanodomains are considerably slowed down and as a result T_{g2} turns out to be much larger than T_{g1}.

More detailed results on the corresponding two glass transition behaviour (Figure 3) in polyureas with various molecular weights of the polyetheramines will be presented in a forthcoming paper.

Acknowledgements The present work was performed in the frame of the COST Action MP0902 (COINAPO – Composites of Inorganic Nanotubes and Polymers). Financial support by the Austrian Science Fund (FWF) P23982-N20 is gratefully acknowledged. Support from Prof. R. Mezzenga (member of the COINAPO Swiss team) is greatly appreciated. We sincerely thank S. Puchegger (Faculty Center for Nanostructure Research, University of Vienna) for providing the SEM images .

References

[1] T. Hanemann and D. V. Szabó, Materials **3**, 3468 (2010).

[2] A. C. Balazs, T. Emrick and T. P. Russel, Science **314**, 1107 (2006).

[3] A. Sánchez-Ferrer, D. Rogez and P. Martinoty, Macromol. Chem. Phys. **211**, 1712 (2010).

[4] A. Sánchez-Ferrer, R. Mezzenga and H. Dietsch, Macromol. Chem. Phys. **212**, 627 (2011).

[5] M. Remskar, A. Mrzel, Z. Skraba, A. Jesih, M. Ceh,J. Demsar, P. Stadelmann, F. Lévy and D. Mihailovic, Science **292**, 479 (2001).

[6] A. Taschin, P. Bartolini, A. Sánchez-Ferrer, R. Mezzenga, A. Mrzel and R. Torre, Materials Science Forum **714**, 79 (2012).

[7] W. Schranz, Phase Transitions **64**, 103 (1997).

[8] A. Taschin, P. Bartolini, A. Sánchez-Ferrer, R. Mezzenga, A. Mrzel and R. Torre, Sensors & Transducers **12**, 46 (2011).

[9] A. Fuith, M. Reinecker, A. Sánchez-Ferrer, R. Mezzenga, A. Mrzel, M. Knite, I. Aulika, M. Dunce and W. Schranz, Sensors & Transducers **12**, 71 (2011).

[10] E.A. Turi, Thermal Characterization of Polymeric Materials, Second Edition, Volume I (Academic Press, Brooklyn, New York, 1997), p. 980.

[11] H. Oh and P. F. Green, Nature Mater. 8, 139 (2009).

[12] A. Bansal, H. Yang, C. Li, B. C. Benicewicz, S. K. Kumar and L. S. Schadler, J. Polym. Sci. B **44**, 2944 (2006).

[13] S. Srivastava and J. K. Basu, Phys. Rev. Lett. **98**, 165701 (2007).

[14] G. Seifert, H. Terrones, M. Terrones, G. Jungnickel and T. Frauenheim, Phys. Rev. Lett. **85**, 146 (2000).

[15] F. W. Starr, T. B. Schrøder and S. Glotzer, Macromolecules **35**, 4481 (2002).

[16] G. Adam and J. H. Gibbs, J. Chem. Phys. **43**, 139 (1965)

[17] E. Hempel, G. Hempel, A. Hensel, C. Schick, and E. Donth, J. Phys. Chem. B **104**, 2460 (2000).

[18] H. Huth, M. Beiner and E. Donth, Phys. Rev. B **61**, 15092 (2000).

[19] B. M. Erwin and R. H. Colby, J. Non-Cryst. Solids **307-310**, 225 (2002).

[20] J. Koppensteiner, W. Schranz and M. A. Carpenter, Phys. Rev. B **81**, 024202 (2010).

[21] D. Fragiadakis, L. Bokobza and P. Pissis, Polymer **52**, 3175 (2011).

[22] J. M. Kropka, K. W. Putz, V. Pryamitsyn,V. Ganesan and P. F. Green, Macromolecules **40**, 5424 (2007).

[23] M. V. Bollinger, K. W. Jacobsen and J. K. Norskov, Phys. Rev. B **67**, 085410 (2003).

[24] G. Tsagaropoulos and A. Eisenberg, Macromolecules **28**, 396 (1995).

[25] G. D. Smith, D. Bedrov, L. Li and O. Byutner, J. Chem. Phys. **117**, 9478 (2002).

[26] M. Labardi and D. Prevosto, J. Vac. Sci. Technol. B **28**, C4D11 (2010).

[27] H. Dodiuk, O. Kariv, S. Kenig and R. Tenne, *The Effect of Tungsten Disulphide Nanoparticles on the Properties of Polyurethane Adhesives*, J. of Adhesion Science and Technology, in press.

[28] E. W. K. Koh, C. H. Chiu, Y. K. Lim, Y.-Wei Zhang and H. Pan, Internat. J. of Hydrogen Energy **37**, 14323 (2012).

8.3 Two glass transitions of polyurea networks: effect of the segmental molecular weight

Journal Name

RSCPublishing

ARTICLE

Two glass transition behaviour of polyurea networks: effect of the segmental molecular weight

Cite this: DOI: 10.1039/xoxxoooooox

Received ooth January 2012,
Accepted ooth January 2012

DOI: 10.1039/xoxxoooooox

www.rsc.org/

Marius Reinecker,*[a] Viktor Soprunyuk,[a] Martin Fally,[a] Antoni Sánchez-Ferrer *[b] and Wilfried Schranz *[a]

Polymer-nanoparticle composites (PNCs) play an increasing role in technology. Inorganic or organic nanoparticles are usually incorporated into a polymer matrix to improve material properties. Polyurea is a spontaneously occurring PNC, exhibiting a phase segregated structure with hard nanodomains embedded in a soft (elastically compliant) matrix. This system shows two glass transitions at T_{g1} and T_{g2}. It has been argued that they are related to the freezing of motion of molecular segments in the soft matrix (usual polymer α–glass transition at T_{g1}) and to regions of restricted mobility near the hard nanodomains (α´-process) at T_{g2}, respectively.
We present detailed dynamic mechanical analysis (DMA) measurements for polyurea networks with different segmental lengths l_c (2.5, 12.1, 24.5 nm) of the polymer chains, i.e. different volume fractions ϕ_x (0.39, 0.12, 0.07) of the hard domains. The two glass transitions show up in two distinct peaks in tanδ at T_α and $T_{\alpha'}$. Analysing the data using a Havriliak-Negami term for the α- and the α´- relaxation, as well as Vogel-Fulcher dependencies for the corresponding relaxations times, it is found, that the α-glass transition at T_{g1} increases strongly (up to ΔT=70 K) with increasing ϕ_x, whereas the α´-transition at T_{g2} remains unchanged. At $\phi_x^c \approx 0.19$ the two curves intersect, i.e. $T_{g1} = T_{g2}$. This value of ϕ_x^c is very close to the percolation threshold of randomly oriented overlapping ellipsoids of revolution with an aspect ratio of about 1:4 - 1:5. We therefore conclude, that around 19% of hard nanodomains polyurea changes from a system of hard nanoparticles embedded in a soft matrix ($\phi_x \leq \phi_x^c$) to a system of soft domains confined in a network of percolated hard domains at $\phi_x \geq \phi_x^c$.

I Introduction

The glass transition remains one of the great mysteries in material science despite of decades of intense research. According to the work of Adam and Gibbs [1] the generally observed drastic slowing down of the dynamics around T_g originates from so called "cooperatively rearranging regions (CRRs)", whose size ξ increases when T approaches T_g. The corresponding relaxation time $\tau_\alpha(\xi)$ is given by [2]

$$\tau_\alpha(\xi) = \tau_0 exp\left[\xi(T)^D \frac{\Delta}{k_B T}\right] \quad (1)$$

Where Δ is a typical energy scale that depends on the details of the glass former and is traditionally assumed to be constant. ξ(T) contains the main T dependence and *D* is the spatial dimension of correlated regions. The glass transition temperature T_g (so called "laboratory glass transition temperature") is usually defined for $\tau_\alpha \approx 100$ s or shear viscosities in the range of about 10^{13} poise. [3] The main question, whether there is a true thermodynamic phase below T_g, or if it is just a kinetic slowing down at T=0 K, is intimately related to the question of a diverging correlation length ξ at a finite temperature T_0 below T_g. Substantial progress has been made in recent years to determine such length scales. Quite different experimental techniques, such as heat capacity spectroscopy,[4] multidimensional NMR,[5,6] dielectric spectroscopy[7] as well as computer simulations[8] have been used to monitor a possible growing length scale accompanying the glass transition in various glass forming materials including molecular liquids and polymers.
It is now generally accepted, that the nature of cooperativity is dynamic and the obtained dynamically correlated regions ξ are increasing when approaching T_g. However, it is very difficult to nail down quantitative values for ξ exactly. To a great extent this is due to the unknown shape of correlated regions, which can change from compact to string like structures with changing temperature.[8,9]

An appealing method to probe correlation lengths in glass forming materials is to restrict their spatial extent *d*. The basic idea is the following: If a growing correlation length $\xi(T)$ for $T \rightarrow T_g$ would be involved in the glass transition, the system should start to "feel" the spatial confinement as soon as $\xi(T_g) \approx d$, and the glass transitions should be finally suppressed for $d < \xi(T_g)$. Indeed, numerous measurements of confined glass forming materials, i.e. of thin polymer films,[10,11] molecular liquids in nanopores,[12,13,14] as well as computer simulations[15,16] support this idea. In most cases confinement leads to a remarkable downshift of T_g, due to so called "confinement induced acceleration of the dynamics". There are however also cases, where a gradual increase of the glass transition temperature with decreasing pore size was reported.[17] It turns out that attractive interactions between the confined glass former and the pore surface can slow down the motion of molecules near the surface, which due to an increase in correlation length can slow down larger regions, leading to an effective upshift of T_g. Interestingly it was found, [18,19] that a second glass transition at $T_{g2}>T_g$ can occur if the interfacial region of slowed down motion is large enough, i.e. of the order of the correlation volume $V_{corr}(T_g)$ of dynamically correlated regions. Effects of confinement on material behaviour including freezing and melting have been discussed in excellent review articles.[20,21]

Exciting interfacial phenomena have been also studied by incorporation of nanoparticles into a polymer host.[22] Depending on the type of interaction (attractive or repulsive) between the polymer chains and the nanoparticles, the relaxation dynamics of the polymer chains close to the nanoparticles may increase (for repulsive interactions) or decrease (for attractive interactions), leading to a down- or upshift of T_g, respectively.[23,24] In case of permanent attachment of polymer chains to nanoparticles one can even obtain two glass transitions : [25] one at T_{g1} associated with polymer chains far from the nanoparticles and a second $T_{g2}>T_{g1}$ associated with chain segments in the vicinity of the nanoparticles. Indeed such polymer nanocomposites (PNCs) are in many respects similar to confined pure polymers or liquid glass formers in nanopores.[26]

Polyurea is a unique material, [27] since it offers the possibility to study the influence of nanoparticles to the glass dynamics without the need to add nanoparticles due to its microphase segregated structure into hard and soft nanodomains, whose volume ratios can be easily varied by changing the molecular weight of the polyetheramines. The type of interaction (attractive vs. repulsive) between the polymer chains near the hard nanodomains is clearly attractive, since the polymer chains are chemically attached to the hard nanodomains. Due to the complex microstructure polyureas display a very broad range of mechanical responses under static and dynamic loading conditions, which favour their use as abrasion/corrosion protection and blast/ballistic-impact mitigation material.

In the present work we use samples of polyurea networks with three different segmental lengths l_c (Table 1) of the polymer backbone (i.e. polyetheramine in our case) resulting in three different volume fractions ϕ_x of the hard nanodomains and perform dynamic mechanical analysis measurements (DMA) as a function of temperature and frequency. Two successive glass transition temperatures at T_{g1} and T_{g2} are found and are attributed to cooperative motions of molecular segments in the soft matrix (T_{g1}) and to regions in the vicinity of the hard domains (T_{g2}), respectively.

Fitting a Havriliak-Negami function with the Vogel-Fulcher relaxation time behaviour to the temperature and frequency dependence of the experimental tanδ - curves, we determine the glass transition temperatures $T_{g1}(\phi_x)$ and $T_{g2}(\phi_x)$ for various concentrations ϕ_x of hard nanodomains.

From the experimental data of the Young´s modulus vs. temperature and frequency $E'(\omega,T)$ we determine the temperature dependence of the linear size ξ and volume V_{corr} of dynamically correlated regions using the multipoint susceptibility approach of Berthier, *et al*. [7] We show that these obtained values are consistent with the hypothesis [25] that the regions of restricted mobility near the hard domains have to exceed a critical size of the order of $V_{corr}(T_g)$ to exhibit their own glass transition at T_{g2}. Moreover, the obtained values of $\xi(T)$ turn out to be large enough to explain the observed increase of T_{g1} with increasing volume fraction of hard nanodomains.

II Experimental

A Samples

For the present study, the three linear hydrophobic diamino-terminated polyetheramines Jeffamine D-400 (M_n = 460 g·mol^{-1}, ρ = 972 kg·m^{-3}), D-2000 (M_n = 2060 g·mol^{-1}, ρ = 991 kg·m^{-3}) and D-4000 (M_n = 4000 g·mol^{-1}, ρ = 994 kg·m^{-3}) from Huntsman International LLC, and the triisocyanate crosslinker Basonat HI-100 (m_w= 504 g·mol^{-1}, ρ = 1174 kg·m^{-3}) from BASF SE, were used as received. Polyurea (PU) networks are formed by the rapid chemical reaction between a triisocyanate and a diamine to build urea moieties, as shown in Fig. 1. Details of the synthesis of these PU elastomers are well described in the literature.[27] Table 1 compares the main structural characteristics for the three used samples JD-400, JD-2000 and JD-4000.

Table 1 Segmental molecular weight ($\bar{M}_c$) of polyetheramines, segmental length (l_c), volume fractions (ϕ_x) of the crosslinker (hard domains) and average distance t between hard domains for all three polyurea elastomers.

Sample	$\bar{M}_c$ (g/mol)	l_c (nm)	ϕ_x	t (nm)
JD-400	428	2.5	0.39	4.8
JD-2000	1990	12.1	0.12	5.4
JD-4000	4024	24.5	0.07	7.5

The structure of polyurea chains is shown in Fig. 1 (top). **U-R-U** represents the hard segment **(HS)** of the polyurea molecule and **R´** the soft segment (**SS**), and thus we can represent the molecules as shown in the bottom of Fig. 1.

Due to strong hydrogen bonding between urea linkages of neighboring chains or neighboring segments in the same chain, hard segments (HS) are usually microphase segregated into so called “hard domains”.

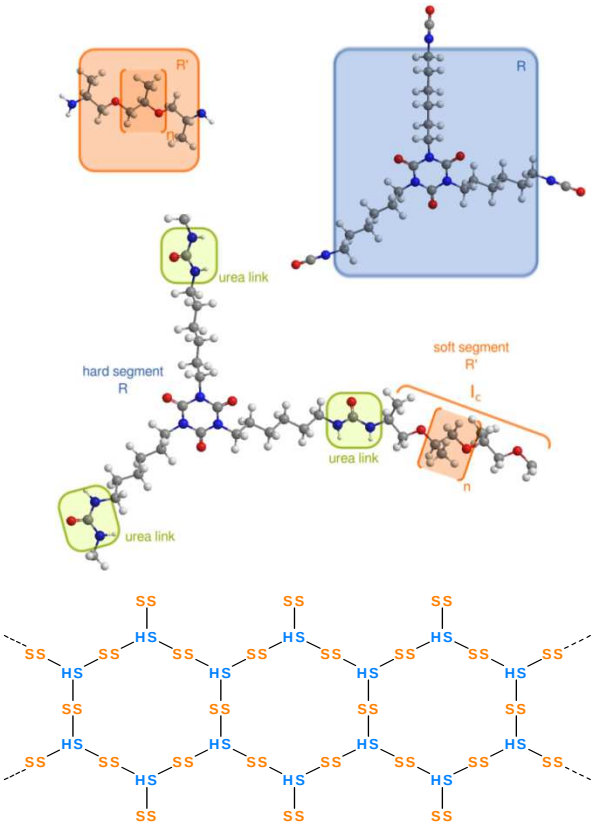

Figure 1 Representation of a typical polyurea chain (top). R represents triisocyanate crosslinker Basonat and R´ denotes the diamino-terminated polyetheramine Jeffamine. The sketch at the bottom shows polyurea molecules built of hard and soft segments.

Atomic force microcopy [28] investigations revealed islands of hard domains embedded in the soft matrix where the average distance between hard domains is of the order of several nm (Table 1).

For small volume fractions of hard nanodomains the topology of phase segregated polyurea is “inverse” to the case of molecular liquids confined in meso- or nano-porous silica frameworks like Vycor or Gelsil. In these systems we recently studied the glass transitions of various glass forming liquids with varying pore diameters. [29,30] E.g. for salol confined in nanoporous silica we detected [29] two glass transitions for pore sizes larger than 5 nm. We could associate the glass transition at $T_{g2}>T_{g1}$ with regions of restricted mobility near the surface of the pores. The glass transition at T_{g1} was attributed to regions well inside the pores. Its dynamics was however also slowed down by surface interactions. This could be proved by silanization of the pore surface: removing the surface interactions resulted in a stronger decrease (as compared to untreated pores) of the bulk glass transition T_{g1} with decreasing pore size and the second glass transition at T_{g2} disappeared.[30]

In polyurea one obtains the inverse geometrical case for small enough volume fractions ϕ_x of hard domains, as the elastically hard domains are suspended in the elastically compliant (soft) matrix. However, with increasing ϕ_x we can expect a crossover to a system that is very similar to the case of glass forming liquids in nanopores.

B Experimental methods

Dynamic mechanical analysis (DMA) is used to measure the temperature dependencies of the low frequency elastic moduli and damping of polyurea at frequencies between 0.1 and 100 Hz. A static force F_{stat} is sinusoidally modulated by a dynamic force $F_{dyn}\sin(\omega t)$ at a chosen amplitude and frequency. The elastic and anelastic response of the sample leads to a change in length u and phase shift δ between force and response amplitude with resolutions for the length and phase shift of $\Delta u\approx 10$ nm and $\Delta\delta\approx 0.1°$, respectively. The knowledge of the sample length u and the phase shift δ allows to determine the real and imaginary parts of a certain component of the complex elastic compliance tensor S_{ii}^*

$$S_{ii}' = S_{ii}\cos\delta \quad \text{and} \quad S_{ii}'' = S_{ii}\sin\delta \qquad (2)$$

The corresponding storage (E´) and loss modulus (E´´) are defined as $E':=1/S_{ii}'$ and $E'':=1/S_{ii}''$, respectively and $\tan\delta=E''/E'$.

DMA experiments are performed on a Perkin Elmer Diamond DMA. The complex elastic compliance can be measured in a frequency range between 0.1 Hz and 100 Hz, and for temperatures between 80 K and 850 K. The minimal (maximal) force that can be applied is 10^{-3} N (10 N) with a resolution of 10^{-5} N. It is transmitted via a steel-rod. The present experiments are performed in tensile stress geometry (Fig.2). For more details concerning the DMA method see e.g. Ref [31]. Typical sample size was $9 \times 2 \times 0.2$ mm^3. The samples were cooled down to about 90 K and heated again with a heating rate between 0.5 and 2 K/min. Up to 5 heating/cooling cycles were performed for each measurement frequency and each sample.

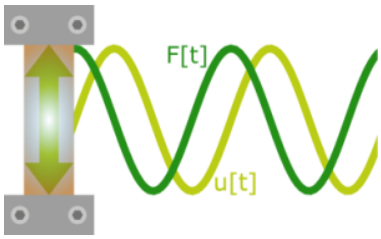

Figure 2 Sketch of DMA measurement in tensile stress geometry.

III Experimental results

Fig. 3 shows the storage modulus E´and tanδ of JD-2000 as a function of temperature at various frequencies.

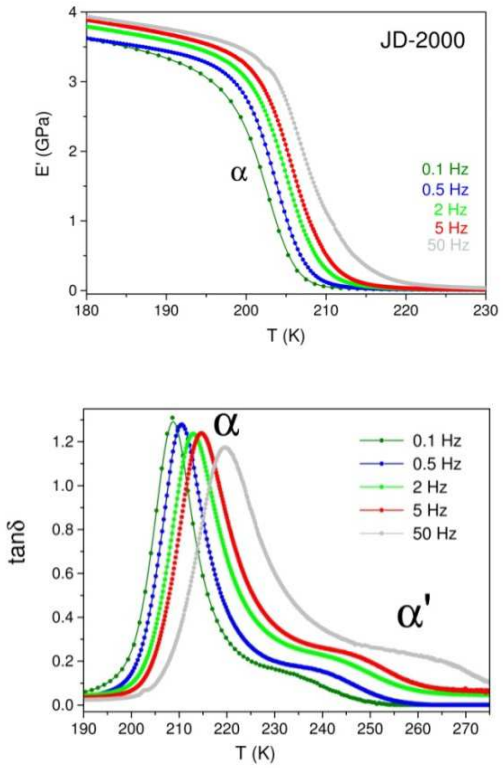

Figure 3 Temperature dependence of storage modulus E´ and tanδ of polyurea JD-2000 at various frequencies.

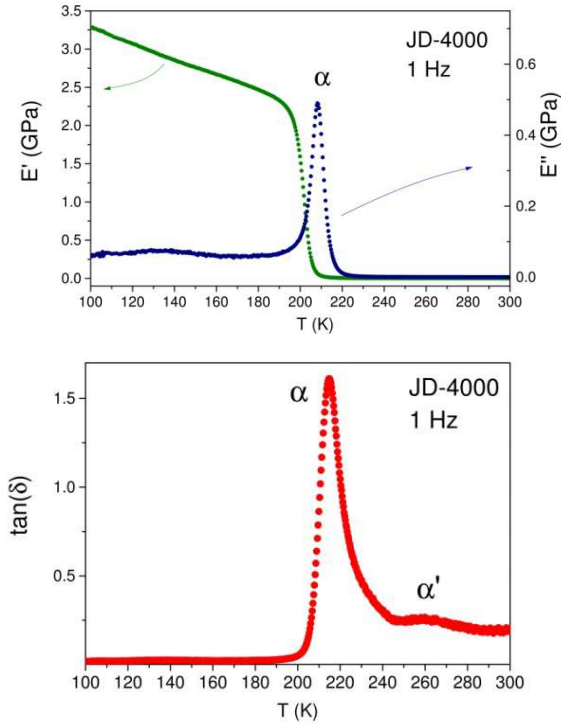

Figure 4 Temperature dependence of storage modulus E´, loss modulus E´´ and tanδ of polyurea JD-4000 measured at f=1Hz.

In Fig. 4 and Fig. 5 the same quantities are plotted for JD-4000 and JD-400, respectively for f=1Hz.

Inspecting Figures 3-5 one recognizes quite similar behaviour for JD-2000 and JD-4000 samples. A typical relaxation behaviour of E´(ω,T) together with the corresponding peak(s) in tanδ whose maximum shifts to higher temperatures with increasing frequency. In JD-2000 and JD-4000 a second peak (α') is observed in tanδ (Fig. 3 and 4). It can be seen in E´´ data only if the scale is increased. The underlying process of this α'-relaxation will be discussed in detail below. Note, that there is only a single broad tanδ-peak in JD-400 (Fig. 5).

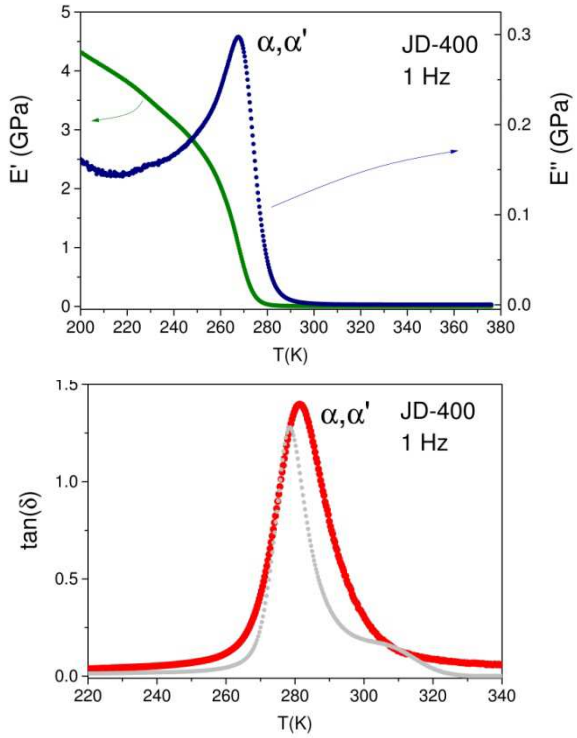

Figure 5 Temperature dependence of storage modulus E´, loss modulus E´´ and tanδ of polyurea JD-400 (red disks) measured at f=1Hz. The grey disks display the shifted (with respect to T) tanδ of JD-2000 (at 0.5 Hz) for comparison to emphasize the broadness of the JD-400 peak.

In all samples we observed also two additional peaks at lower temperatures, often denoted as β– and γ– relaxations. They are related to motions of side groups and other local molecular motions and have been also observed in previous DMA measurements of polyurea. [32] As we focus on the α- and α'-process here we will show these details in a forthcoming paper.

IV Discussion

The segmental dynamics of polyurea was already previously studied by dynamic mechanical analysis [32,33] as well as by dielectric spectroscopy. [34] Contrary to these DMA [32,33] and specific heat [34] measurements our DMA data clearly show (in

tanδ of JD-2000 and JD-4000) a second relaxation process (α') at a temperature higher than the α-peak (Fig. 3 and Fig. 4). As we shall show below, for JD-400 (Fig. 5) the two glass transitions can only be separated by a careful fitting procedure.

In dielectric spectroscopy measurements [34] a similar second relaxation process was found (denoted there also as α´-process) and turned out to be about 3 orders of magnitude slower than the α – relaxation. Calorimetric data show [34], that the α- transition in polyurea is very broad with a ΔT ≈ 30 - 35 K. This indicates a rather heterogeneous dynamics. Such a broad distribution of relaxation times can be accounted for by fitting a double Havriliak-Negami [35] term for the α- and the α´-relaxation to the data

$$E^*(\omega) = E_\infty - \sum_{j=1}^{2} \frac{\Delta E_j}{\left[1+(i\omega\tau_j)^{\alpha_j}\right]^{\beta_j}} \qquad (3)$$

where j=1,2 correspond to the α- and α'-relaxation, respectively. E_∞ is the unrelaxed (high frequency limit) Young´s modulus, $\Delta E_1 = E_\infty - E_{s1}$ and $\Delta E_2 = E_{s1} - E_{s2}$ (E_{s1} and E_{s2} are the static moduli of the corresponding process). The exponents α_j and β_j describe the broadness and asymmetry of the corresponding spectra.

The temperature dependencies of the two relaxation times τ_j can be written in terms of Vogel-Fulcher relations as [36]

$$\tau_j = \tau_{0j} exp\left(\frac{B_j}{T - T_{0j}}\right) \qquad (4)$$

where τ_{0j} describe attempt rates, B_j the activation energies and T_{0j} the corresponding Vogel-Fulcher temperatures of the α- and α'-process, respectively.

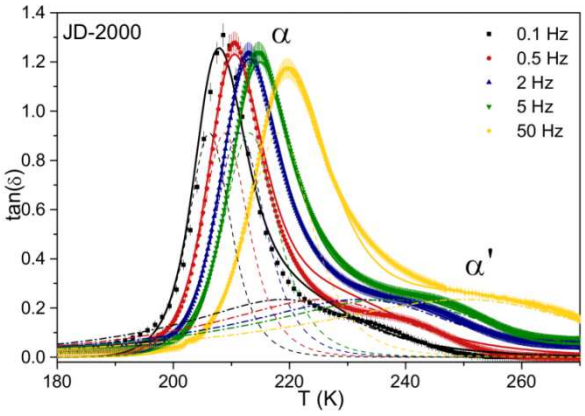

Figure 6 Measured temperature dependence of tanδ of polyurea JD-2000 (disks). The full lines show a simultaneous fit for all measured frequencies with Eqs. (3) and (4). Dotted lines are generated by considering either the α- or the α´-relaxation.

Fig. 6, 7 and 8 show fits of tanδ to the corresponding data of JD-2000, JD-4000 and JD-400 using Eq.(3) and Eq.(4). The resulting fitting parameters are displayed in Table 2.

Contrary to JD-2000 and JD-4000 the tanδ curve of JD-400 exhibits only a single peak (Fig. 8), and hence does not obviously display two relaxation processes. However, it is impossible to fit the data assuming a single relaxation process in Eq.(3). On the other hand we cannot uniquely separate the α and α´- contributions. Therefore we varied the relaxation contributions ΔE_1 and ΔE_2 in Eq.(3), resulting in fits of similar quality characterized by chi-square values ranging from 0.28 to 0.39. However, while T_{g1} is determined with high accuracy the uncertainty of T_{g2} is ± 10.6 K.

Taking into account, that mechanically measured relaxation times are usually shorter than dielectrically determined ones [37] the fitting parameters in Table 2 are in reasonable agreement with those determined from dielectric spectroscopy data.[34] Moreover, the main fitting parameters for the polyureas with different hard/soft segment ratios turn out to be rather similar.

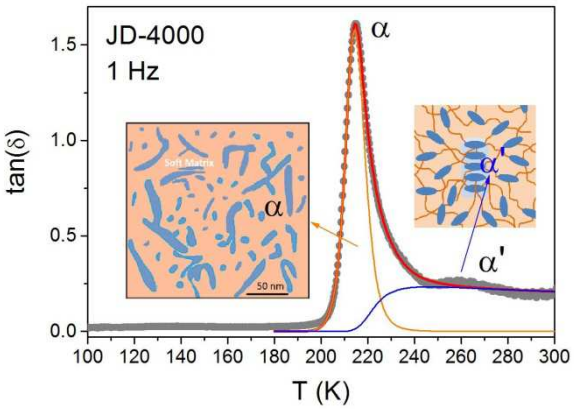

Figure 7 Measured temperature dependence of tanδ of polyurea JD-4000 (grey disks). The red full line shows a fit with Eqs. (3) and (4). Orange and blue lines are generated by considering either the α- or the α´-relaxation. The inset sketches the spatial regions of α and α' relaxations.

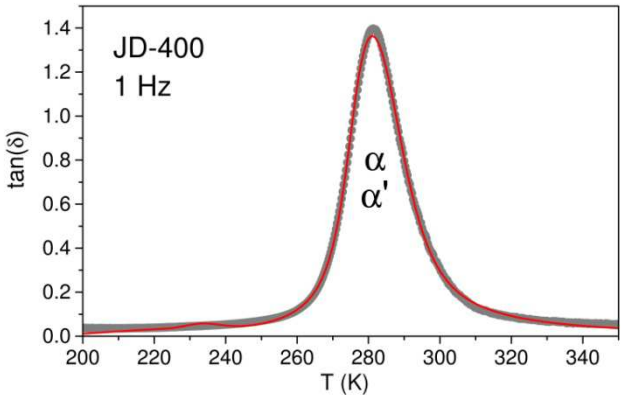

Figure 8 Measured temperature dependence of tanδ of polyurea JD-400 (grey disks). The red line shows a fit with Eqs. (3) and (4). Here we do not show separate curves, since we cannot uniquely disentangle the α and α´- contributions.

Table 2 α and α' relaxation parameters for the three polyureas JD-4000, JD-2000 and JD-400 obtained from fits with Eq. (3) and Eq.(4).

	JD-4000	JD-2000	JD-400
T_{01} (K)	156.6	153.8	221.5
α1	0.78	0.7	0.66
β1	0.48	0.39	0.001
τ_{01}(s)	10^{-15}	10^{-15}	10^{-15}
B_1 (K)	1755	1755	1755.2
$\Delta E_1/E_\infty$	0.99	0.97	0.7
T_{02}(K)	206.3	92	171.8
α2	0.16	0.57	0.61
β2	0.36	0.098	0.17
τ_{02}(s)	10^{-13}	10^{-13}	10^{-13}
B_2 (K)	565.7	4010	1388
$\Delta E_2/E_\infty$	0.0099	0.026	0.299

In the following we will calculate the temperature dependence of dynamically correlated regions when approaching the glass transition in polyurea JD-2000 using the multipoint susceptibility approach of Ref. 7. In their work the authors proposed a very general but straightforward method to calculate a number of dynamically correlated units - which they call $N_{corr,4}(T)$ - in glass forming materials. Relating un-measurable four-point correlations to an easily accessible response function, e.g. the temperature derivative of a dynamic two-point correlation function they obtain [38]

$$N_{corr,4}(T) = \frac{k_B N_A}{\Delta C_P \bar{M}_c} T^2 \{\max_\omega \chi_T(\omega,T)\}^2 \qquad (5)$$

where ΔC_P [$Jg^{-1}K^{-1}$] is the specific heat anomaly at the glass transition temperature, N_A the Avogadro constant, $\bar{M}_c$ the segmental molecular weight of the polyetheramines (soft segments) and $\chi_T(\omega,T)=(1/E_\infty)dE'(\omega,T)/dT$ is the temperature derivative of a suitable correlation function (here the real part of the complex Young´s modulus E´ normalized with respect to E_∞). In these units we obtain $N_{corr,4}$ in terms of the number of correlated soft segments. To calculate an appropriate length scale ξ we then have to multiply $N_{corr,4}$ by the corresponding segmental length l_c (Table 1).

Fig. 9 shows the temperature derivatives of the Young´s modulus of JD-2000 as a function of frequency for various temperatures near the α-glass transition. From the corresponding maxima, we have calculated $N_{corr,4}(T)$, which is increasing with decreasing temperature. Values of $N_{corr,4}$ for many glass forming materials are reported in the literature, [2,7,38] and it was shown that this quantity indeed increases when approaching T_g, implying that dynamical correlations increase when approaching the glass transition.

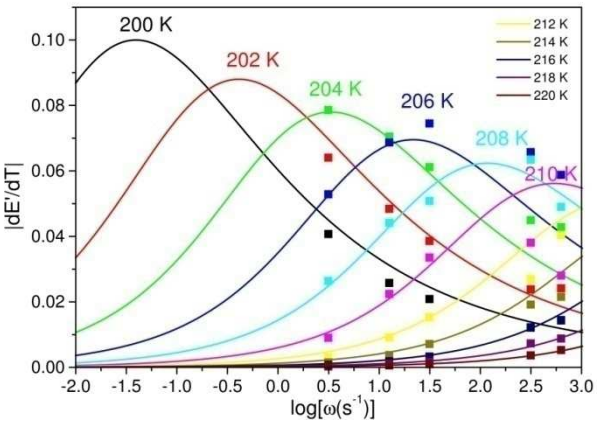

Figure 9 Temperature derivatives of normalized Young´s moduli as function of frequency for various temperatures. Points are from experimental data of JD-2000 (Fig. 3) and lines are calculated from the corresponding fits to E'(ω,T).

It is nontrivial to relate the value of $N_{corr,4}$ to certain values of spatially correlated regions. This is due to the fact, that there is no need for the associated correlation volume V_{corr} to be compact and therefore to scale as $V_{corr} = N_{corr,4}/\rho \sim\xi^3$ as is the case for isotropic correlations. Although some theories, like e.g. the random first-order transition theory (RFOT) of glasses predicts that these correlated regions are compact, computer simulations suggest that CRRs are string-like. [8,9,39]

To get a reliable estimation of the spatial correlations in polyurea we proceed as follows. Exploiting the approach described above, we calculate $N_{corr,4}(T)$ (with [34] ΔC_P=0.5 $JK^{-1}g^{-1}$) and further the correlation volume $V_{corr}(T)$ (Fig. 10). At the laboratory glass transition T_{g1}=198.6 K, defined as $\tau_1(T_{g1})$=100 s, we obtain $V_{corr}(T_{g1})\approx$10.2 nm^3. Assuming a compact correlation volume and isotropic correlations this would imply $\xi\approx V_{corr}^{1/3}$, leading to $\xi(T_{g1})\approx$2 nm. If however, we assume the dynamic correlations in polyurea to be string-like we can estimate their approximate length scale following two different approaches, which turn out to yield almost identical results (Fig. 10). For the first one, we assume that cylindrically shaped strings have an approximate thickness of a polyurea molecule [40], i.e.2r ≈ 0.56 nm – with $\xi = V_{corr}/(r^2\pi)$ – this leads to the blue disks in Fig. 10. For the second approach we calculate ξ(T) (green disks in Fig. 10) from the number of correlated segments $N_{corr,4}$ using Eq.(5) with the corresponding segmental length (l_c=12.1 nm for JD-2000) of Table 1.

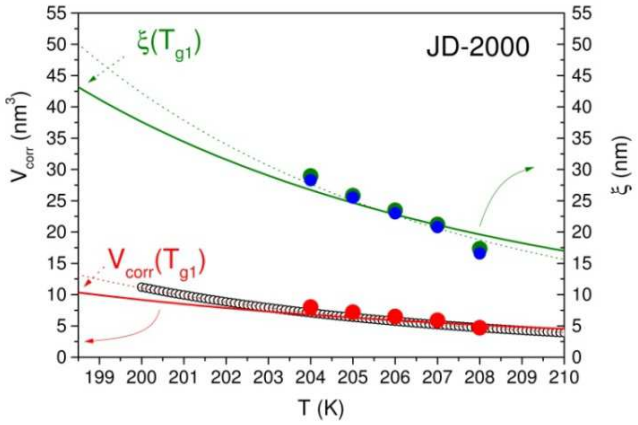

Figure 10 Temperature dependencies of dynamically correlated regions approaching the α-glass transition in polyurea JD-2000. The few full circles between 204 and 208 K are determined from the experimental values of E´(ω,T) using Eq.(5) together with $V_{corr}=N_{corr,4}/\rho$ (red disks), $\xi=V_{corr}/(r^2\pi)$ (blue) and $\xi=l_c N_{corr,4}$ (green disks) . The black open circles of V_{corr} are determined by extrapolating the experimental data of dE'/dT by the fitted ones to 200 K. The full lines are fits with Eq.(7) using the fitting parameters B_1 and T_{01} of Table 2. Dotted lines were obtained by varying the exponent in Eq.(7) from 4 to 5.3.

Fig. 10 shows the temperature dependencies of V_{corr} and ξ. The points represent the experimentally determined values using Eq.(5) and the procedures described above. The lines are fits using the relation [2,38]

$$V_{corr}(T) = \frac{N_{corr,4}(T)}{\rho} \propto \frac{k_B}{\rho \Delta C_P} T^2 \left(\frac{d \ln \tau}{dT}\right)^2 \quad (6)$$

which by using the Vogel-Fulcher temperature dependence Eq.(4) for τ(T) Eq.(6) can be written as

$$V_{corr}(T) = \frac{N_{corr,4}(T)}{\rho} \propto \frac{k_B}{\rho \Delta C_P} T^2 \frac{B^2}{(T-T_0)^4} \quad (7)$$

leading to $\xi(T_{g1})\approx 43$ nm.

After these data evaluations we arrive at the following picture for the two-glass transition behaviour of polyurea. For the α-process dynamical correlations between molecules are increasing with decreasing temperature (Fig. 10) leading to a collective slowing down of (most probably string-like) molecular motions in the soft matrix.

We argue that the α'-process is related to a freezing of the motion of soft segments of restricted mobility in the vicinity of the hard domains for the following reasons: Contrary to the α-transition, the α'-transition affects the real part of the complex Young´s modulus only very little (from Table 2 we obtain $\Delta E_2 \approx 0.027 \Delta E_1$), which is in agreement with the assumption, that the α'-transition takes place in a very small shell surrounding the hard domains (Fig. 7).

The size of the hard nanodomains is of the order of ≈ 3 – 4 nm. This nanodomain size was calculated taking into account the volume fraction of both hard and soft domains, the average distance between two hard nanodomains (Table 1) which was obtained from the maximum intensity peak in the SAXS region ($d = 2\pi/q$),[27] and the packing of spheres as an ideal model – primitive cubic (PC), body-centered cubic (BCC) and face-centered cubic (FCC). The estimated radius of this hard domains is proportional to the product of the lattice parameter times the square root of the volume fraction of the crosslinker ($r \propto a\ \phi_{HD}^{1/2}$); PC: $r = a[3\phi_{HD}/(4\pi)]^{1/2}$, BCC: $r = a[3\phi_{HD}/(8\pi)]^{1/2}$, and FCC: $r = a[3\phi_{HD}/(16\pi)]^{1/2}$. From the calculated areas of the tanδ peaks with respect to the α- and the α´-transition, we have estimated the thickness of the surrounding layer of restricted mobility to be of the order of λ≈0.2 nm for JD-2000 when considering a packing of such model spheres with a hard-to-hard domain distance of d = 5.4 nm and volume fraction of 0.04 and 0.84 for the polymer segment directly attached to the hard nanodomain interface and the bulk polymer, respectively.

The corresponding volume of this surrounding shell, which then is of the order of ≈30 nm^3, is larger than the correlation volume $V_{corr}(T_{g1})$ ≈10 nm^3 (Fig. 10). It implies that the region of restricted mobility is large enough to exhibit its own glass transition at T_{g2}. Similar estimations hold also for JD-4000 and for JD-400.

Using the fitting parameters (Table 2) one obtains (Fig. 11), that in the vicinity of the α'-peak the dynamics of these motions is indeed several orders of magnitude slower as compared to the dynamics of the polymer chain motions in the soft matrix (α–process).

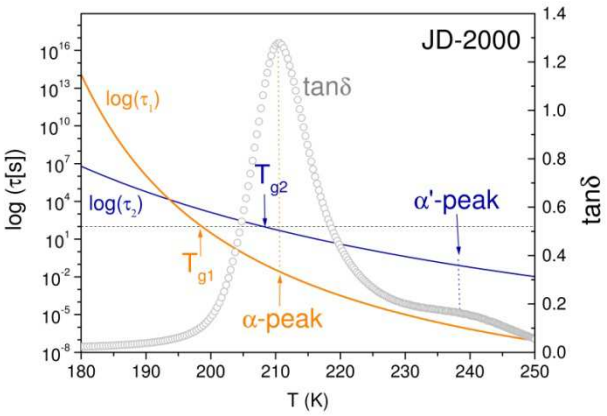

Figure 11 Temperature dependencies of relaxation times τ_1 and τ_2 for JD-2000 calculated from Eq.(4) with the parameters of Table 2. Tanδ was measured at 0.5 Hz.

Computer simulations [15,23,41] show, that the relaxations of chain segments in the vicinity of nanoparticles are necessarily slowed down, if there is an attractive interaction between nanoparticles and polymer chains. This is certainly the case here, since the soft segments (SS) are chemically attached to the hard domains. Under such conditions of permanent attachment PNCs have shown to exhibit two glass transition temperatures: [42] one associated with polymer chains in the soft matrix far from the

nanoparticles (hard domains in our case), and the other one at higher temperature is associated with chains in the vicinity of the nanoparticles (hard domains).
Table 3 gives the glass transition temperatures for the three polyureas obtained from the fitting parameters of Table 2.

Table 3 Glass transition temperatures calculated from fitting parameters of Table 2 using $\tau(T_g)$=100 s.

Sample	Tg_1 (K)	Tg_2 (K)
JD-400	266.3 ± 0.2	217.2 ± 10.6
JD-2000	198.6 ± 0.4	208.2 ± 2.1
JD-4000	201.4 ± 0.2	222 ± 1.4

Fig. 12 shows the dependencies of the glass transition temperatures on the volume fractions ϕ_x of the crosslinker (hard domains) and a fit with the relation [43]

$$T_{g1} = T_{g1}^0 + k\frac{\phi_x}{1-\phi_x} \quad (8)$$

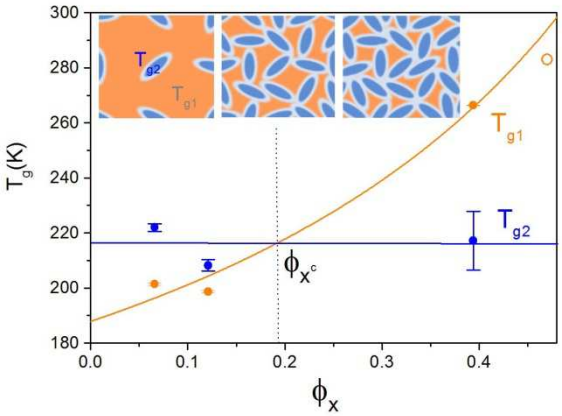

Figure 12 Glass transition temperatures of three polyurea networks JD-4000, JD-2000 and JD-400 vs. volume fractions ϕ_x of the hard nanodomains. The orange line is a fit with Eq. (8), yielding T_{g1}^0=(187.9 ± 6.6) K and k=(119.6 ± 17.2) K. The polyurea elastomer [27] ET-403 with a volume fraction of ϕ_x =0.47 (orange open circle) follows the trend rather well.

Inspecting Fig. 12 we observe, that around the critical volume fraction of $\phi_x^c \approx 0.19$ the two glass transitions reverse order, implying $T_{g1} = T_{g2}$ for ϕ_x^c. This value of 0.19 corresponds to the percolation threshold of randomly oriented overlapping ellipsoids[44] of revolution with an aspect ratio of about 1:4 – 1:5. It implies, that for ϕ_x less than 19% the system consists of hard nanodomains embedded in a soft matrix. At ϕ_x^c the hard nanodomains percolate. For $\phi_x > \phi_x^c$ the system consists of soft islands surrounded by a percolated network of hard nanodomains.
Finally we will discuss the physical origin of the strong increase of T_{g1} with increasing ϕ_x. Because the size ξ of CRRs increases for $T \rightarrow T_{g1}$ (Fig. 10), the molecules of polymer chains at distances $r \leq \xi$ away from the surface of the hard nanodomains will "feel" the surface induced slowing down. Since the average distance between the hard nanodomains is smaller than $\xi(T_{g1}) \approx 43$ nm, the dynamics of the soft domains is considerably slowed down, rationalizing the observed increase of the glass transition temperature.
A very similar behaviour was recently found for nanocomposites of polyurea JD-2000 filled with 1 wt% of MoS_2 nanotubes and $Mo_6S_2I_8$ nanowires.[45] Although the inorganic nanoparticles are much larger (100 nm diameter, 10μm length) and their concentration is 1-2 orders of magnitude smaller as compared to the hard nanodomains, a clear increase of T_{g1} was observed in the presence of nanoparticles, whereas T_{g2} remained constant (Fig. 13). Also in this case the increase of T_{g1} results from a slowing down of molecular motions near the nanoparticle surface, which due to an increase of the correlation length ξ extends deeply into the matrix.

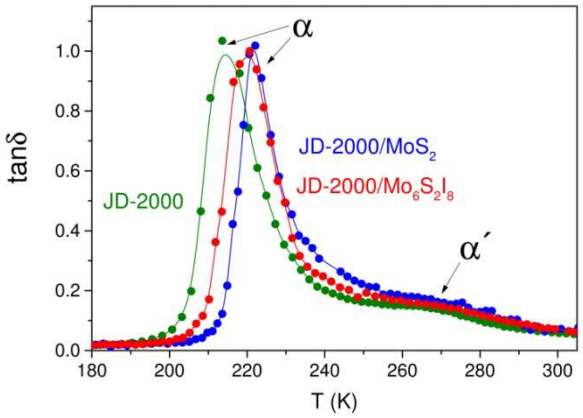

Figure 13 tanδ of pure polyurea JD-2000 compared with the nanocomposites JD-2000/MoS_2 and JD-2000/$Mo_6S_2I_8$ (1wt.% of MoS_2 and $Mo_6S_2I_8$). The measurements were performed at a frequency of 1Hz.

V Summary and conclusions

We have studied the glass transitions in microphase segregated polyurea networks by measuring the dynamic elastic susceptibility in a broad temperature range and at frequencies between 0.1 – 100 Hz. By varying the chain length l_c of the soft part of the polyurea molecules between 24.5 nm and 2.5 nm, the volume fractions ϕ_x of hard nanodomains increased from 7% to 39%, implying that the average distance *t* between the hard nanodomains decreases with decreasing chain length l_c.
Two distinct peaks in tanδ were clearly resolved at T_α and $T_{\alpha'} > T_\alpha$ for samples with 7 and 12 vol% of hard nanodomains. They were attributed to glass transitions in the soft matrix (α-peak) and at the interface between the hard nanodomains and the matrix (α'-peak), respectively. We have fitted the two tanδ peaks with two Havriliak-Negami terms and Vogel-Fulcher dependencies of the corresponding relaxation times τ_α and $\tau_{\alpha'}$. Using these fitting parameters we have determined the glass transition temperatures $T_{g1}(\phi_x)$ and $T_{g2}(\phi_x)$, corresponding to the α and the α´-process, respectively. It turns out, that T_{g1}

increases strongly with increasing volume fraction of the hard nanodomains, whereas T_{g2} remains almost constant.

The strong increase of T_{g1} with increasing ϕ_x results from the fact, that due to the observed strong increase of a dynamical correlation length ξ with $T \rightarrow T_{g1}$, the interfacially slowed down regions near the hard nanodomains extend deep into the soft matrix, and the longest relaxation time τ_α increases, resulting in an increase of the average T_{g1}. The effect increases with increasing density of the nanodomains. Molecular dynamics simulations [15,23,39,46] corroborate such a picture. On the other hand the molecules near the hard nanodomains are already strongly (chemically) attached, so that their dynamics is substantially slowed down and thus T_{g2} is not expected to be much influenced by an increase of ϕ_x, in agreement with the observations.

At the critical value of $\phi_x^c \approx 0.19$ the two glass transition temperature curves intersect, implying that at this concentration of hard nanodomains one cannot longer separate the dynamics of molecular motions close to the nanodomain interface from that of the soft matrix. At this critical concentration, the hard nanodomains start percolating and microphase segregated polyurea changes from a system of hard nanodomains embedded in a soft matrix to the opposite case of a soft polymer confined in a network of interconnected hard domains. This is also accompanied by a strong reinforcement effect, i.e. the Young´s modulus at 100 K changes from 4 GPa (for ϕ_x=0.07) to 8 GPa (for ϕ_x=0.39). The critical concentration of about 0.19 corresponds to the percolation threshold [44] of overlapping ellipsoids with an aspect ratio between 1:4 and 1:5. Of course such a simple geometrical model has at this stage to be taken with caution. E.g. if instead of rotational ellipsoids one would take overlapping spherocylinders, the observed percolation threshold [47] would imply D/L≈1:2-1:3 (D=diameter, L=length of the spherocylinder). Although such shapes of nanodomains are in reasonable agreement with some previous AFM measurements [28], more detailed investigations are needed to test these predictions which are based on a rather idealized geometrical model.

Summarizing, our findings lead to interesting insights into the two-glass transition behaviour of microphase segregated polyurea which are valid for other NPCs, too. However, as they are based on a rather macroscopic approach and phenomenological analysis they should be complemented by microscopic measurements as well as computer simulations. Detailed AFM measurements are required to reveal the morphologies of nanodomains in polyureas with different hard/soft segment ratios of the chains and to determine the corresponding average distances between the hard nanodomains as well as their exact shape. Molecular dynamics simulations of the type of Ref. 39 could help to considerably improve the quality of fitting of dynamic susceptibility data. At present we know, that in the vicinity of nanoparticles $\tau(r,T)=\tau_0(r)\exp\{\xi(r,T)\Delta(r)/T\}$ with $\tau(r\rightarrow\infty) > \tau$ (pure polymer) and we do not have a clue on the specific r-dependencies of τ_0, B and T_0 in the corresponding Vogel-Fulcher equation. Given the spatial dependence of the relaxation time – like the one shown in Fig. 11 of Ref. 39 – in an analytic form, would help to reduce the number of fitting parameters considerably and would give more physical meanings to the parameters, as compared to the rather phenomenological Havriliak-Negami fitting procedure.

In addition to the obtained fundamental insights, the present work yields results that may be also interesting from the applications point of view: The properties of polyurea can be easily tuned by varying the segmental molecular weight of polyetheramines, i.e. the volume fraction ϕ_x of hard nanodomains. The glass transition temperature increases from – 75°C for ϕ_x= 0.07 to – 7°C for ϕ_x= 0.39, i.e. with decreasing molecular weight and is accompanied by a strong reinforcement effect of 100%. In principle these properties could be further improved if the density of nanodomains could be still increased. It has been shown that packing fractions of more than 0.7 can be reached for ellipsoids [48] and superellipsoids. [49] Inserting this value into Eq. (8) one obtains a theoretical glass transition temperature of 194°C. Although such high values may not be reached in practice, the polyurea elastomer ET-403 [27] with a volume fraction of ϕ_x=0.47 yields a glass transition temperature of +10°C, which is well predicted by Eq.(8) with the fitting parameters of the present work (Fig. 12).

Acknowledgements

The present work was performed in the frame of the COST Action MP0902 (COINAPO – Composites of Inorganic Nanotubes and Polymers). Financial support from the Austrian Science Fund (FWF) P23982-N20 is gratefully acknowledged.

[a]Faculty of Physics, University of Vienna, Boltzmanngasse 5, 1090 Vienna, Austria

[b]Department of Health Sciences and Technology, ETH Zurich, Institute of Food, Nutrition and Health, Food and Soft Materials Science Group, Schmelzbergstrasse 9, LFO, E29, 8092 Zurich, Switzerland

References

[1]G. Adam and J. H. Gibbs, J. Chem. Phys., 1965, **43**, 139.

[2]S. Capaccioli, G. Ruoccoand F. Zamponi, J. Phys. Chem. B, 2008, **112**, 10652.

[3]P. Debenedetti and F. H. Stillinger, Nature, 2001, **410**, 259.

[4]G. Hempel, A. Hempel, A. Hensel, C. Schick and E. Donth, J. Phys. Chem. B, 2000, **104**, 2460.

[5]S. A. Reinsberg, A. Heuer, B. Doliwa, H. Zimmermann and H. W. Spiess, J. Non-Cryst. Sol., 2002, **307-310**, 208.

[6]X.H. Qiu and M. D. Edinger, J. Phys. Chem. B, 2003, **107**, 459.

[7]L. Berthier, G. Biroli, J.-P. Bouchard, L. Cipelletti, D. ElMasri, D. L´Hote, F. Ladieu and M. Pierno, Science, 2005, **310**, 1797.

[8]C. Donati, J. F. Douglas, W. Kob, S. J. Plimpton, P. H. Poole and S. C. Glotzer, Phys. Rev. Lett., 1998, **80**, 2338.

[9]J. D. Stevenson, J. Schmalian and P. G. Wolynes, Nature Physics, 2006, **2**, 268.

[10]J. A. Forrest and J. Mattsson, Phys. Rev. E, 2000, **61**, R53.

[11]B. Jérome and J. Commandeur, Nature, 1997, **386**, 589.

[12]P. Pissis, A. Kyritsis, D. Daoukaki, G. Barut, R. Pelster and G. Nimtz, J. Phys.: Condens. Matter, 1998, **10**, 6205.

[13]C. L. Jackson and G. B. McKenna, Chem. Mater., 1996, **8**,2128.

[14]W. Schranz, M. R. Puica, J. Koppensteiner, H. Kabelka and A. V. Kityk, Europhys. Lett., 2007, **79**, 36003.

[15]P. Scheidler, W. Kob and K. Binder, Europhys. Lett., 2000, **52**, 277.

[16]P. Scheidler, W. Kob and K. Binder, Europhys. Lett., 2002, **59**, 701.

[17]O. Trofymluk, A. A. Levchenko and A. Navrotsky, J. Chem. Phys., 2005, **123**, 194509.

[18]J.-Y. Park and G. B. McKenna, Phys. Rev. B, 2000, **61**, 6667.

[19]C. LeQuellec, G. Dosseh, F. Audonnet, N. Brodie-Lindner, C. Alba-Simionesco, W. Häussler and B. Frick, Eur. Phys. J. Special Topics, 2007, **141**, 11.

[20]M. Alcoutlabi and G. B. McKenna, J. Phys.: Condens. Matter, 2005, **17**, R461.

[21]C. Alba-Simionesco, B. Coasne, G. Dosseh, G. Dudziak, K. E. Gubbins, R. Radhakrishnan and M. Sliwinska-Bartkowiak, J. Phys.: Condens. Matter, 2006, **18**, R15.

[22]H. Oh and P. F. Green, Nature Materials, 2009, **8**, 139.

[23]F. W. Starr, T. B. Schroder and S. Glotzer, Macromolecules, 2002, **35**, 4481.

[24]G. D. Smith, D. Bedrov, L. Li and O. Byutner, J. Chem. Phys., 2002, **117**, 9478.

[25]G. Tsagaropoulos and A. Eisenberg, Macromolecules, 1995, **28**, 6067.

[26]J. M. Kropka, V. Pryamitsyn and V. Ganesan, Phys. Rev. Lett., 2008, **101**, 075702.

[27]A. Sánchez-Ferrer, D. Rogez and P. Martinoty, Macromol. Chem. Phys. 2010, **211**, 1712.

[28]M. Grujicic, B. Pandurangan, T. He, B. A. Cheeseman, C.-F.Yen and C. L. Randow, Mater.Sci. Eng.A, 2010, **527**, 7741.

[29]J. Koppensteiner, W. Schranz and M. R. Puica, Phys. Rev. B, 2008, **78**, 054203.

[30]J. Koppensteiner, W. Schranz and M. A. Carpenter, Phys. Rev. B, 2010, **81**, 024202.

[31]W. Schranz, Phase Transitions, 1997,**64**, 103.

[32]J. Yi, M. C. Boyce, G. F. Lee and E. Balizer, Polymer, 2006, **47**, 319.

[33]J. A. Pathak, J. N. Twigg, K. E. Nugent, D. L. Ho, E. K. Lin, P. H. Mott, C. G. Robertson, M. K. Vukmir, T. H. Epps III and C. M. Roland, Macromol. 2008, **41**, 7543.

[34]D. Fragiadakis, R. Gamache, R. B. Bogoslovov and C. M. Roland, Polymer, 2010, **51**, 178.

[35]S. Havriliak and S. Negami, Journal of Polymer Science Part C-Polymer Symposium, 1966, 14PC, 99.

[36]F. Kremer and A. Schönhals, *Broadband dielectric spectroscopy*. Berlin; New York: Springer; 2003.

[37]N. G. McCrum, B. E. Read and G. Williams, *Anelastic and dielectric effects in polymeric solids.* New York: Dover Publications, 1991.

[38]C. Dalle-Ferrier, C. Thibierge, C. Alba-Simionesco, L. Berthier, G. Biroli, J. P. Bouchaud, F. Ladieu, D. L´Hote and G. Tarjus, Phys. Rev. E, 2007, **76**, 041510.

[39]B. A. Pazmino Betancourt, J. F. Douglas and F. W. Starr, Soft Matter, 2013, **9**, 241.

[40] P. D. Godfrey, R. D. Brown and A. N. Hunter, J. Molecular Structure, 1997, **413-414**, 405.

[41] M. Vacatello, Macromolecules, 2001, **34**, 1946.

[42]G. Tsagaropoulos and A. Eisenberg, Macromolecules, 1995, **28**, 396.

[43] H. Stutz, K.-H. Illers and J. Mertes, J. Polymer Sci.: Part B: Polymer Phys., 1990, **28**, 1483.

[44] E. J. Garboczi, K. A. Snyder, J. F. Douglas and M. F. Thorpe, Phys. Rev. E, 1995, **52**, 819.

[45] M. Reinecker, A. Fuith, V. Soprunyuk, A. Sánchez-Ferrer, A.Mrzel, R. Torre and W. Schranz, Phys. Stat. Sol. A, 2013, **210**, 2320.

[46] M. Vacatello, Macromolecules, 2001, **34**, 1946.

[47] B. Nigro, C. Grimaldi, P. Ryser, A. P. Chatterjee and P. van der Schoot, Phys. Rev. Lett., 2013, **110**, 015701.

[48] A. Donev, F. H. Stillinger, P.M. Chaikin and S. Torquato, Phys. Rev. Lett. 2004, **92**, 255506-1.

[49] G. W. Delaney and P. W. Cleary, Europhys. Lett. 2010, **89**, 34002-p1.

9 Acknowledgements

I would like to express my heartfelt thanks to my supervisor, Prof. Dr. Wilfried Schranz for his scientific enthusiasm and immeasureable patience. His steady, motivating support and optimistic, insightful approach to any problem proved invaluable in finishing this work. I also owe a large debt of gratitude to Dr. Antoni Sánchez-Ferrer for manufacturing the samples, many fruitful discussions and his absolutely essential scientific input, which resulted in the publications included here. I also would like to thankfully mention Dr. Aleš Mrzel, who manufactured the nanoparticles and provided valuable help.

Furthermore, I am deeply grateful for the cooperation and help provided by the PCCL (Polymer competence center) Leoben, in particular Astrid Rauschenbach, and the Faculty Center for Nanostructure Research of the University of Vienna, especially Prof. Dr. Herwig Peterlik and Dr. Johanna Akbarzadeh. It is also my privilege to convey my thanks to Phil Robinson of Ruston Services Ltd., who taught me a lot about thermal analysis, in a way that was both entertaining and intensely informative. Continous helpful technical support was also faciliated and provided by Franz Öller of Solutions for Science and Johann Krautgasser of Perkin Elmer.

The financial support of the Austrian Science Fund (FWF) P23982-N20 and the COST Action MP0902 (COINAPO – Composites of Inorganic Nano-tubes and Polymers) is also gratefully acknowledged.

List of Figures

3.1 The phase image of polyurea JD-400 shows small hard islands which appear elevated from the soft matrix . . . 17
3.2 In the topographic view of polyurea JD-400 the small hard islands can be clearly seen as light spots . . . 17
3.3 The phase image of JD-2000 is less conclusive than the one of JD-400, but the hard domains are still discernible. . . . 17
3.4 In the topographic view of polyurea JD-2000 more hard islands can be discerned, and the dark areas representing the soft matrix occupy less space compared to JD-400. Extensive areas of restricted molecular mobility are also visible, indicated by mid-tone colors. . . . 17
3.5 On the phase image of JD-4000 it is very difficult to recognize the difference between the soft from the hard areas. . . . 17
3.6 Only a few small dark spots representing the soft matrix remain in the topographic image of JD-4000. . . . 17
3.7 AFM phase (left column) and topographic (right column) images of JD-400 (top row), JD-2000 (second row) and JD-4000 (bottom row) . . . 17
3.8 SAX-image of JED with C1 MoS_2 nanotubes, $1 \cdot 10^{-}1$ weight-% . The slightly elliptic shape suggests a direction of preference in the distribution of the nanotubes. As the rings are not sharply defined, but rather diffuse, the clusters of nanotubes have a rather wide size distribution. . . . 18
3.9 SAX-image of JED with C1 MoS_2 nanotubes, 1 weight-% . The diffraction rings appear to be perfectly concentric, leading to the conclusion that the nanotube-clusters are randomly oriented. . . . 18
3.10 SEM-image of JED with C2 MoS_2 nanotubes, „bottom“ side with respect to the orientation during manufacture of the sample in horizontal orientation in a petri dish, showing that the nanotubes have sunk to the bottom during the polimerization process in spite of having been stirred as long as possible. . . . 18

3.11 SEM-image of JED with C2 MoS_2 nanotubes, „top“ side with only very few individual nanotubes visible as most have sunk down into the sample in relation to the orientation during manufacture. . . . 18
3.12 JED with C1 MoS_2 nanotubes . . . 19
3.13 JED with C1 MoS_2 nanotubes . . . 19
3.14 JED with C1 MoS_2 nanotubes . . . 19
3.15 JED with C2 MoS_2 nanotubes . . . 20
3.16 JED with C2 MoS_2 nanotubes . . . 20
3.17 JED with C2 MoS_2 nanotubes . . . 20

4.1 Typical representation of a glass transition measured with DMA. The elastic contribution E' to the complex modus, shown in **red**, changes very little until the glass transition temperature is approached, when it drops drastically, possibly severeal orders of magnitude. The damping $tan(\delta)$, shown in **blue**, which is defined as the ratio of the viscous contribution E" to E', exhibits a pronounced peak in the same temperature region as the drop in E' occurs. The dashed line marks the definition of the glass transition temperature $\boldsymbol{T_g}$ used in this work. . . . 26
4.2 Unmodified Perkin Elmer Diamond DMA. An insulated hose connects the liquid nitrogen dewar to the instrument's furnace. . . . 27
4.3 Modified Perkin Elmer Diamond DMA. The insulated liquid nitrogen reservoir is mounted directly on the furnace. The top covering of the reservoir was removed and is not shown in the picture. . . . 27

5.1 Real (E') and imaginary (E'') part of the complex Young's modulus for the pure polyurea elastomer (PU) and the two nanocomposites (PU-MoS_2 and PU-$Mo_6S_2I_8$). 28
5.2 Second $tan\ \delta$-peak in polyurea JD-2000 . . . 29
5.3 E' of PNC JD-2000/MoS_2 . . . 31
5.4 $tan\ \delta$ of PNC JD-2000/MoS_2 . . . 31
5.5 E' of PNC JED-2003/MoS_2 The inset shows the drop in the elastic modulus E' due to the removal of the hydrogen bonds. . . . 31
5.6 E'' of PNC JED-2003/MoS_2 . . . 31
5.7 $\boldsymbol{E'}$, $\boldsymbol{E''}$ and $\boldsymbol{tan\ \delta}$ of JD-4000 . . . 32
5.8 $\boldsymbol{E'}$, $\boldsymbol{E''}$ and $\boldsymbol{tan(\delta)}$ of JD-400. The grey discs show the $tan(\delta)$ of **JD-2000**, shifted with respect to temperature, to illustrate the relative breadth of the $\boldsymbol{tan(\delta)}$ of **JD-400**. 33
5.9 Temperature dependencies of dynamically correlated regions . . . 36

5.10 Glass transition temperatures dependent on the volume fraction of hard domains. Insets show 2-dimensional comics of the configurations of the hard domains and their shells of restricted mobility inside the soft matrix. The first inset on the left shows widely dispersed hard domains without any contact of the slowed down regions around it, corresponding to the situation in JD-2000 and JD-4000. The inset in the middle gives an impression of how the hard domains start to continuously interconnect over long distances, and the third inset on the right shows densely interlocked hard domains, as they can be found in JD-400. The actual situation is more complex because the domains are not perfectly eliptically shaped. They are also not of precisely the same size. Moreover, the real arrangement of the domains is naturally 3-dimensional. 37

List of Illustrations

3.1 Typical polyurea segment. Carbon atoms are shown in **black**, **hydrogen** in white, **nitrogen** in blue and **oxygen** in red. 10
3.2 Hydrogen bonds between urea-moieties 11
3.3 Typical single wall MoS_2-nanotube sulfur shown in yellow, molybdenum colored turquoise 13

4.1 Principle of DMA measurements. The periodically modulated force $\boldsymbol{F}$ is shown in red, the corresponding length change of the sample $\boldsymbol{\Delta l}$ in blue. δ denotes the phase shift between them. The time-axis is labeled t. 22
4.2 Tension mode 24
4.3 Shear mode. Two identical samples are needed for this setup. 24

5.1 2 methods for calculating the correlation length in polyurea based on DMA-data . . . 35

Literature

[1] Johannes Koppensteiner. "The glass transition in nanoscaled confinement probed by dynamic mechanical spectroscopy". supervisor: Wilfried Schranz. PhD thesis. Universität Wien, Fakultät für Physik, 2009.

[2] G. Grundmeier, W. Schmidt, and M. Stratmann. "Corrosion protection by organic coatings: electrochemical mechanism and novel methods of investigation". In: *Electrochimica Acta* 45.15–16 (2000), pp. 2515–2533. ISSN: 0013-4686. DOI: 10.1016/S0013-4686(00)00348-0. URL: http://www.sciencedirect.com/science/article/pii/S0013468600003480.

[3] M. Grujicic, B. Pandurangan, T. He, B. A. Cheeseman, C.-F. Yen, and C. L. Randow. "Computational investigation of impact energy absorption capability of polyurea coatings via deformation-induced glass transition". In: *Materials Science and Engineering: A* 527 (2010), pp. 7741–7751.

[4] Thomas Hanemann and Dorothée Vinga Szabó. "Polymer-Nanoparticle Composites: From Synthesis to Modern Applications". In: *Materials* 3.6 (2010), p. 3468. ISSN: 1996-1944. DOI: 10.3390/ma3063468. URL: http://www.mdpi.com/1996-1944/3/6/3468.

[5] M.R. Bockstaller and E.L. Thomas. "Optical Properties of Polymer-Based Photonic Nanocomposite Materials". In: *The Journal of Physical Chemistry B* 107.37 (2003), pp. 10017–10024. DOI: 10.1021/jp035286j. eprint: http://pubs.acs.org/doi/pdf/10.1021/jp035286j. URL: http://pubs.acs.org/doi/abs/10.1021/jp035286j.

[6] D. Fragiadakis, R. Gamache, R.B. Bogoslovov, and C.M. Roland. "Segmental dynamics of polyurea: Effect of stoichometry". In: *Polymer* 51 (2010), pp. 178–184.

[7] Ning Hu, Zen Masuda, Cheng Yan, Go Yamamoto, Hisao Fukunaga, and Toshiyuki Hashida. "The electrical properties of polymer nanocomposites with carbon nanotube fillers". In: *Nanotechnology* 19 (2008), p. 215701.

[8] Jonathan N. Coleman, Martin Cadek, Kevin P. Ryan, Antonio Fonseca, Janos B. Nagy, Werner J. Blau, and Mauro S. Ferreira. "Reinforcement of polymers with carbon nanotubes. The role of an ordered polymer interfacial region. Experiment and modeling". In: *Polymer* 47.26 (2006), pp. 8556–8561. ISSN: 0032-3861. DOI: 10.1016/j.polymer.2006.10.014. URL: http://www.sciencedirect.com/science/article/pii/S0032386106011785.

[9] D.K. Avasthi, Y.K. Mishra, D. Kabiraj, N.P. Lalla, and J.C. Pivin. "Synthesis of metal-polymer nanocomposite for optical applications". In: *Nanotechnology* 18.12 (2007), p. 125604. URL: http://dx.doi.org/10.1088/0957-4484/18/12/125604.

[10] K. P. Menard. *Dynamic Mechanical Analysis*. 2nd ed. 2008.

[11] G. Tsagaropoulos and A. Eisenberg. In: *Macromolecules* 28 (1995), p. 6067.

[12] A. Eisenberg, B. Hird, and R.B. More. In: *Macromolecules* 23 (1990), p. 4098.

[13] E. Hempel et al. "Characteristic Length of Dynamic Glass Transition near Tg for a Wide Assortment of Glass-Forming Substances". In: *J. Phys. Chem. B* 104 (2000), p. 2460.

[14] J. Koppensteiner, W. Schranz, and M.R. Puica. "Confinement effects on glass forming liquids probed by dynamic mechanical analysis". In: *Phys. Rev. B* 78 (2008), p. 054203.

[15] J. Koppensteiner and W. Schranz. "Dynamic Mechanical Analysis of Confined Glass Forming Liquids". In: *Phase Transitions* 83 (2010), p. 744.

[16] A.C. Comer, A.L. Heilman, and D.S. Kalika. "Dynamic relaxation characteristics of polymer nanocomposites based on poly(ether imide) and poly(methyl methacrylate)". In: *Polymer* 51.22 (2010), pp. 5245–5254. ISSN: 0032-3861. DOI: 10.1016/j.polymer.2010.08.053. URL: http://www.sciencedirect.com/science/article/pii/S0032386110007548.

[17] M. Vacatello. In: *Macromolecules* 34 (2001), p. 1946.

[18] F.W. Starr, T.B. Schroder, and S.C. Glotzer. In: *Macromolecules* 35 (2002), p. 4481.

[19] M. Remskar et al. In: *Science* 292 (2001), p. 479.

[20] A. Kis et al. In: *Small* 3 (2007), p. 1544.

[21] Firouzeh Sabri, John D. Boughter Jr, David Gerth, Omar Skalli, Thien-Chuong N. Phung, George-Rudolph M. Tamula, and Nicholas Leventis. "Histological Evaluation of the Biocompatibility of Polyurea Crosslinked Silica Aerogel Implants in a Rat Model: A Pilot Study". In: *PLoS ONE* 7.12 (Dec. 2012), e50686. DOI: 10.1371\/journal.pone.0050686. URL: http://dx.doi.org/10.1371%5C/journal.pone.0050686.

[22] A. Sánchez-Ferrer, D. Rogez, and P. Martinoty. "Synthesis and Characterization of New Polyurea Elastomers by Sol/Gel Chemistry". In: *Macromol. Chem. and Phys.* 211 (2010), p. 1712.

[23] A. Sánchez-Ferrer, R. Mezzenga, and H. Dietsch. "Orientational Behavior of Ellipsoidal Silica-Coated Hematite Nanoparticles Integrated within an Elastomeric Matrix and its Mechanical Reinforcement". In: *Macromol. Chem. Phys.* 212 (2011), pp. 627–634.

[24] A. Sánchez-Ferrer, M. Reufer, R. Mezzenga, P. Schurtenberger, and H. Dietsch. "Inorganic-Organic Elastomer Nanocomposites from Integrated Ellipsoidal Silica-Coated Hematite Nanoparticles as Crosslinking Agents". In: *Nanotechnology* 21 (2010), pp. 185603/1–7.

[25] Gotthard Seifert, Humberto Terrones, Mauricio Terrones, Gerd Jungnickel, and Thomas Frauenheim. "Structure and Electronic Properties of MoS_2 Nanotubes". In: *Phys. Rev. Lett.* 85 (1 July 2000), pp. 146–149. DOI: 10.1103/PhysRevLett.85.146. URL: http://link.aps.org/doi/10.1103/PhysRevLett.85.146.

[26] A. Fuith, M. Reinecker, A. Sánchez-Ferrer, R. Mezzenga, A. Mrzel, M. Knite, I. Aulika, M. Dunce, and W. Schranz. "Dynamic- and thermo- mechanical analysis of inorganic nanotubes/elastomer composites". In: *Sensors & Transducers* 12 (2011), p. 71.

[27] Hyunjoon Oh and Peter F. Green. "Polymer chain dynamics and glass transition in athermal polymer/nanoparticle mixtures". In: *Nat Mater* 8.2 (Feb. 2009), pp. 139–143. ISSN: 1476-1122. DOI: 10.1038/nmat2354. URL: http://dx.doi.org/10.1038/nmat2354.

[28] Marius Reinecker, Viktor Soprunyuk, Martin Fally, Antoni Sánchez-Ferrer, and Wilfried Schranz. "Two glass transitions of polyurea networks: effect of the segmental molecular weight". In: *Soft Matter* 10 (31 2014), pp. 5729–5738. DOI: 10.1039/C4SM00979G. URL: http://dx.doi.org/10.1039/C4SM00979G.

[29] Berthier L., G. Biroli, J.-P. Bouchaud, L. Cipelletti, D. El Masri, D. L'Hôte, F. Ladieu, and M. Pierno. "Direct experimental evidence of a growing length scale accompanying the glass transition". In: *Science* 310 (2005), p. 1797. DOI: 10.1126/science.1120714.

[30] H. Stutz, K.-H. Illers, and J. Mertes. "A generalized theory for the glass transition temperature of crosslinked and uncrosslinked polymers". In: *Journal of Polymer Science Part B: Polymer Physics* 28.9 (1990), pp. 1483–1498. ISSN: 1099-0488. DOI: 10.1002/polb.1990.090280906. URL: http://dx.doi.org/10.1002/polb.1990.090280906.

[31] E. J. Garboczi, K. A. Snyder, J. F. Douglas, and M. F. Thorpe. "Geometrical percolation threshold of overlapping ellipsoids". In: *Phys. Rev. E* 52 (1 July 1995), pp. 819–828. DOI: 10.1103/PhysRevE.52.819. URL: http://link.aps.org/doi/10.1103/PhysRevE.52.819.

[32] M. V. Bollinger, K. W. Jacobsen, and J. K. Nørskov. "Atomic and electronic structure of MoS_2 nanoparticles". In: *Phys. Rev. B* 67 (8 Feb. 2003), p. 085410. DOI: 10.1103/PhysRevB.67.085410. URL: http://link.aps.org/doi/10.1103/PhysRevB.67.085410.

[33] J. Koppensteiner, W. Schranz, and M.A. Carpenter. “Revealing the pure confinement effect in glass-forming liquids by dynamic mechanical analysis”. In: *Phys. Rev. B* 81 (2010), p. 024202.

Author's contributions

[1] L. Zhang, G. Rogl, A. Grytsiv, S. Puchegger, J. Koppensteiner, F. Spieckermann, H. Kabelka, M. Reinecker, P. Rogl, W. Schranz, M. Zehetbauer, and M.A. Carpenter. "Mechanical properties of filled antimonide skutterudites". In: *Materials Science and Engineering B* (2010). doi:10.1016/j.mseb.2010.02.022, pp. 1409–1417.

[2] E.K.H. Salje, J. Koppensteiner, M. Reinecker, W. Schranz, and A. Planes. "Jerky elasticity: Avalanches and the martensitic transition in $Cu_{74.08}Al_{23.13}Be_{2.79}$ shape-memory alloy". In: *Applied Physics Letters* 95 (2009). doi:10.1063/1.3269578, p. 231908.

[3] M. Falmbigl, G. Rogl, P. Rogl, M. Krigisch, H. Müller, E. Bauer, M. Reinecker, and W. Schranz. "Thermal expansion of thermoelectric type-I-clathrates". In: *Journal of Applied Physics* 108 (2010). doi:10.1063/1.3465637, p. 043529.

[4] Long Zhang, Andrij Grytsiv, Peter Franz Rogl, Ernst Bauer, Johannes Koppensteiner, Marius Reinecker, Heinz Kabelka, and Wilfried Schranz. "High Temperature Thermoelectric Performance and Mechanical Properties of Macro- and Nano-MmyFe4-x{Co, Ni}x{Sb}12 Skutterudites". In: The 28^{th} International Conference on Thermoelectrics and The 7^{th} European Conference on Thermoelectrics (ICT 2009 & ECT 2009) Freiburg Deutschland. 2009.

[5] Gerda Rogl, Andrij Grytsiv, Ernst Bauer, Peter Franz Rogl, Marius Reinecker, Johannes Koppensteiner, and Michael Zehetbauer. "Novel Skutterudites (Pr,Nd)1-y(Fe1-xCox)4Sb12 and (Pr,Nd)1-y(Fe1-xNix)4Sb12". In: The 28^{th} International Conference on Thermoelectrics and The 7^{th} European Conference on Thermoelectrics (ICT 2009 & ECT 2009) Freiburg Deutschland. 2009.

[6] Marius Reinecker and Bair Damdinov. *Shear viscoelastic properties of Nd:YAG nanoparticles dispersed in ethylene glycol*. The 2^{nd} International Conference "Nanomaterials and technologies" in Ulan-Ude Buryatia. 2009.

[7] A. Fuith, M. Reinecker, A. Sánchez-Ferrer, R. Mezzenga, A. Mrzel, M. Knite, I. Aulika, M. Dunce, and W. Schranz. "Dynamic- and thermo- mechanical analysis of inorganic nanotubes/elastomer composites". In: *Sensors & Transducers* 12 (2011), p. 71.

[8] M. Reinecker, A. Fuith, M. Fally, A. Sánchez-Ferrer, R. Mezzenga, A. Mrzel, and W. Schranz. *Dynamic mechanical analysis of polyurea and nanoparticle–elastomer composites*. Poster at: COST Action MP0902 COINAPO Workshop in Llubljana. 2011.

[9] J. Koppensteiner, M. Reinecker, A. Fuith, A. Sánchez-Ferrer, R. Mezzenga, and W. Schranz. *Glass transitions of confined liquids and polyurea-elastomers*. Poster at: COST Action MP0902 COINAPO Workshop in Praha. 2012.

[10] M. Reinecker, V. Soprunyuk, A. Sánchez-Ferrer, R. Mezzenga, and W. Schranz. *Glass transition behaviour in polyurea elastomers with varying soft to hard nanodomain ratios*. Poster at: COST Action MP0902 COINAPO Workshop in Naples. 2013.

[11] G. Rogl, Z. Aabdin, E. Schafler, J. Horky, D. Setman, M. Zehetbauer, M. Kriegisch, O. Eibl, A.Grytsiv, E. Bauer, M. Reinecker, W. Schranz, and P. Rogl. "Effect of HPT processing on the structure, thermoelectric and mechanical properties of Sr0.07Ba0.07Yb0.07Co4Sb12". In: *Journal of Alloys and Compounds* (2012), pages. ISSN: 0925-8388. DOI: 10.1016/j.jallcom.2012.05.011. URL: http://www.sciencedirect.com/science/article/pii/S0925838812008080?v=s5.

[12] Zhiying Zhang, Nathan Church, Sophie-Charlotte Lappe, Marius Reinecker, Armin Fuith, Paul J Saines, Richard J Harrison, Wilfried Schranz, and Michael A Carpenter. "Elastic and anelastic anomalies associated with the antiferromagnetic ordering transition in Wüstite, Fe_xO". In: *J. Phys.: Condensed Matter* 24.21 (2012), p. 5404.

[13] A. E. Böhmer, P. Burger, F. Hardy, T. Wolf, P. Schweiss, R. Fromknecht, M. Reinecker, W. Schranz, and C. Meingast. "Nematic Susceptibility of Hole-Doped and Electron-Doped $BaFe_2As_2$ Iron-Based Superconductors from Shear Modulus Measurements". In: *Phys. Rev. Lett.* 112 (4 Jan. 2014), p. 047001. DOI: 10.1103/PhysRevLett.112.047001. URL: http://link.aps.org/doi/10.1103/PhysRevLett.112.047001.

[14] Marius Reinecker, Armin Fuith, Viktor Soprunyuk, Antoni Sánchez-Ferrer, Aleš Mrzel, Renato Torre, and Wilfried Schranz. "Influence of inorganic nanoparticles on the glass transitions of polyurea elastomers". In: *physica status solidi (a)* (2013), n/a–n/a. ISSN: 1862-6319. DOI: 10.1002/pssa.201329317. URL: http://dx.doi.org/10.1002/pssa.201329317.

[15] Marius Reinecker, Viktor Soprunyuk, Martin Fally, Antoni Sánchez-Ferrer, and Wilfried Schranz. "Two glass transitions of polyurea networks: effect of the segmental molecular weight". In: *Soft Matter* 10 (31 2014), pp. 5729–5738. DOI: 10.1039/C4SM00979G. URL: http://dx.doi.org/10.1039/C4SM00979G.

10 Curriculum vitae

Education and professional activities

Physics

2015	talk at the Physics of functional materials research groups seminar at the University of Vienna
	teaching at the University of Vienna: Exercise course in Introductory Physics I
	teaching at the University of Vienna: Exercise course in Introductory Physics II
2014	talk at the Physics of functional materials research groups seminar at the University of Vienna
	talk at the Perkin Elmer Material 2014 Seminar in Vienna
	teaching at the University of Vienna: Exercise course in Introductory Physics I
2013	teaching at the University of Vienna: Exercise course in Introductory Physics I
	poster presentation at COST Action MP0902 COINAPO Workshop in Naples
2012	poster presentation at COST Action MP0902 COINAPO Workshop in Praha
2011	poster presentation at COST Action MP0902 COINAPO Workshop in Ljubljana
2011	poster presentation at the 8^{th} Liquid matter conference in Vienna
2009	talk at the 2^{nd} International Conference Nanomaterials and technologies in Ulan-Ude, Buryatia
2008-	PhD Thesis Viscoelastic Properties of Polymer-Nanocomposites,
	Supervisor Ao. Prof. Dr. Wilfried Schranz
2002-2007	study of physics at the University of Vienna
	Master thesis Zucht von NaCL-Einkristallen nach dem Bridgeman-Stockbarger-Verfahren,
	Supervisor Ao. Prof. Dr. Armin Fuith
1998-2000	study at the College of Graphics and Design in Vienna
1993-1998	study of physics at the University of Vienna

Communications design in natural sciences and related fields

2015 -	development of CI and CD for Solutions for Science Handels GmbH
2014 - 2015	graphics design and prepress work together with Dr. Anna-Marie B. Hermann for the exhibiton The University of Vienna on the Ringstraße
2014	complete graphics design and prepress work for the opening ceremony of the Opening of the Danube Center for Atomistic Modeling in Vienna
2013	complete graphics design and prepress work together with Dr. Anna-Marie B. Hermann for the DyProSo XXXIV symposium in Vienna
2011	complete graphics design and prepress work for 8^{th} Liquid matter conference in Vienna
-	more design and prepress work for scientific posters at diverse conferences than I care to mention